Fault Detection and Isolation in Spacecraft Attitude Control System Using Parity Space Method

Golnaz Nakhaie Ashtiani

A thesis

in

The Department

of

Electrical and Computer Engineering

Present in Partial Fulfillment of Requirements
For the Degree of Master of Applied Science (Electrical Engineering) at
Concordia University
Montreal, Quebec, Canada

April 2007

Your file Votre référence
ISBN: 978-0-494-28922-8
Our file Notre référence
ISBN: 978-0-494-28922-8

Abstract

FAULT DETECTION AND ISOLATI IN SPACECRAFT ATTITUDE CONTROL SYSTEM USING PARITY EQUATION METHOD

Golnaz Nakhaie Ashtiani

In this thesis, the problem of fault detection and diagnosis in the spacecraft attitude control system is considered. For this purpose, a fault or a failure in a spacecraft is first defined. This is followed up by description and details on the spacecraft architecture, and specifically the spacecraft attitude control system (ACS). The method developed for fault detection and diagnosis is the parity space or the parity equation approach. This method is applied to one type of actuators, namely reaction wheels that are commonly used in the spacecraft attitude control system. The capabilities of this method for fault detectability are studied through extensive numerical simulations. The proposed method is validated by comparing the obtained results with those of a fault detection method based on linear observer approach. Among the various variables in a reaction wheel of the attitude control system, bus voltage and actuator current components are of particular interest in this thesis, due to their influence in performance of the ACS of the spacecraft. Different types of fault signatures are used for these two components, and the simulated results are compared through two different approaches for fault detection. The advantages of the proposed and designed parity space-based method over a linear observer-based approach for fault detection and diagnosis is shown to be significant especially in detecting faults in the pitch axis of the spacecraft.

Acknowledgment

I would like to thank my supervisor Prof. Khashayar Khorasani, who has been a good supervisor, teacher and friend in all steps of doing this thesis, and assisted me in numerous ways and supported me during my graduate studies and research.

I am grateful to my family, who supported me in all senses during my work. I would like to thank them for preparing me such a good opportunity to do this job and make a big step to my goals in my life. This job couldn't be done without their encouragement.

I want to thank Prof. Yumin Zhang from Denmark University, who authorized me to have access to his lecture notes and documentations.

I can not end without thanking my friends Mr. Behzad Samadi for his guidelines and Mr. Vahid Mirjalili for his reviews.

Contents

Chapter 1 : Introduction 1

1.1. Statement of the Problem 1

1.2. Justification 3

1.3. Methodology 4

1.4. Contribution of Thesis 8

1.5. Outline of Thesis 8

Chapter 2 : Fault Detection, Isolation, and Recovery (FDIR) 10

2.1. Concept of a Fault 10

2.2. Modeling a Faulty System 11

2.3. Fault Detection System Characteristics 13

2.4. Model Based Approaches to Fault Detection and Isolation 14

2.4.1. Residual Generation Techniques 16

2.5. Conclusion 28

Chapter 3 : Spacecraft Attitude Control System 29

3.1. Reference Frame 29

3.1.1. Spacecraft Fixed Body Reference 30

3.1.2. Spacecraft Principal Axes Reference Frame 30

3.1.3. Spacecraft Orbital Reference Frame 31

3.1.4. Inertial Reference Frame 31

3.2. Attitude Control System Dynamics and Control Laws 32
3.2.1. Spacecraft Attitude Dynamics and Disturbance Torques 33
3.2.2. Actuator Dynamics 37
3.2.3. Controller Dynamics 46
3.3. Conclusion 58
Chapter 4 : Parity Space and Linear Observer-based Customized Design 59
4.1. Parity Space FDD Design 59
4.1.1. Simulation Results 66
4.2. Linear Observer FDI Design (State Estimation Approach) 72
4.2.1. Simulation Results 73
4.3. Safe Limits 78
4.4. Conclusion 84
Chapter 5 : Comparative Analysis and Simulation Results 85
5.1. Fault in K_t 85
5.1.1. Sensitivity 85
5.1.2. Permanent Faults 91
5.1.3. Intermittent Faults 94
5.2. Fault in the V_{BUS} 97
5.2.1. Sensitivity 98
5.2.2. Permanent and Intermittent Faults 99
5.3. Multiple Faults in K_t and V_{BUS} 103
5.4. Conclusion 119

Chapter 6 : Conclusions and Future Work..... 120

List of Figures

Figure 2-1: The controlled system and fault topology [24] 11

Figure 2-2: Structure of the model based FDI system [24] 15

Figure 2-3: Parameter estimation method using equation error [24] 17

Figure 2-4: Parameter estimation method using output error 19

Figure 2-5: General structure of the state estimator 21

Figure 2-6: The process and the state observer method [24]. 23

Figure 3-1: Spacecraft fixed body reference frame [55] 30

Figure 3-2: Spacecraft orbital reference frame [55] 31

Figure 3-3: Spacecraft inertial reference frame [55] 32

Figure 3-4: ITHACO reaction wheel 38

Figure 3-5: High fidelity reaction wheel block diagram [5] 39

Figure 3-6: Static imbalance representation [5] 45

Figure 3-7: Dynamic imbalance representation [5] 45

Figure 3-8: The three axis stabilized spacecraft attitude control system 47

Figure 3-9: Single axis control block diagram 47

Figure 3-10: Transient response specifications 49

Figure 3-11: Nearly ideal reaction wheel [5] 53

Figure 3-12: The set point reference commands for a scheduled different maneuvers for the spacecraft (a) roll axis, (b) pitch axis and (c) yaw axis 56

Figure 3-13: The actual outputs of the closed loop non-linear spacecraft following the desired reference commands shown in Figure 3-12 (a) roll axis, (b) pitch axis and (c) yaw axis 57

Figure 4-1: The linear block diagram of a single axis spacecraft attitude control system (pitch axis) 60

Figure 4-2: A one axis FDI system block diagram 62

Figure 4-3: Parity equation approach to fault detection and diagnosis as applied to the linear single axis model of the spacecraft 66

Figure 4-4: The residual signal generated corresponding to the input signal of (a) 1°, (b) 7°, and (c) 15° 67

Figure 4-5: Residual generated corresponding to different initial conditions applied through different input signals of (a), (b) and (c). 71

Figure 4-6: The residual signal generated corresponding to the input signal of (a) 1°,(b) 7°, and (c) 15° 74

Figure 4-7: Residual generated corresponding to different initial conditions applied for different input signals (a), (b) and (c). 77

Figure 4-8: Safe limits derived and applied to the roll axis residual (parity space) 81

Figure 4-9: Safe limits derived and applied to the pitch axis residual (parity space) 81

Figure 4-10: Safe limits derived and applied to the yaw axis residual (parity space) 81

Figure 4-11 : Safe limits derived and applied to the roll axis residual (linear observer).. 83

Figure 4-12: Safe limits derived and applied to the pitch axis residual (linear observer) 83

Figure 4-13: Safe limits derived and applied to the yaw axis residual (linear observer).. 83

Figure 5-1: The minimum amount of fault in the roll axis that is detected by (a) linear observer-based and (b) Parity space-based schemes for a reference set point angle of 1° 87

Figure 5-2: The minimum amount of fault in the roll axis that is detected by (a) linear observer-based and (b) parity space-based scheme for a reference set point angle of 5° 88

Figure 5-3: The effects of noise and disturbances on the residual generated by the pitch axis of a spacecraft when (a) faults occur in the roll axis, (b) faults occur in the pitch axis, and (c) faults occur in the yaw axis of the spacecraft 90

Figure 5-4: The delay in detecting of a fault in the roll axis by using (a) linear observer and (b) parity space approaches 92

Figure 5-5: The delay in detecting of a fault in the pitch axis by using (a) linear observer-based and (b) parity space-based approaches 94

Figure 5-6: Intermittent fault 95

Figure 5-7: Intermittent fault detection in the roll axis for the (a) linear observer-based and (b) parity space-based approaches 97

Figure 5-8: Minimum V_{BUS} fault in the roll axis detected by (a) linear observer-based and (b) parity space-based approaches 98

Figure 5-9: Permanent fault detection in the pitch axis for (a) linear observer-based and (b) parity space-based approaches 101

Figure 5-10: Detection of the intermittent fault in the V_{BUS} in the roll axis for the (a) linear observer-based and (b) parity space-based approaches 103

Figure 5-11: Multiple faults in V_{BUS} in the roll axis and K_t in the pitch axis that are detected by (a) linear observer-based, and (b) parity space-based approaches 107

Figure 5-12: Multiple faults in V_{BUS} in the roll axis and K_t in the yaw axis that are detected by (a) linear observer-based, and (b) parity space-based approaches 109

Figure 5-13: Multiple faults in K_t in the roll and pitch axes that are detected..... 111

Figure 5-14: Multiple faults in K_t in the roll and yaw axes that are detected by (a) linear observer-based, and (b) parity space-based approaches 113

Figure 5-15: Multiple faults in V_{BUS} in the roll and pitch axes that are detected by (a) linear observer-based, and (b) parity space-based approaches 115

Figure 5-16: Multiple faults in V_{BUS} in the roll and yaw axes that are detected by (a) linear observer-based, and (b) parity space-based approaches 117

List of Tables

Table 1-1: Fault detection and isolation methods 5

Table 3-1: The reaction wheel parameters values [5] 40

Table 3-2: ACS control design specifications 50

Table 5-1: Sensitivity of the two fault detection (FD) approaches to occurrence of faults in the component K_t 89

Table 5-2: Detection times for the linear observer-based and parity space-based approaches to fault detection 93

Table 5-3: Detection time for the linear observer-based and parity space-based schemes to intermittent faults 96

Table 5-4: Sensitivity of the linear observer-based and parity space-based approaches to fault detection to the occurrence of faults in the V_{BUS} component 99

Table 5-5: Detection time of the linear observer-based and parity space-based approaches to a permanent fault 101

Table 5-6: Detection time of the linear observer and parity space approaches to intermittent faults 102

Table 5-7: Multiple fault scenarios and case studies 104

Table 5-8: Detectability and the detection time for the linear observer scheme to multiple faults in the roll, pitch and the yaw axes according to Table 5-7 118

Table 5-9: Detectability and the detection time for the parity space scheme to multiple faults in the roll, pitch and the yaw axes according to Table 5-7. 118

Chapter 1 : Introduction

1.1. Statement of the Problem

Spacecraft or satellite is a vehicle designed to leave the atmosphere and to operate in outer space. It contains different subsystems [1, 2], which can be varied depending on the mission [3] for which this spacecraft has been designed and developed. Among these subsystems, one can mention the Attitude Control System (ACS), the Communication System (COMS), the Thermal Control System (TCS), the power system, the propulsion system, the payload subsystems and other electronic and control devices.

All of the above subsystems can be subject to occurrences of faults or failures. In this thesis, the problem of fault detection and isolation (FDI) in the attitude control system (ACS) of a spacecraft is investigated.

Attitude control system (ACS) is employed for an accurate orientation of a satellite and its payloads in three dimensions according to a reference frame [4]. It is composed of sensors (e.g. inertial guidance system, star tracker, etc) and actuators (e.g. thrusters, reaction wheels, etc) together with a control algorithm. In general, the ACS should perform the following functionalities:

- Controlling the rotation of the solar arrays,
- Controlling the rotation of cameras,
- Providing actuator's command for repositioning and station keeping,

- Controlling the orientation of the antenna,
- Providing sun and earth sensor telemetry data for ground based satellite attitude determination, and
- Providing the capability to recover the satellite from failure conditions.

The performance of the ACS is entirely conjoined to the performance of its actuators. Actuators can be defined as devices that convert electrical control signals to a rotational or linear motion. In this thesis, the actuator considered is a high fidelity reaction wheel [5] which converts a reference command voltage to torque. This torque is then applied to the spacecraft to reach the required orientation. Reaction wheel is a device that is very susceptible to fault. The reaction wheel plays an important role in the performance of the spacecraft, hence any fault or failure in this device may have a serious impact in the spacecraft mission. For example, the *Far Ultraviolet Spectroscopic Explorer (FUSE)* [6] satellite was at the peak of its scientific productivity when on November 25 and December 10, 2001, it lost the use of two of its four reaction wheels required for pointing control. The pitch and yaw wheels failed due to the excessive friction between the rotors and the wheel housings. As another example, one can mention the *Hayabusa* satellite, as its two reaction wheels failed in 2005 where the X-axis wheel failed on July 31 and the Y-axis on October 2 [7].

These examples among others have initiated an intensive desire to develop solutions to the fault detection and isolation (FDI) problem in the spacecraft's reaction wheel and this has also been the main motivation for conducting this research in this thesis.

1.2. Justification

A safe and reliable operation of a spacecraft is of great importance for the protection of human life, the environment with enormous ramifications and the cost diminution during a spacecraft mission. To have a safe spacecraft mission, fault detection and isolation has recently gained a significant attention in the literature [8-23]. The early detection of faults is crucial in avoiding performance degradation and damage to the machinery or human life. Accurate diagnosis also helps to make the right decisions on emergency actions and repairs which lead to lower expenses.

Traditionally, the ground system has been responsible for spacecraft Health and Safety (H&S). For a ground based fault detection and diagnosis, many sensors should have been used to provide sufficient information for numerous devices. Furthermore, the ground personnel should have adequate knowledge and expertise of sensor outputs to be able to detect faults and to recognize their sources.

The needs for an autonomous and onboard fault detection, isolation and recovery (FDIR) arose due to the following observations:

1- Increasing the number of sensors in use, for the purpose of providing more information, together with limited knowledge of space and uncertainties, increase the risk of wrong evaluation. False signals might arise either due to sensor failures, or unknown space disturbances and noise.
2- A real time response is a critical issue to avoid catastrophes in safety critical systems. This may, in general, not be satisfied by the ground based systems.

Although, the above mentioned problems are not the only reasons [24], they are among the main points in developing and designing an onboard autonomous FDIR system. The envisaged design for the FDIR should discriminate between faults and disturbances to make the appropriate decision for the isolation and recovery of the faults and/or failures.

Towards this end, the role of advanced computers can not be neglected, since these devices enable the space vehicle to accomplish many tasks onboard. In addition, they have reduced the utilization and the number of physical sensors and consequently the amount of false alarms. Fault Detection and Diagnosis (FDD) has become a major area of research introducing major advantages for this new technology. Several techniques have been introduced, which are suitable for a special class of fault or system [24, 25]. These methods are briefly reviewed and categorized in the next section.

1.3. Methodology

Numerous methods for fault detection and diagnosis have been developed and investigated since 1970 [26, 27]. These methods are summarized in Table 1-1. According to Table 1-1, there are two general methods introduced for fault detection and isolation: model free FDI, and model based FDI.

Traditional approaches to FDI are model free. These methods are either knowledge based or signal based. The knowledge based technique includes the fault tree approach, the pattern recognition approach and the expert system approach to FDI.

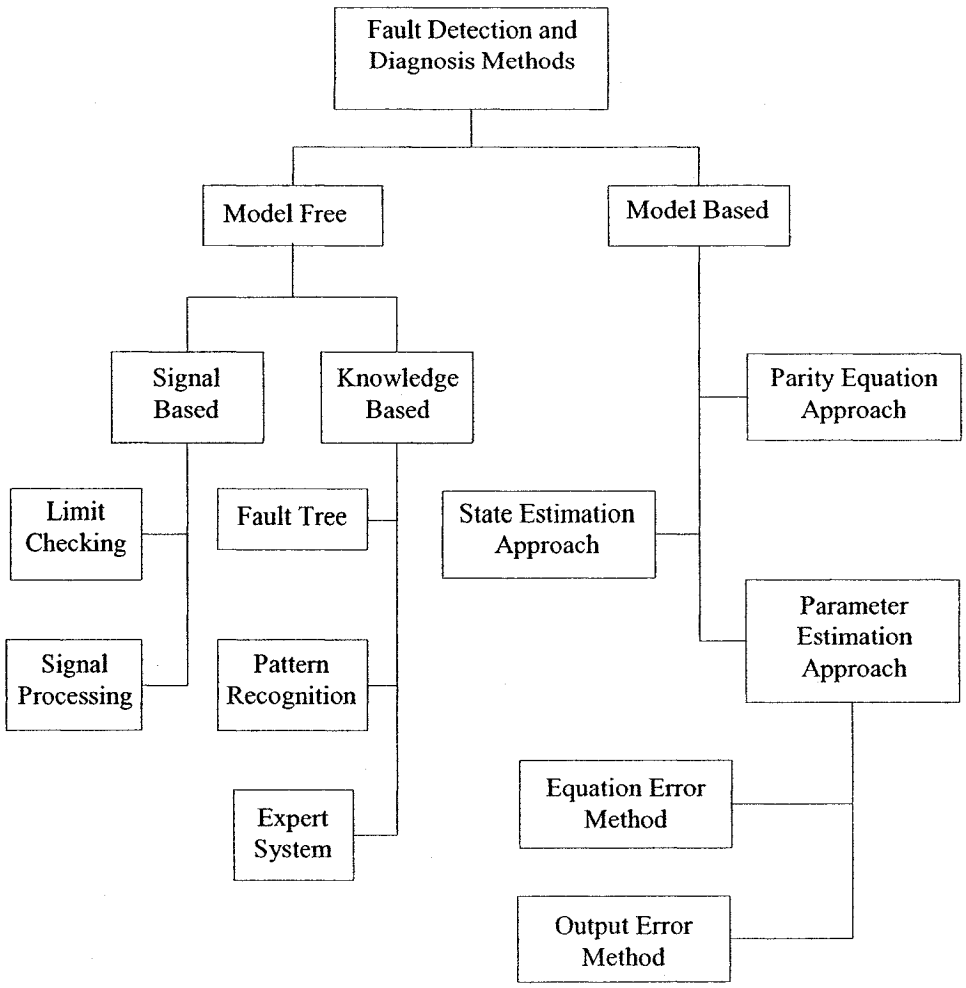

Table 1-1: Fault detection and isolation methods

The Fault Tree Analysis (FTA) is a formal deductive procedure for determining the combinations of component failures and human errors leading to the occurrence of specified undesired events at system levels. This method can be used to analyze the vast majority of the reliability problems related to the industrial systems. In this method the identified failures can be arranged in a tree structure in such a way that their relations can be characterized and evaluated [44]. Pattern recognition method however is developed due to the fact that a unique pattern can be specified for any system. Using signal

processing, it is possible to design a system to recognize the difference between the pattern related to the healthy system and that of the faulty system [37]. An expert system approach, normally used in managing computer systems, performs based on statistical algorithm for abnormal performance detection [54].

In signal based techniques, sufficient information for fault detection is provided using some sort of redundancy [28]. A redundancy is a parameter used to make consistency checks between related variables. In safety critical systems, redundancy is supplied by extra hardware, known as hardware redundancy. A critical component, e.g. a sensor, is then duplicated or triplicated and voting schemes are then used to monitor signal levels and trends to detect and locate faulty sensors. Then the decision can be made by

- *Limit value checking* of directly measurable signals, or
- *Signal analysis* of direct measurable signals using a model signal.

Hardware redundancy may be replaced by analytical redundancy where the redundancy is supplied by a process model instead of an extra hardware. Using this method, there would be no need for extra hardware and duplication of certain components, which have an important role in cost efficiency. Furthermore, model-based methods are of more interest in the literature as it gives a better intuition of the internal characteristics of the system [24, 25].

The model based fault detection and diagnosis methods aim at using all the available system information, such as input and output signals, to generate a signal referred to as the residual. This signal measures the difference between the output of the faulty system

and that of the healthy system (that is without a fault). Residual is supposed to be zero when there is no fault and nonzero when there exists a fault and/or a failure. The residual signal should then be analyzed to decide whether a fault or a failure has been occurred in the system and to isolate this fault and/or failure. At the higher levels of design, the residual should provide sufficient information in the case of multiple faults or failures. In Table 1-1, three different techniques for model based fault detection and diagnosis are specified. These methods are briefly introduced in next chapter. In the context of this thesis, the word diagnosis is referred to the detection and location of a faulty component.

To obtain a residual, the fault scenarios associated with the system should be described. Hence, we need to implement and apply one or more faults to the components of the actuator (reaction wheel) in the attitude control system of a satellite. Having the faulty system, one may then uses different methods to generate the residual signals.

Among the three model-based approaches introduced in Table 1-1, in this thesis the parity space approach to fault detection and diagnosis is developed and applied to the spacecraft's attitude control system. The simulated results for the residual under different faulty scenarios are studied using the state estimation approach as a benchmark and reference technique. Due to the following reasons the parity space approach is selected considering the state estimation approach as a benchmark and a reference point:

1. As it will be explained in the next chapter, in this method the state space block diagram is used and so is in the state estimation method; therefore a single block diagram of the attitude control system as well as the same mathematics can be used for both methods.

2. The state estimation approach is developed based on the assumption that the faults contaminate the states of the system, and consequently the outputs of the system. However, in parity equation approach, the parity parameters are designed to be independent of the states of the system. In this approach it is assumed that the fault or failure behaves like a system input. This difference provides more information on the concept of fault in the attitude control system of a spacecraft.

Early detection of a fault or a failure together with accurate information of the size, type, and location of the fault are the main goals of research in these areas.

1.4. Contribution of Thesis

In this thesis, a model based technique known as parity equations has been developed and applied to a high fidelity model of a reaction wheel in the spacecraft's attitude control system. Residual signals are generated to detect two types of faults in two components of the non-linear model of the reaction wheel. To gain a better understanding of the sensitivity and the advantages of this technique and to further justify its use for a satellite, comparison studies between the results of the proposed technique and those of the standard and conventional linear observer technique are investigated extensively.

1.5. Outline of Thesis

A brief introduction to different types of faults and failures as well as different approaches for model based fault detection and diagnosis are addressed in Chapter 2. The architecture of a spacecraft attitude control system accompanied by the dynamics of the

satellite are provided in Chapter 3. In Chapter 4, a fault detection system using parity space approach is designed and developed, and the convergence properties of this method is verified and validated. Furthermore, its safe limits are specified in this chapter. Simulation results related to the linear observer and parity space approaches are implemented and compared in Chapters 5. Finally, concluding remarks and future work are covered in Chapter 6.

Chapter 2 : Fault Detection, Isolation, and Recovery (FDIR)

In this chapter, we will provide a review of the basic concepts of faults. Then, a general faulty model of a control system is introduced and modified to be used in implementing the spacecraft attitude control system. Finally, this chapter concludes by studying various model based fault detection approaches.

2.1. Concept of a Fault

Fault can be specified as an abnormal condition, defect, or an unexpected change at a component, equipment, or sub-system. It may lead to a failure or an unacceptable system performance. Here, there is a preference for using the word fault rather than failure, to denote a malfunction rather than a catastrophe.

Malfunction is defined as an unacceptable functionality in the performance of a system that can lead to a catastrophe or a hazardous situation if not recovered. Malfunction is different from catastrophe as this type of functionality can be encircled and recovered, like a failed component which can be isolated, quarantined and its performance can be substituted by those of some other components.

Various faults can be classified considering the components they contaminate i.e. a sensor, an actuator, etc, or the way the fault affect the output of the system. Faults may

infect the output of the system by adding or multiplying it with another parameter [24, 29 and 30]. Depending on the class to which a fault belongs and the type of the infected system, different methods for fault recovery can be applied to a faulty system to avoid catastrophe [31, 32 and 33].

2.2. Modeling a Faulty System

A faulty system is defined as a system that is contaminated by any type of a fault, such that the desired output cannot be provided. A system is composed of different components. Faults may infect any of these components, leading to a faulty system. To further explain this concept, a general architecture of a control system is illustrated in the block diagram of Figure 2-1. It is assumed that the output of the actuator is not observable. This is the assumption made in the concept of this thesis for the real dynamics of the system. The main components of a control system (sensors, actuators, plant and controllers) are illustrated in the block diagram of Figure 2-1.

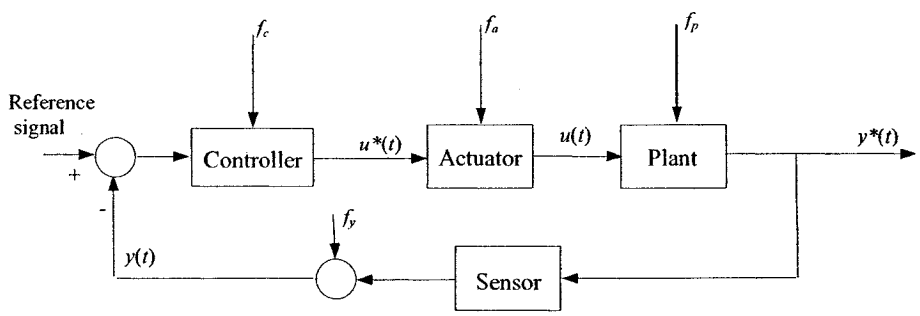

Figure 2-1: The controlled system and fault topology [24]

Faults and failures that may infect each block are shown by arrows. In this figure, f_c, is the controller fault, f_a, refers to the fault and the failure that may infect the actuator block, and f_p represents the plant fault. Output sensor's faults are implemented by f_y, as well. The

signal $u^*(t)$ is the controlled input that is applied to the plant through the actuator block, and $u(t)$ is considered as the actuator output and will be different from $u^*(t)$, if the actuator is faulty. The variable $y^*(t)$ shows the real output of the plant block, while y is the observed output signal through the output sensors.

Assuming the controller faults are equal to zero, from Figure 2-1 we can obtain the state space representation of the faulty spacecraft system as follows [24]:

$$\begin{cases} \dot{x}(t) = Ax(t) + Bu(t) + f_p \\ y^*(t) = Cx(t) \end{cases} \tag{2.1}$$

and,

$$y(t) = y^*(t) + f_y(t) \tag{2.2}$$

where $x(t)$ is the state vector of dimension n, A is an $n \times n$ state matrix, B is a constant (column) n-dimensional vector and C is a constant (row) n-dimensional vector.

Given that in this thesis we are concerned with the occurrence of a fault in the actuator block, we can assume the sensor and plant block's faults to be zero. Consequently we will have:

$$\begin{cases} \dot{x}(t) = Ax(t) + Bu(t) \\ y(t) = Cx(t) \end{cases} \tag{2.3}$$

$u(t)$ in the above equation may be approximated by following equation:

$$u(t) = u^*(t) + f_a(t) \tag{2.4}$$

By combining equations (2.3)and(2.4) we will have:

$$\begin{cases} \dot{x}(t) = Ax(t) + Bu^*(t) + Bf_a(t) \\ y(t) = Cx(t) \end{cases} \tag{2.5}$$

As B is a constant n-dimensional vector, the expression Bf_a represents the effects of actuator fault in the system and may be shown by f_A. Consequently, equation (2.7) can be reduced into following equation:

$$\begin{cases} \dot{x}(t) = Ax(t) + Bu^*(t) + f_A(t) \\ y(t) = Cx(t) \end{cases} \tag{2.6}$$

Equation (2.6), will be used in this thesis to explain a faulty spacecraft attitude control system, both in the explanation of the FDI approaches, and to implement the faulty scenarios for the verification of the methods.

2.3. Fault Detection System Characteristics

An inaccurate detection and diagnosis of a fault will have potentially significant consequences, as discussed in Chapter 1 to the satellite mission. To avoid these consequences, an appropriate FDI system, that is employed in a spacecraft or for that matter in any other complex dynamical system, should satisfy the following requirements [38, 30]:

- ***Low detection time delay***- which is the difference time between when a fault has occurred and when it has been correctly detected;
- ***High rate of correct detection (sensitivity)***- which means that the system should be sensitive to a fault;
- ***Low rate of false alarms***- being sensitive to fault may have consequences as being sensitive to noise and increasing the rate of false alarms.

- ***Detectibility***- refers to the ability of the FDI system to detect the fault from the designed residual;
- ***Isolability***- which is the ability of the diagnostic system to distinguish between different failures that occur in different parts of the system;
- ***Novelty identifiability***- which is the ability to find the source of abnormal behavior of a system. It specifies whether the cause is a *known* malfunction or an *unknown*, novel malfunction;
- ***Adaptability***- there are changes in the behavior of the system because of the changes in the mission requirements or unanticipated disturbances and noise. It is important for the FDI system to adapt itself with these changes in external inputs or structural changes due to retrofitting and so on;
- ***Multiple fault identifiablity***- which is the ability to identify multiple faults in different components; and
- ***Low cost***- this is an important goal in designing any device and execution of any process.

Investigation of these requirements in any proposed FDI system leads to a better justification of the designed method.

2.4. Model Based Approaches to Fault Detection and Isolation

A model based FDI system normally performs the following tasks:

- ***Fault detection***: the possibility of the occurrence of a fault should be determined in this task;
- ***Fault isolation***: the faulty component will be located in this task; and

- ***Fault identification***: this task is concerned with estimating the size and the type or the nature of the fault.

The general idea in a model based FDI system is to generate a residual signal to detect a fault. The signal is then evaluated to specify the characteristics of the fault. The performance of the method can be evaluated based on its ability to generate and elaborate a residual signal. The structure of a model based FDI system is illustrated in Figure 2-2 [46]. The two basic blocks are described below:

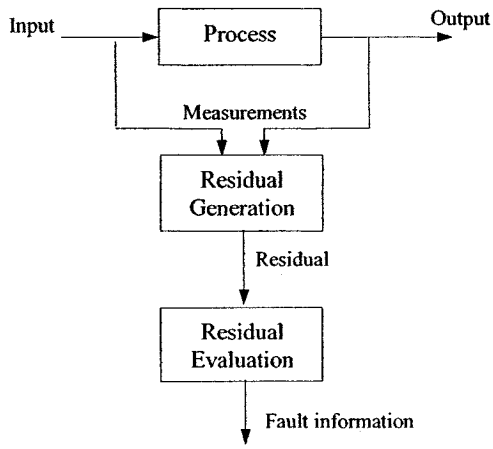

Figure 2-2: Structure of the model based FDI system [24]

- **Residual generation**: The residual is going to be generated in this block using available information such as input and output signals. The generated residual should provide sufficient information for fault detection, isolation and identification. Normally, the residual is zero or very close to zero (considering model uncertainties), for the system with no fault. Unlike a healthy system, for a faulty system the residual should distinguishably diverges from zero. The difference between the very close to zero and the non zero signal can be specified

by applying specific fixed or variable thresholds that are known as "safe limit" or "healthy limit".

- **Residual evaluation**: After the residual is generated, this signal is examined to decide whether the fault has occurred or not. It should be evaluated to decide about the location, size and nature of the fault [24]. To further improve this technique, a number of residual signals can be generated. Any of these residuals are designed to be sensitive to a special type of fault. This simplifies the process of the residual evaluation.

2.4.1. Residual Generation Techniques

Generating an accurate residual signal is important in the process of evaluating the fault signal. Different methods of residual generation are considered in this section. These methods, which can be referred to as model based fault detection methods are classified as: (a) parameter estimation approach, (b) state estimation approach, and (c) parity equation (parity space) approach [24]. Following sections explain each of these methods in detail.

2.4.1.1. Fault Detection with Parameter Estimation

Parameter estimation can be used when the process parameters are not partially known, or are not known at all [36, 37]. This approach is based on the assumption that the faults are reflected in the *physical system parameters*. Basic idea of this method is to estimate the parameters of an actual fault free process on-line, using well-known parameter estimation methods. This way, we obtain an estimation of a fault free process outputs as

well, which will be referred to as the reference outputs. Any changes in the process parameters will then reflect in the system outputs and result in discrepancy between the system outputs and reference outputs. These discrepancies will be transformed into residual signals. There are two approaches for parameter estimation method: 1- the equation error method, and 2- the output error method.

1. Equation Error Method

A block diagram corresponding to the equation error method is illustrated in Figure 2-3. In this block diagram, $u(t)$ is the input signal which is provided by the actuator block in Figure 2-1. $\frac{B(s)}{A(s)}$, implements the Laplace transformation of the actuator and plant block in which $A(s)$ and $B(s)$ are polynomials of s. The coefficients of the polynomials $A(s)$ and $B(s)$ are known as the parameters of the system. $\hat{A}(s), \hat{B}(s)$ are the estimates of $A(s)$ and $B(s)$, which are obtained through the parameter estimation block. $e(t)$, known as the equation error, specifies the differences between the system function, $\frac{B(s)}{A(s)}$, and its estimate, $\frac{\hat{B}(s)}{\hat{A}(s)}$.

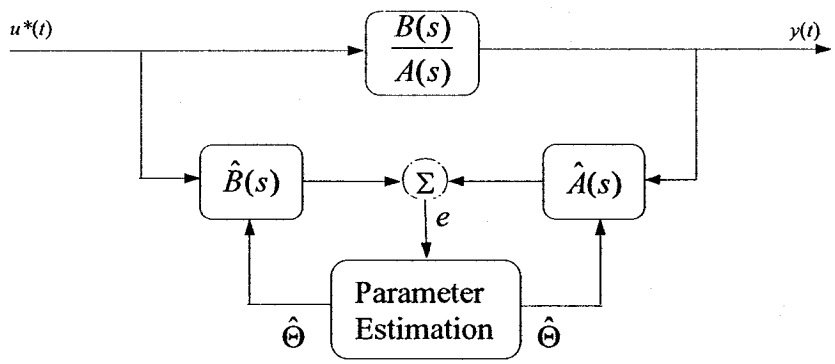

Figure 2-3: Parameter estimation method using equation error [24]

To describe this method, a general dynamic system can be specified by the following differential equation in the time domain [24, 37]:

$$a_n \frac{d^n y}{dt^n} + a_{n-1} \frac{d^{n-1} y}{dt^{n-1}} + \cdots + a_0 y = b_m \frac{d^m u}{dt^m} + b_{m-1} \frac{d^{m-1} u}{dt^{m-1}} + \cdots + b_0 \tag{2.7}$$

This equation can be presented in the following form:

$$y(t) = \Psi^T \Theta \tag{2.8}$$

where

$$\Theta^T = [a_1 ... a_n, b_1 ... b_n] \tag{2.9}$$

referred to as the parameter vector and

$$\Psi^T = \left[y^{(1)} ... y^{(n)} u^{(1)} ... u^{(n)} \right] \tag{2.10}$$

is the data vector. According to Figure 2-3, the equation error is given by

$$e(t) = y(t) - \Psi^T \Theta \tag{2.11}$$

or if

$$\frac{y(t)}{u(t)} = \frac{B(s)}{A(s)} \tag{2.12}$$

is the transfer function of the process, the equation error via the Laplace transformation becomes:

$$e(t) = \hat{B}(s)u(t) - \hat{A}(s)y(t). \tag{2.13}$$

The equation error, $e(t)$, is designed such that it tends to be zero in steady state for a healthy system. Due to the occurrence of a fault or failure, according to the assumption made earlier, the system parameters (the coefficients of $A(s)$ and $B(s)$) are infected. Consequently, $\hat{A}(s)$ and $\hat{B}(s)$ are not the correct estimate of $A(s)$ and $B(s)$ and $e(t)$ will not remain zero. This property of $e(t)$ has enabled it to be considered as a residual signal.

2. **Output Error Method**

The output error method is depicted in Figure 2-4. In Figure 2-4, $\frac{B(s)}{A(s)}$ indicates the Laplace transfer function of the system. $u(t)$ is the system input which is provided by the controller and $y(t)$ is the output of the system . The estimate of the system transfer function, i.e. $\frac{\hat{B}(s)}{\hat{A}(s)}$, is used to calculate the estimated output of the system, $\hat{y}(t)$, in which $\hat{A}(s)$ and $\hat{B}(s)$ are the estimates of $A(s)$ and $B(s)$ obtained through the parameter estimate Θ. The output error is then defined as

$$e(t) = y(t) - \hat{y}(\Theta, t) \tag{2.14}$$

where

$$\hat{y}(\Theta, s) = \frac{\hat{B}(s)}{\hat{A}(s)} u(s) \tag{2.15}$$

is the estimated model output.

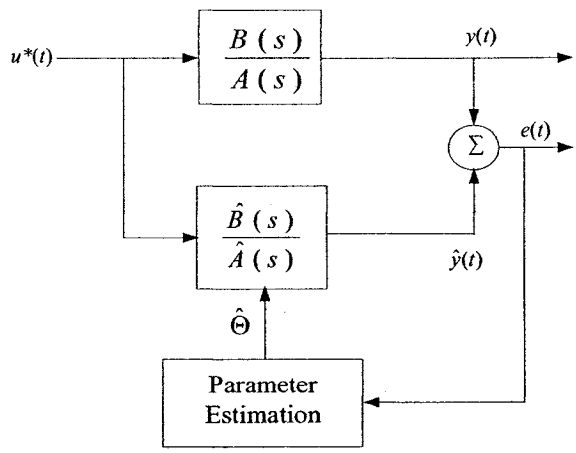

Figure 2-4: Parameter estimation method using output error

When a fault occurs in the system, it changes the process parameters by $\Delta\Theta(t)$. Consequently, the output signal changes for small deviations according to

$$\Delta y(t) = \Psi^T(t)\Delta\Theta(t) + \Delta\Psi^T(t)\Theta(t) + \Delta\Psi^T\Delta\Theta(t) \tag{2.16}$$

and the parallel estimator indicates a change of $\Delta\Theta$.

Generally, the process parameters Θ depends on the physical process coefficients p (e.g. stiffness, damping factor, resistance, etc)

$$\Theta = f(p) \tag{2.17}$$

via the above non-linear algebraic equation. If one inverts the relationship

$$p = f^{-1}(\Theta) \tag{2.18}$$

(assuming that it exists), then the changes Δp of the process coefficients can be calculated. These changes in the coefficients are in many cases directly related to the faults.

2.4.1.2. Fault Detection with State Estimation

This approach is based on the assumption that faults are reflected in the *physical system states,* rather than parameters. Basic idea of this method is to estimate the states of the actual fault free process, on-line, using the state estimation methods, as illustrated in Figure 2-5 [47]. Any changes in the state of the system leads to a discrepancy between the system states and their estimates generating a residual signal.

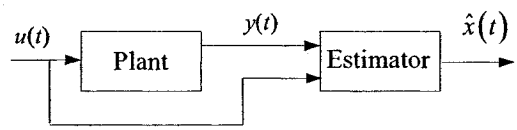

Figure 2-5: General structure of the state estimator

In Figure 2-5, the state-space representation of the plant block is specified by the following equation:

$$\begin{aligned} \dot{x}(t) &= Ax(t) + Bu(t); \qquad x \in R^n,\ u \in R,\ y \in R \\ y(t) &= Cx(t) \end{aligned} \tag{2.19}$$

In equation (2.19), $x(t)$ is an n-dimensional state vector, A is a constant nxn matrix, B and C are known constant column and row n-dimensional vectors, respectively.

The estimator equation of Figure 2-5 can be expressed as:

$$\dot{\hat{x}}(t) = F\hat{x}(t) + Hu(t) + Gy(t); \qquad u \in R,\ y \in R \tag{2.20}$$

We need to choose the matrices F, G and H such that $\hat{x}(t)$ is an accurate estimate of $x(t)$. To do this, the transfer function from $u(t)$ to $x(t)$ must be equal to the transfer function from $u(t)$ to $\hat{x}(t)$:

$$\frac{\hat{X}(s)}{U(s)} = \frac{X(s)}{U(s)}. \tag{2.21}$$

Obtaining the Laplace transfer function of the equation (2.19), we have:

$$\begin{cases} sX(s) - x(0) = AX(s) + BU(s) \\ Y(s) = CX(s) \end{cases} \tag{2.22}$$

in which the initial value $x(0)$ is unknown, and A, B and C are known matrices as expressed earlier. $\frac{X(s)}{U(s)}$ can be obtained from the following equation, neglecting the initial conditions:

$$X(s) = (sI - A)^{-1} BU(s). \tag{2.23}$$

To obtain the Laplace transfer function of the estimator, we assume that the initial conditions are zero, as well. The transfer function of the estimator is expressed by:

$$\begin{aligned} & s\hat{X}(s) = F\hat{X}(s) + HU(s) + Gy(s) \\ & y(s) = CX(s) \\ & \therefore s\hat{X}(s) = F\hat{X}(s) + HU(s) + GCX(s) \\ & \therefore \hat{X}(s) = (sI - F)^{-1}\left[HU(s) + GCX(s)\right] \\ & \qquad = (sI - F)^{-1}\left[H + GC(sI - A)^{-1}B\right]U(s) \end{aligned} \tag{2.24}$$

Since equation (2.21) should be satisfied:

$$(sI - A)^{-1} B = (sI - F)^{-1}\left[H + GC(sI - A)^{-1}B\right]. \tag{2.25}$$

Collecting $(sI - A)^{-1} B$ terms:

$$\left[I - (sI - F)^{-1} GC\right](sI - A)^{-1} B = (sI - F)^{-1} H. \tag{2.26}$$

Since $(sI - F)^{-1}(sI - F) = I$, we have:

$$(sI-F)^{-1}[sI-F-GC](sI-A)^{-1}B=(sI-F)^{-1}H$$
$$\therefore [sI-F-GC](sI-A)^{-1}B=H \tag{2.27}$$

Therefore,

$$(sI-A)^{-1}B=(sI-F-GC)^{-1}H \tag{2.28}$$

The equation (2.28) is satisfied if we chose:

$$\begin{cases} F=A-GC \\ H=B \end{cases} \tag{2.29}$$

In the above equation, the gain matrix G is chosen such that an acceptable transient response for the state estimator is achieved. The detailed state space block diagram of the state estimator is illustrated in Figure 2-6:

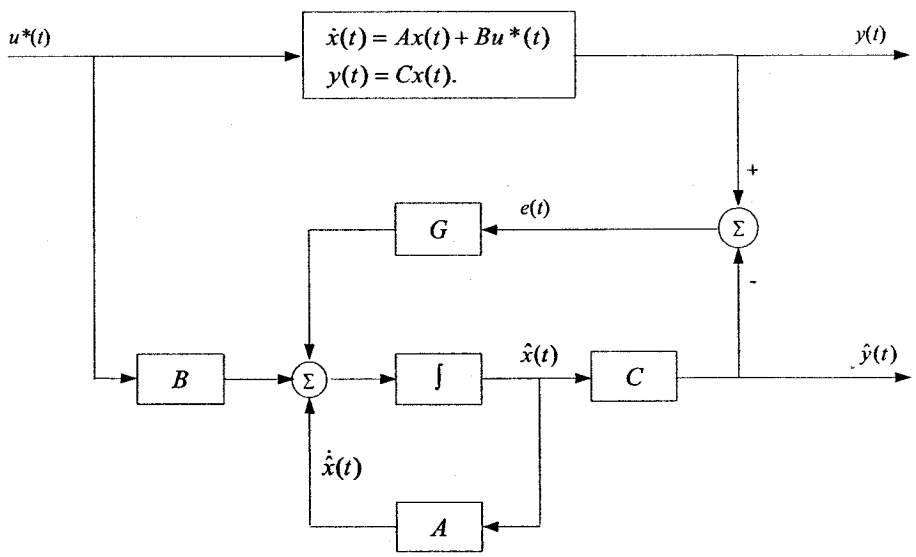

Figure 2-6: The process and the state observer method [24].

This way we can obtain an estimation of the fault free process outputs, which will be considered as the reference outputs. Any changes in the process states will then be reflected in the system outputs and result in a discrepancy between the system output and the reference outputs. These discrepancies or mismatches will be transformed into the residual signals. The advantage of using the observer is the flexibility in the selection of its gains, *G*, leading to a rich variety of FDI schemes [48, 49]. In order to implement this approach for the system designed in Figure 2-1, a state space dynamic model for the process (Plant in Figure 2-1) is considered as:

$$\begin{cases} \dot{x}(t) = Ax(t) + Bu^*(t) + f_A(t) \\ y(t) = Cx(t) + Du^*(t) \end{cases} \tag{2.30}$$

Assuming that all the matrices A, B, and C are perfectly known, an observer is used to reconstruct the system states based on the measured input $u(t)$ and the output $y(t)$ where $u(t)$ is obtained from the controller.

In Figure 2-6, let us define $e_x(t)$ as the state estimate error, that is the difference between the states and their estimated values, namely:

$$\begin{cases} e_x(t) = x(t) - \hat{x}(t) \\ \dot{e}_x(t) = (A - HC)e_x(t) \end{cases} \tag{2.31}$$

The state estimate error $e_x(t)$ and the measurement estimate error $e(t) = y(t) - \hat{y}(t)$ vanish asymptotically if the observer is asymptotically stable, which can be achieved by the proper design of the observer feedback gain, G [47].

Both signals, $e(t)$ and $e_x(t)$, represent dynamic behaviors, and can therefore be taken as the residuals. For the generation of the residual with special properties, (i.e. transient and steady state response properties), the design of the observer feedback matrix, G, is of interest. The necessary strict conditions are the stability and sensitivity against disturbances. In this thesis, the signal $e(t)$ is considered as the residual signal. If faults appear as any changes in the systems states, $e_x(t)$ and consequently $e(t)$ differ from zero.

2.4.1.3. Fault Detection with Parity Equation

A straight forward model based fault detection is to take a fixed model and run it in parallel to the process, thereby forming an output error, namely,

$$R(s) = \left(\frac{A(s)}{B(s)} - \frac{\hat{A}(s)}{\hat{B}(s)} \right) U(s) \tag{2.32}$$

As mentioned in Section 2.3 for a linear time invariant (LTI) system, the existence of fault can be specified according to the following formula in the state space:

$$\begin{cases} \dot{x}(t) = Ax(t) + Bu^*(t) + f_A(t) \\ y(t) = Cx(t) + Du^*(t) \end{cases} \tag{2.33}$$

where $x(t)$ is the system state vector, $u(t)$ is the input signal and $y(t)$ is the output of the system. The matrices A, B, C and D are the system matrices with appropriate dimensions, and f_A is the component fault vector affecting the system.

By obtaining the first derivative of the output of the system, we have:

$\dot{y}(t) = C\dot{x}(t) + D\dot{u}^*(t)$

By replacing $\dot{x}(t)$ obtained from equation (2.33) in the above formula, we will have:

$$\dot{y}(t) = CAx(t) + CBu^*(t) + Cf_A + D\dot{u}^*(t)$$

In the same way, by obtaining the second derivative of the output, we will have:

$$\ddot{y}(t) = CA^2x(t) + CABu^*(t) + CAf_A(t) + CB\dot{u}^*(t) + C\dot{f}_A(t) + D\ddot{u}^*(t)$$

Consequently, we can introduce the following matrix notation for the relation between the input signal and its derivatives, and the output signal and its derivatives, namely,

$$\begin{bmatrix} y \\ \dot{y} \\ \ddot{y} \\ \vdots \\ y^{(n)} \end{bmatrix} = \begin{bmatrix} C \\ CA \\ CA^2 \\ \vdots \\ CA^n \end{bmatrix} x(t) + \begin{bmatrix} D & 0 & \cdots & 0 & 0 \\ CB & D & \cdots & 0 & 0 \\ CAB & CB & \cdots & 0 & 0 \\ \vdots & \vdots & \vdots & \vdots & \vdots \\ CA^{n-1}B & CA^{n-2}B & \cdots & CB & D \end{bmatrix} \begin{bmatrix} u^* \\ \dot{u}^* \\ \ddot{u}^* \\ \vdots \\ u^{(n)*} \end{bmatrix} + \begin{bmatrix} 0 & 0 & \cdots & 0 & 0 \\ C & 0 & \cdots & 0 & 0 \\ CA & C & \cdots & 0 & 0 \\ \vdots & \vdots & \vdots & \vdots & \vdots \\ CA^{n-1} & CA^{n-2} & \cdots & C & 0 \end{bmatrix} \begin{bmatrix} f_A \\ \dot{f}_A \\ \ddot{f}_A \\ \vdots \\ f^{(n)}{}_A \end{bmatrix} \tag{2.34}$$

in which n=1,2,…,k or in a compact form

$$Y(t) = Tx(t) + QU(t) + VF(t) \tag{2.35}$$

where

$$Y = \begin{bmatrix} y & \dot{y} & \cdots & y^{(n)} \end{bmatrix}^T,\ T = \begin{bmatrix} C^T & (CA)^T & \cdots & (CA^n)^T \end{bmatrix}^T,\ U = \begin{bmatrix} u^* & \dot{u}^* & \cdots & u^{(n)*} \end{bmatrix}^T,$$

$$Q = \begin{bmatrix} D & 0 & \cdots & 0 \\ CB & D & \cdots & 0 \\ \vdots & \vdots & \cdots & \vdots \\ CA^{n-1}B & CA^{n-2}B & \cdots & D \end{bmatrix},\ V = \begin{bmatrix} 0 & 0 & \cdots & 0 \\ C & 0 & \cdots & 0 \\ \vdots & \vdots & \cdots & \vdots \\ CA^{n-1} & CA^{n-2} & \cdots & 0 \end{bmatrix} \text{ and}$$

$$F = \begin{bmatrix} f_A & \dot{f}_A & \cdots & f^{(n)}{}_A \end{bmatrix}^T$$

Now we define a parity vector Ω (an n+1 row dimensional vector) as follows:

$$\begin{cases} \Omega = [\omega_1 \quad \omega_2 \quad \omega_3 \quad \dots \quad \omega_{n+1}] \\ \Omega \neq 0 \end{cases} \tag{2.36}$$

multiplying both sides of equation (2.35) by the parity vector, Ω, yields:

$$\Omega Y(t) = \Omega\big(Tx(t) + QU(t) + VF(t)\big) \tag{2.37}$$

which can be rearranged as:

$$\Omega\big(Y(t) - QU(t)\big) = \Omega\big(Tx(t) + VF(t)\big) \tag{2.38}$$

If we want to consider equation (2.38) as the residual signal, it should not be influenced by the state variables. Therefore, $\Omega T = 0$. This adds another element which should be considered in choosing the parity vector (Ω) parameters. Under the above conditions, equation (2.38) becomes:

$$r = \Omega\ \big(Y(t) - QU(t)\big) = \Omega\ VF(t) \tag{2.39}$$

where r is the residual signal and Ω is the parity vector. According to the above equation, the residual signal r will be zero if the fault vector $F(t)$ becomes zero, and it is nonzero if there exists a fault. The vector r will satisfy all the residual conditions and can be considered as a residual signal [43, 50, 51].

To obtain the number of the derivatives required for this approach, k, the well known Caley-Hamilton theorem is used [45]. According to this theorem, assuming the system is observable through its outputs, there is an $\overline{n}$, $1 \leq \overline{n} \leq n$, such that

$$\text{Rank } T(n) = \begin{cases} n+1 & n \prec \overline{n} \\ \overline{n} & n \geq \overline{n} \end{cases} \tag{2.40}$$

The system states can be observed by the matrix $T(\bar{n}\text{-}1)$. On the other hand, any component of the states lying in this matrix affects the outputs of the system.

2.5. Conclusion

Different approaches to model based fault detection and diagnosis were presented in this chapter. The fault detection problem has been formalized using a system framework and the mathematical description of the system. Within this framework, the residual generation has been identified as the main issue in the model based FDI and the residual generator has been summarized in three different residual generation structures. It is obvious that the success of a fault diagnosis system depends on the quality of the residuals.

Chapter 3 : Spacecraft Attitude Control System

The motion of a spacecraft is described by three parameters: position, velocity, and attitude. Position and velocity are the subjects of orbital mechanics and are similarly referenced to some coordinate frames. They give the location, speed and direction of motion of the spacecraft. Attitude, however, is the subject of attitude dynamics, i.e. the motion and orientation of the spacecraft about a reference system. It describes how spacecraft body axes are oriented relative to an inertial or rotating coordinate system.

In this chapter, the dynamic model of a spacecraft that is used in this thesis is described to some details. This follows by the design of the attitude control system (ACS) for the spacecraft. Attitude control system design contains two tasks, one deals with the design and development of the actuator, and the other deals with the design and development of a controller to obtain a desired actuation signal.

3.1. Reference Frame

As stated above, a reference frame is required to describe the attitude control system of a satellite. Any reference frame will lead to a correct description, if applies consistently, and the difference is in the number of necessary calculations and algebraic transformations. Therefore, selecting an appropriate reference frame would help us reduce the computation time and resources [38, 36].

3.1.1. Spacecraft Fixed Body Reference

Fixed body reference, as it is obvious from its name, is a body-fixed frame of reference. Its origin is located at the spacecraft center of mass and its orientation is based on the spacecraft geometry. The x-axis and the y-axis are considered along two of the solar panels on the bottom side of the satellite and the z-axis is considered along the height. This reference frame is depicted in Figure 3-1.

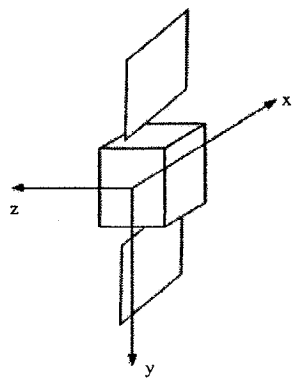

Figure 3-1: Spacecraft fixed body reference frame [55]

3.1.2. Spacecraft Principal Axes Reference Frame

The principal axis reference frame, like the fixed body frame, is a frame that is fixed to the body of the spacecraft with its origin located at the center of the spacecraft mass. The orientation of this reference frame is along the principal directions of the spacecraft body. It should be noted that the principal directions are the eigenvectors of the spacecraft inertia matrix and that the resulting dynamic equations may be expressed more conveniently in this frame.

3.1.3. Spacecraft Orbital Reference Frame

The orbital reference frame as shown in Figure 3-2, is chosen to be the well-known Earth-pointing reference system where the x-axis (Roll) is along the satellite velocity vector, the z-axis (Yaw) points toward the center of the earth and the y-axis (Pitch) completes the right-hand triad.

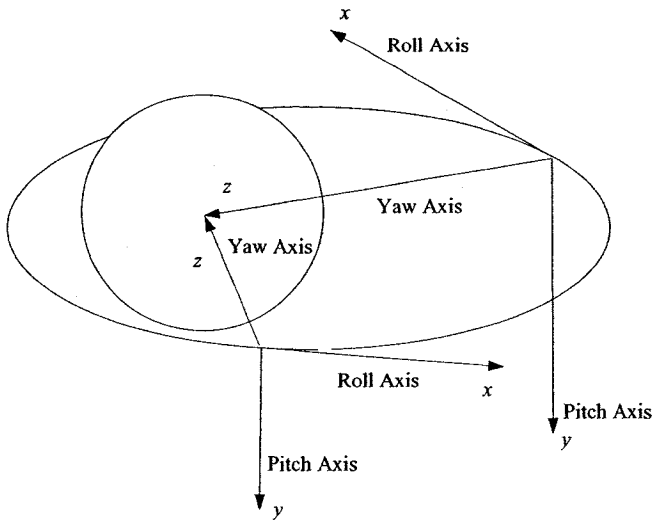

Figure 3-2: Spacecraft orbital reference frame [55]

3.1.4. Inertial Reference Frame

As is obvious from Figure 3-3, this is a non-rotating Earth-fixed frame. Its origin is located at the center of the Earth with x-axis points through the Greenwich Meridian in the equatorial plane. Its z-axis is the same direction as the Earth's rotation axis, and the y-axis completes the right hand triad.

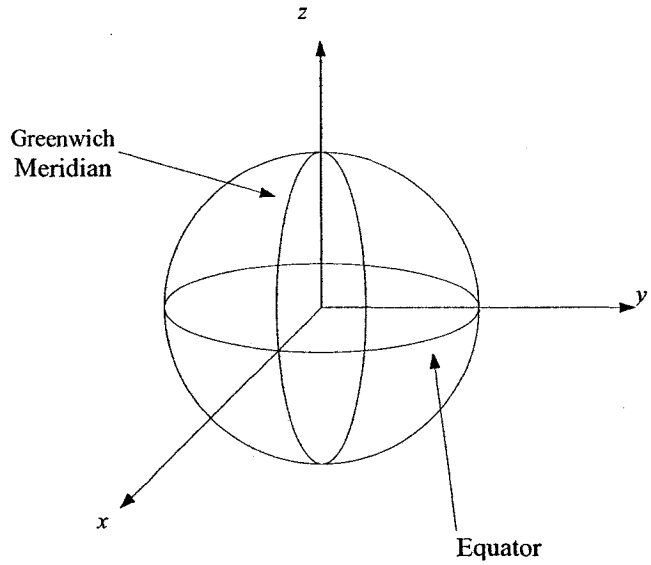

Figure 3-3: Spacecraft inertial reference frame [55]

3.2. Attitude Control System Dynamics and Control Laws

The spacecraft attitude control system, as explained earlier in Chapter 1, performs slew-and-hold maneuvers to satisfy the spacecraft pointing and stability requirements. This component has been developed to meet the high accuracy requirements established by the desired missions. The ACS designed in this thesis includes a three-axis reaction wheel with specified pointing requirements. Pointing requirements for the roll, pitch, and yaw axes are equal to 0.02° (i.e. a navigation error of 0.02° for the roll and pitch and yaw axes is acceptable) [52, 53]. The pointing requirements must be maintained by the control system under the influence of disturbance torques. The first step to design and analyze the control system is to derive a mathematical model of the system. In this work, the control system is designed to provide an appropriate input signal for the reaction wheels using the reference command signal and the feedback signals received from the spacecraft outputs. According to the input signal provided by the controller, the reaction

wheel produces and applies the proper torque to the satellite to obtain the desired pointing requirements. Consequently, the mathematical model of the system, required to design the controller, includes the spacecraft and the three-axis actuator (3-axis reaction wheel).

3.2.1. Spacecraft Attitude Dynamics and Disturbance Torques

The attitude control system stabilizes the vehicle and orients it during the mission, despite the external disturbance torques acting on it. Hence, the mathematical modeling of the spacecraft attitude dynamics includes both the dynamics of the spacecraft as well as the disturbance torques applied to it.

3.2.1.1. Spacecraft Attitude Dynamics

The nonlinear equations of the attitude motion of the satellite can be derived considering a torque about the satellite's center of mass. With reference to an absolute coordinate system, Newton's second law defines the relationship between the torque and the angular momentum, namely:

$$\tau = \dot{\vec{H}} \tag{3.1}$$

where τ is the actuator torque and H is defined as angular momentum.

If the body reference system has an angular velocity $\vec{\omega}$ as observed from the inertial reference frame, then $\dot{\vec{H}}$ in the above equation becomes

$$\tau = \dot{\vec{H}} + \vec{\omega} \times \vec{H} \tag{3.2}$$

In the above equation, the first part, $\dot{\vec{H}}$ represents any changes in the magnitude of the components of H, and the cross-product term represents changes in direction of the component of H. Replacing "$\vec{\omega} \times \vec{H}$" in the above equation by

$$\vec{\omega} \times \vec{H} = (\omega_y H_z - \omega_z H_y)i + (\omega_z H_x - \omega_x H_z)j + (\omega_x H_y - \omega_y H_x)k \tag{3.3}$$

where i, j and k denote the unit reference vectors, leads to:

$$\vec{\tau} = (\dot{H}_x + \omega_y H_z - \omega_z H_y)i + (\dot{H}_y + \omega_z H_x - \omega_x H_z)j + (H_z + \omega_x H_y - \omega_y H_x)k \tag{3.4}$$

Equation (3.4) can be written as a set of three differential equations relating the torque components to the angular momentum components. These equations are known as the Euler's momentum equations and are given by:

$$\begin{aligned} \tau_y &= \dot{H}_y + \omega_z H_x - \omega_x H_z \\ \tau_x &= \dot{H}_x + \omega_y H_z - \omega_z H_y \\ \tau_z &= \dot{H}_z + \omega_x H_y - \omega_y H_x \end{aligned} \tag{3.5}$$

Angular momentum components, H_x, H_y, and H_z, are related to the angular velocity components, ω_x, ω_y and ω_z, through the inertia matrix I, given by:

$$
\begin{aligned}
H_x &= I_{xx}\omega_x - I_{xy}\omega_y - I_{xz}\omega_z \\
H_y &= I_{yy}\omega_y - I_{xy}\omega_x - I_{yz}\omega_z \\
H_z &= I_{zz}\omega_z - I_{yz}\omega_y - I_{xz}\omega_x
\end{aligned}
\tag{3.6}
$$

If the spacecraft body frame is parallel to its principal axis, where the products of inertias are zero, substituting equations (3.6) into equations (3.5), yields:

$$
\begin{aligned}
\tau_x &= \dot{\omega}_x I_{xx} + \omega_y \omega_z \left(I_{zz} - I_{yy}\right) \\
\tau_y &= \dot{\omega}_y I_{yy} + \omega_z \omega_x \left(I_{xx} - I_{zz}\right) \\
\tau_z &= \dot{\omega}_z I_{zz} + \omega_x \omega_y \left(I_{yy} - I_{xx}\right)
\end{aligned}
\tag{3.7}
$$

where x, y and z now represent the principal axes of inertia.

Although, the general attitude motion of a rigid body may be modeled by equations (3.7), they have no general solution unless we specify the components of $\vec{\tau}$ which are the outputs of the actuators. Note that the equations are nonlinear and coupled.

3.2.1.2. Disturbance and Noise Signals

A body in space is subject to small but persistence disturbance torques from a variety of sources. Since, these torques would quickly reorient the vehicle, the effects of these disturbance torques on the overall system cannot be disregarded and should be modeled. The sources of the disturbances can be summarized as follows:

- **Gravity Gradient Torque**

The gravitational disturbance torques appear as a result of the gravitational torque variations over the unsymmetrical mass distribution of the satellite body. This variation is due to the variation of the radius vector from the center of Earth to the center of mass of the satellite in the body frame of reference. It can be estimated by the following equation [3]:

$$T_g = \frac{3\mu}{2R^3}\left|I_z - I_y\right|\sin(2\theta) \tag{3.8}$$

where T_g is the maximum gravity torque, μ is the Earth's gravity constant (3.986×10^{14} m^3/s^2), R is the orbit radius (m), θ is the maximum deviation of the Z-axis from the local vertical axis in radians, and I_z and I_y are the moments of inertia about z and y (or x, if smaller) axes in $kg.m^2$.

- **Earth's Magnetic Torque**

The Earth's magnetic field is closely approximated by the magnetic field of a dipole positioned at the centre of the Earth. This field is defined as series spherical harmonics. This magnetic field imposes a torque on the satellite, known as Earth's magnetic field. It can be obtained from the following equation

$$T_m = DB \tag{3.9}$$

where T_m is the magnetic torque on the spacecraft, D is the residual dipole of the spacecraft ($A.m^2$), and B is the Earth's magnetic field. B can be approximated as:

$$B = 2M / R^3 \tag{3.10}$$

In this equation, M is the magnetic momentum of the Earth, 7.96×10^{15} $tesa.m^3$, and R is the radius from Earth center to the spacecraft in m [3].

- **Solar Pressure Torque**

The solar pressure torque is a result of the accumulative force imparted by the sun and other solar masses on the satellite body orbiting the Earth. For a spacecraft with its size about $2\times 1.5m$, this torque is approximated to be: 6.6×10^{-6} $N.m$ [3].

- **Aerodynamic Disturbance Torque**

The aerodynamic disturbance torque is due to the accumulative force imposed by the molecules found in the upper atmosphere. Aerodynamic torque can be obtained from following equation:

$$T_a = F(c_{pa} - c_g) = FL \tag{3.11}$$

where T_a, is the aerodynamic torque, c_{pa} is the center of aerodynamic pressure and c_g is the center of gravity, F is the force that is imposed on the spacecraft and can be obtained from following equation:

$$F = 0.5(\rho C_d A V^2) \tag{3.12}$$

where C_d is the drag coefficients (usually between 2 and 2.5 [3]), ρ is the atmospheric density, A is the surface area, and V is the spacecraft velocity [3].

3.2.2. Actuator Dynamics

Conservation of the vehicle angular momentum requires that only external torques change the spacecraft net angular momentum. Actuators are devices which provide

reaction torque. They are employed in the system to apply any desired changes in the angular momentum and to resist the torques imposed by external disturbances [52]. In this section, the mathematical model of a high fidelity reaction wheel -the type of the actuator that has been used in the ACS system in this thesis- is introduced.

In general, a reaction wheel consists of a rotating flywheel, typically suspended on ball bearings and driven by an internal brushless DC motor.

Figure 3-4 shows a view of ITHACO reaction wheel. A detailed block diagram of reaction wheel is required to provide us with a fundamental understanding of a high fidelity mathematical model of the reaction wheel system [5]. This structure is presented by Figure 3-5.

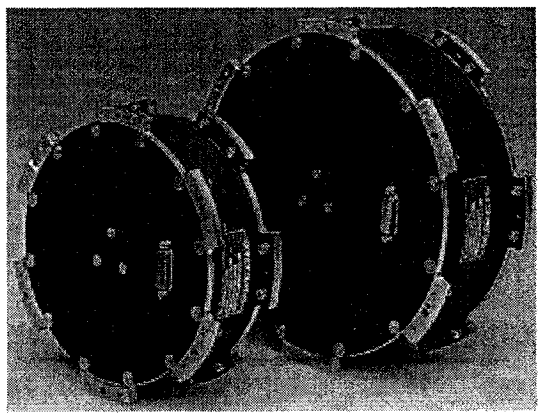

Figure 3-4: ITHACO reaction wheel

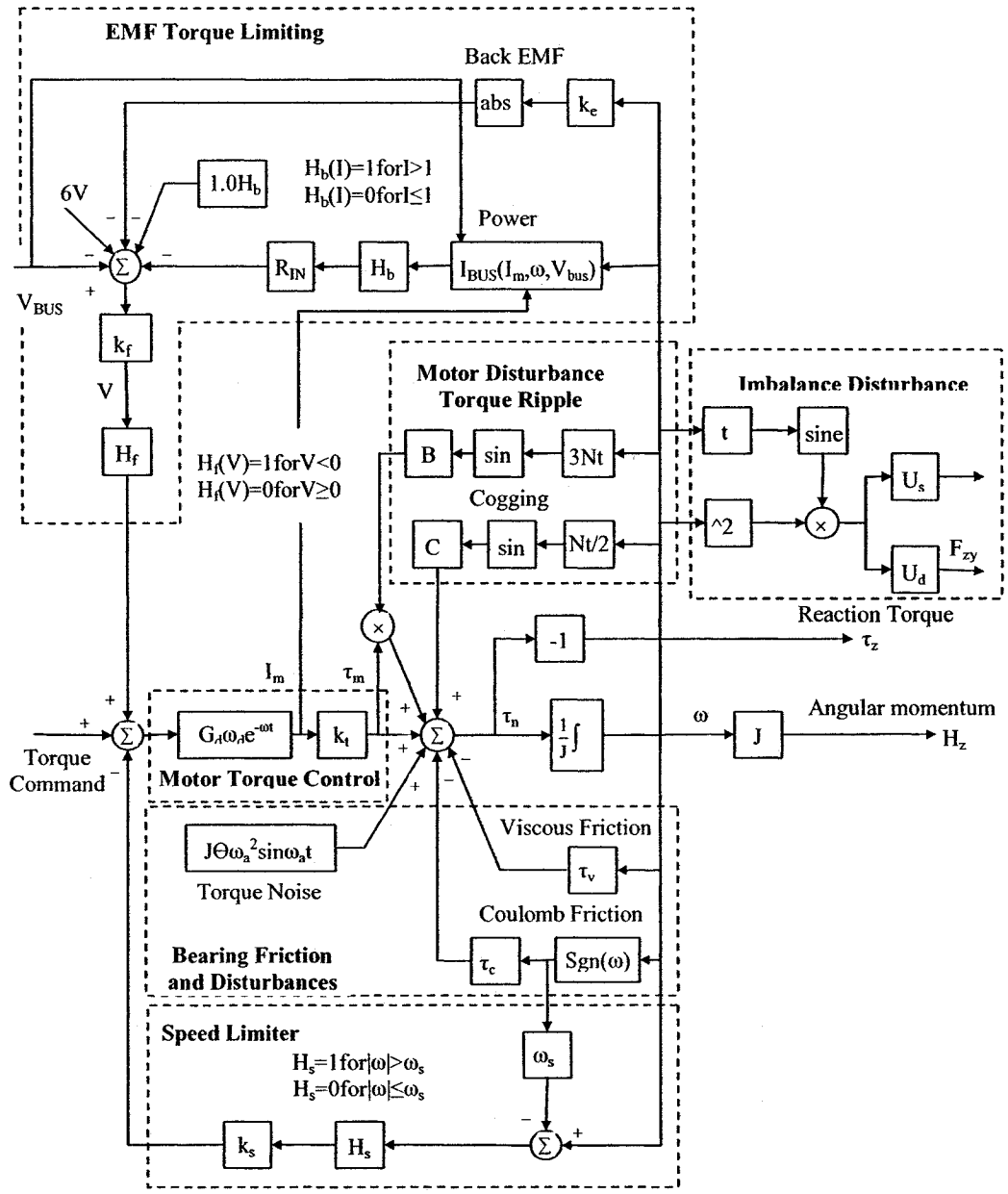

Figure 3-5: High fidelity reaction wheel block diagram [5]

The values of the parameters for different components and their units in this model can be found in Table 3.1. The constants in this table are considered for ITHACO's Type A reaction wheel [5].

Variable	Nomenclature	Units	Type A RWA
G_d	Driver Gain	A/V	0.19
ω_d	Driver Bandwidth (-3dB)	Rad/sec (Hz)	2000 (318)
K_t	Motor Torque Constant	N-m/A	0.029
τ_e	Motor Back-EMF	V/rad/sec	0.029
k_s	Overspeed Circuit Gain	V/rad/sec	95
ω_s	Overspeed Circuit Threshold	Rad/sec (rpm)	690 (6600)
τ_c	Coulomb Friction	N-m	0.002
J	Flywheel Inertia	N-m-s^2	0.0077
N	Number of Motor Poles	-	36
B	Motor Torque Ripple Coefficient	N-m	0.22
C	Cogging Torque Amplitude	-	Zero
R_{IN}	Input Resistance	Ω	2.0
P_q	Quiescent Power	W	3.0
R_B	Bridge Resistance	Ω	2.0
	Torque Command Range	V	5
k_f	Voltage Feedback Gain	V/V	0.5
θ_a	Torque Noise Angle Deviation	rad (degrees)	0.05 (3)
ω_a	Torque Noise High Pass Filter Frequency	rad/sec	0.2

Table 3-1: The reaction wheel parameters values [5]

The subsystems of a high fidelity reaction wheel illustrated in Figure 3-5 are described in following subsections.

3.2.2.1. Motor Torque Control

The motor driver is a current source with a gain, G_d, controlled by a command voltage. The purpose of this block is to deliver the current directly proportional to the torque command voltage. Torque constant, K_t in Figure 3-5 provides torque proportional to the current delivered into it, I_m.

3.2.2.2. Speed Limiter

In order to prevent the flywheel from reaching unsafe speeds, a speed limiter circuit is employed. The speed limiter senses wheel speed and if the wheel speed, ω, exceeds a hold threshold, ω_s, the block H_s will activate a negative feedback which returns the flywheel speed with a negative high gain, K_s, into torque command.

3.2.2.3. EMF Torque Limiting

Any change in the magnetic environment of a coil of wire will induce an electric field and therefore a voltage (emf) in a coil. No matter how the change is produced, the voltage will be generated (Faraday's Law). When an emf is generated by a change in magnetic flux according to Faraday's Law, the polarity of the induced emf produces a current whose magnetic field opposes the change which produces it (Lenz's Law).

In the presence of a magnetic field, when an emf is applied to the ends of the coils of the motor, they rotate. The magnetic flux threading through the area between the coils therefore changes constantly. By Faraday's law of induction, this induces an emf that, by Lenz's law, opposes the motion of rotation; it is a *back emf.*

At high speeds, because of the high rate of change in magnetic field, there will be a big increase in the amount of back emf, τ_e which according to the Lenz's Law, will oppose the rotation. Therefore, there will be a threshold for the rotation speed, which exceeding that threshold will apply limitation in the rotation speed and corollary the motor torque. This can be compensated by a high V_{BUS}. But in low bus voltage, from the disturbance point of view, the available motor torque is coupled directly to the V_{BUS} and any change or fluctuation will be considered as torque disturbance which should be modeled in the block diagram. The back emf limiting is coupled with I_{BUS} as has been shown in Figure 3-5. I_{BUS} is a function of motor current, angular velocity and bus voltage which can be specified by the following equation [5]:

$$I_{BUS} = \left(\frac{1}{V_{BUS} - 1}\right)\left(I_m^2 R_B + 0.04|I_m|V_{BUS} + P_q + \omega I_m k_e\right) \tag{3.13}$$

where V_{BUS} is the bus voltage of the wheel, I_m is the motor current, R_B is a constant known as bridge resistance and P_q is a constant known as quiescent power.

3.2.2.4. Friction and Torque Noise

Another important parameter that influences the motor torque is friction and the noise related to the friction. These parameters should be considered as disturbance torques and modeled carefully in the high fidelity mathematical modeling. To simplify the study and the modeling of the friction, it can be broken down into viscose friction and coulomb friction and torque noise.

- ***Viscous Friction, τ_v-*** Viscous friction is a parameter that depends on speed and temperature. The viscous friction is generated in the bearings due to the bearing lubricant. Since, the lubricant has a strong sensitivity to the temperature; the viscosity is a temperature dependent variable. This torque has been characterized by the following equation [5]:

$$\tau_v = \left(0.049 - \frac{0.0002}{^\circ C}(T + 30^\circ C)\right)\frac{mN - m}{rad/\sec} \tag{3.14}$$

- ***Coulomb Friction, τ_c-*** Coulomb friction is a constant parameter with polarity dependence on wheel direction of rotation. The coulomb friction, τ_c is caused by rolling friction within the bearing. This loss torque is independent of wheel speed and temperature and is primarily of interest as a disturbance source. The coulomb friction is assumed to be *0.002 Nm.*
- ***Torque Noise, τ_a-*** Torque noise is a very low frequency torque with the lubricant dynamic source. This torque can be specified as a deviation from the ideal location of the spacecraft. It can be approximated by the following formula [5]:

$$\tau_a = J\theta_a\omega_a^2 \sin\omega_a t \tag{3.15}$$

where θ_a represents the angle applied due to this torque noise, ω_a is the torque noise high pass filter frequency (This filter is used to determine the torque noise angle) and where J is the wheel inertia.

3.2.2.5. Imbalance Disturbance

The imbalance of the flywheel is often considered to be one of the most significant sources of disturbance from a reaction wheel or momentum wheel to the spacecraft. The imbalance is specified as sum of the two errors in the symmetry of the flywheel with respect to the axis of rotation, known as static and dynamic imbalance [5].

- ***Static Imbalance***-The static imbalance is the offset of the center of gravity of the flywheel from the rotation axis as illustrated in Figure 3-6. As a result, it produces a rotating radial force which appears sinusoidal from a fixed reference, at a frequency corresponding to once per flywheel revolution and an amplitude given by:

$$F_{x,y} = mr\omega^2 \tag{3.16}$$

The static imbalance is a flywheel mass property defined by:

static imbalance = $U_s = mr$. The radial force is given by:

$$F_{x,y} = U_s\omega^2 \sin \omega t \tag{3.17}$$

- ***Dynamic Imbalance***- The dynamic imbalance is caused by the angular misalignment of the principal axis of the wheel and the spin axis. It is modeled as two equal masses, m, placed 180° apart at the radial distance, r, and an axial distance, d, from the center of the flywheel as shown in Figure 3-7. This causes a once-per-revolution rotating couple given by:

$$\tau_{x,y} = mrd\omega^2 \tag{3.18}$$

The dynamic imbalance is a flywheel mass property defined by:

Dynamic imbalance = $U_d = mrd$

The magnitude of the disturbance torque is then simply the dynamic imbalance times the square of the flywheel speed or:

$$\tau_{x,y} = U_d\omega^2 \sin\omega t \tag{3.19}$$

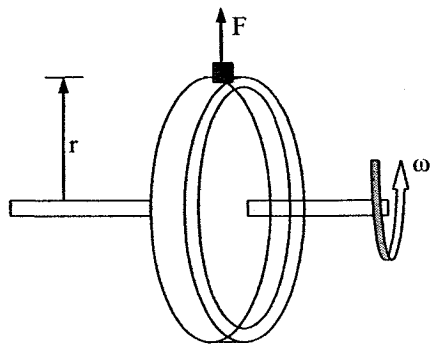

Figure 3-6: Static imbalance representation [5]

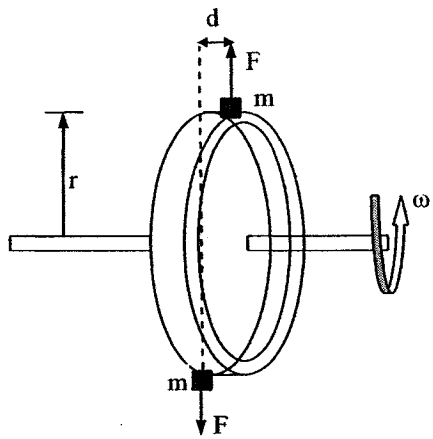

Figure 3-7: Dynamic imbalance representation [5]

3.2.2.6. Motor Disturbances

The brushless DC motor used in reaction wheel is another source of disturbance torques. The amount of the disturbance torques generated by the brushless DC motor is different depending on the frequency the machine is working with. In this thesis, the motor disturbance is considered in the commutation frequency, which is also known as *torque ripple*, and the frequency corresponding to the number of motor poles and rate of rotation, namely *cogging*.

3.2.3. Controller Dynamics

Having the spacecraft and the reaction wheel mathematical model, an automatic controller is used to compare the actual output of the plant with the desired one. Using these two signals, the controller produces a control signal to reduce the difference between these two signals to zero or to a small acceptable value. Figure 3-8 illustrates the three axis stabilized spacecraft attitude control system. The dynamics of the reaction wheel and spacecraft are described earlier in previous chapters. A PID controller is used in the controller blocks due to having the following properties [38]:

1- It can perform as an amplifier to adjust the gain due to its proportional parameter,
2- The integral factor can be used to minimize the steady state error to zero,
3- The derivative factor, however, can stabilize the system; and
4- It can easily be adjusted to the desired application.

Since, the focus of this thesis is on the fault detection problem, the above conditions are satisfactory for the purpose of controller design.

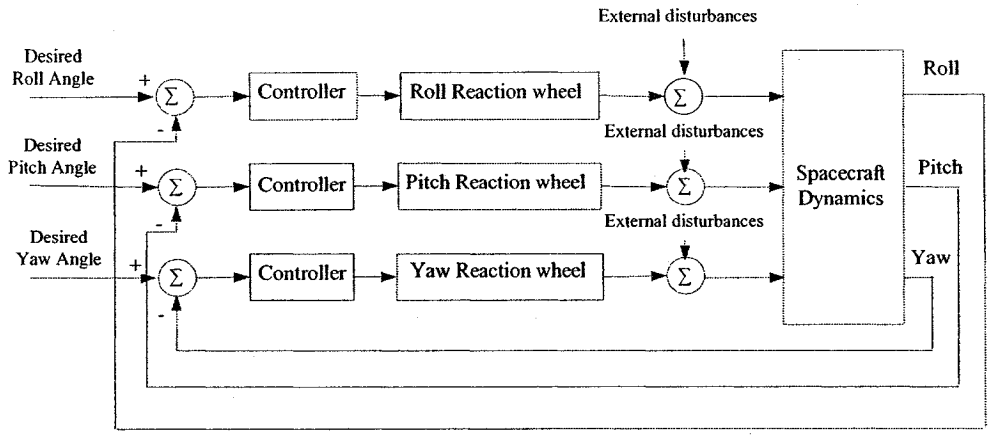

Figure 3-8: The three axis stabilized spacecraft attitude control system

To design the PID controller parameters it is first assumed that there is no coupling properties between different axes. This assumption eliminates the coupling term in equations (3.7). Consequently, the spacecraft dynamic will turn out to be:

$$\begin{aligned} \tau_x &= \dot{\omega}_x I_{xx} \\ \tau_y &= \dot{\omega}_y I_{yy} \\ \tau_z &= \dot{\omega}_z I_{zz} \end{aligned} \tag{3.20}$$

Considering the above equations for the dynamics of the satellite, a single axis system as shown in Figure 3-9 can be employed to design the controller, and then the design can be applied to the other two axes.

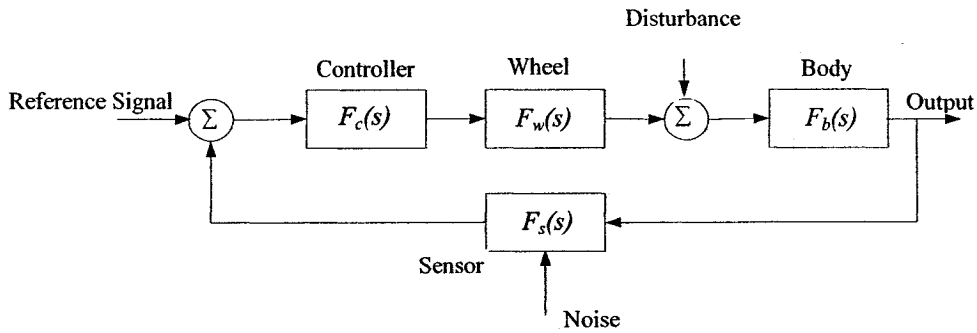

Figure 3-9: Single axis control block diagram

In this figure, $F_c(s)$ indicates the controller transfer function, F_w specifies the wheel transfer function, and F_b describes the body transfer function which can be obtained from equation (3.20).

The above controller designed for a linear system, is now applied to the non-linear model in all three axes. Considering the model mismatches, the difference between the output signal of the satellite and the desired ones are then compensated by further tuning and some modifications in the controller parameters.

3.2.3.1. Attitude Control System Design Using Classical Control (PID)

The desired response of the ACS can be characterized by system specifications. Any input can be approximated as a linear combination of step signals. Consequently, for a LTI system if the response of the system to a step input is known, it is mathematically possible to obtain the response of the system to any other input. Due to this property of LTI systems, specification of a control system is determined in terms of the response of the system to a step input. These specifications in time domain are as follows [38]:

- ***Delay time, t_d-*** which is the time required for the response to reach half the final value for the very first time,
- ***Rise time, t_r-*** which can be specified as the time required for the response to rise from 10% to 90%, or 5% to 95%, or 0% to 100% of its final value, depending on the designer,
- ***Peak time, t_p-*** which is the time required for the response to reach the first peak of the overshoot,

- ***Maximum overshoot, M_p***- which can be determined as the maximum peak value of the response curve. Maximum overshoot should be specified with respect to the steady state response. As a result, maximum percent overshoot is used instead of maximum overshoot. And,
- ***Settling time, t_s***- which is the time required for the response curve to reach and stay within 2% to 5% of its final value.

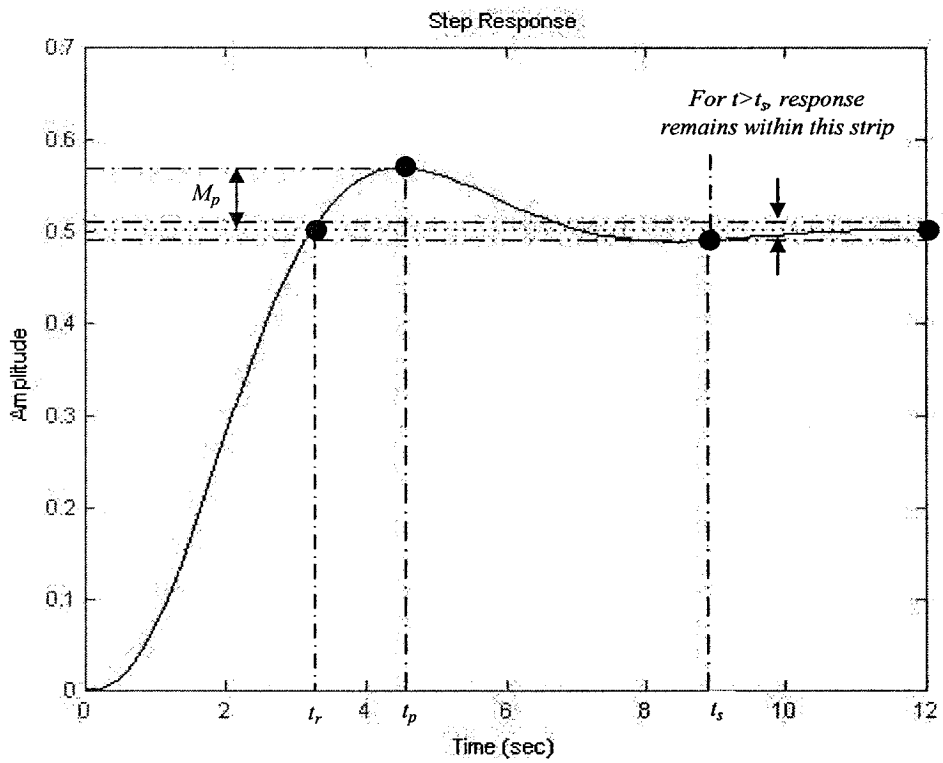

Figure 3-10: Transient response specifications

The above specifications are illustrated in Figure 3-10. It should be noted that not all of the above specifications are required, but depending on the system requirements some of them can be employed.

In the design of spacecraft, delay time, rise time and peak time are of no concern. When a reference command signal is applied to the spacecraft, we need our spacecraft output to

not pass a threshold (max overshoot), and becomes stable after a specific time (settling time). Since, the focus of this thesis is in fault detection, the precise formalization of system specifications are not of major concern. Toward designing the controller, the required specifications are selected to be: settling time, t_s, and the maximum overshoot, M_p. The two specifications are selected according to Table 3-2.

Specification	Desired Amount
Settling time (t_s)	≤500 sec
Maximum overshoot (M_p)	≤10%

Table 3-2: ACS control design specifications

Given that the primary emphasis in spacecraft operations is safety rather than a fast transient response, the settling time of 500 sec is quite reasonable for a Low Earth Orbit that is generally lasting 100 minutes.

To control a system, whatever the mechanism is, one generally approximates it by a second order system. A general second order system is specified by the following transfer function in the Laplace domain:

$$\frac{Y(s)}{U(s)} = \frac{\omega_n^2}{s^2 + 2\varsigma\omega_n s + \omega_n^2} \tag{3.21}$$

where ζ is known as the damping ratio, ω_n is the undamped natural frequency and $\varsigma\omega_n$ usually specified by the parameter σ is known as the damping factor. The relation between these parameters and system specifications are determined by the following equations:

$$t_s = \frac{4.6}{\sigma}$$
$$\varsigma = 0.6(1 - M_p) \tag{3.22}$$

The desired second order system which can satisfy our specifications is given by the equation:

$$\frac{Y(s)}{U(s)} \approx \frac{0.2^2}{s^2 + 2 \times (0.01)s + 0.2^2} \tag{3.23}$$

Equation (3.23), indicates a second order system with a behavior that is desired for our system.

Basically to design a PID controller for this system, the whole dynamics of the system as shown in Figure 3-9 should be expressed by Laplace transfer functions. The relation between input and output of the system from this figure is used to obtain the system transfer function. This relation can be specified as follows:

$$\theta = \theta_\Delta F_c F_w F_b + z(s) F_b \tag{3.24}$$

where θ is the controlled attitude angle, and

$$\theta_\Delta = \theta_c - \theta_s \quad \text{with } \theta_s = \theta F_s \tag{3.25}$$

which when combined results in the following general expression

$$\theta(s)[1+F_b(s)F_w(s)F_c(s)F_s(s)]=z(s)F_b(s)+\theta_c(s)F_b(s)F_w(s)F_c(s) \tag{3.26}$$

Assuming that the disturbance torque $z(s)$ is zero, we can obtain the transfer function as follows:

$$F(s)=\frac{\theta(s)}{\theta_c(s)}=\frac{F_b(s)F_w(s)F_c(s)}{1+F_b(s)F_w(s)F_c(s)F_s(s)}=\frac{F_w(s)F_c(s)}{\frac{1}{F_b(s)}+F_w(s)F_c(s)F_s(s)} \tag{3.27}$$

in which $F_b(s)$ is the body transfer function, $F_w(s)$ represents the wheel transfer function, $F_c(s)$ is the controller transfer function, and $F_s(s)$ specifies the sensor transfer function.

The disturbance transfer function $D(s)=\frac{\theta(s)}{z(s)}$ is calculated assuming that the control command $\theta_c(s)$ is set to zero. The disturbance transfer function $D(s)$ becomes:

$$D(s)=\frac{\theta(s)}{z(s)}=\frac{F_b(s)}{1+F_b(s)F_w(s)F_c(s)F_s(s)}=\frac{1}{\frac{1}{F_b(s)}+F_w(s)F_c(s)F_s(s)} \tag{3.28}$$

It is obvious from equation (3.27) that to obtain the transfer function of the system each block's transfer function is required. These are described individually below:

- **Sensor Transfer Function**

Sensors are used to measure the pitch, roll, and yaw angles of the satellite. The transfer function that is considered for this block can be as simple as unity gain, namely:

$$F_s=K_s=1 \tag{3.29}$$

- **Reaction Wheel Transfer Function**

The reaction wheel block diagram described earlier by Figure 3-5, is approximated by a linear model as illustrated in Figure 3-11. The input to the system is a voltage which controls motor current and therefore motor torque, τ_m. The output of the system is the reaction torque, τ_z which is applied to the spacecraft. Friction torque, τ_d and back EMF torque, τ_e have been considered in this model. Because of the consideration of these two factors in this model, it is not an ideal model of the reaction wheel, so we have named it nearly ideal model of the reaction wheel. In Figure 3-11 J is the flywheel inertia, G_d is the motor gain, and K_t is the motor torque constant.

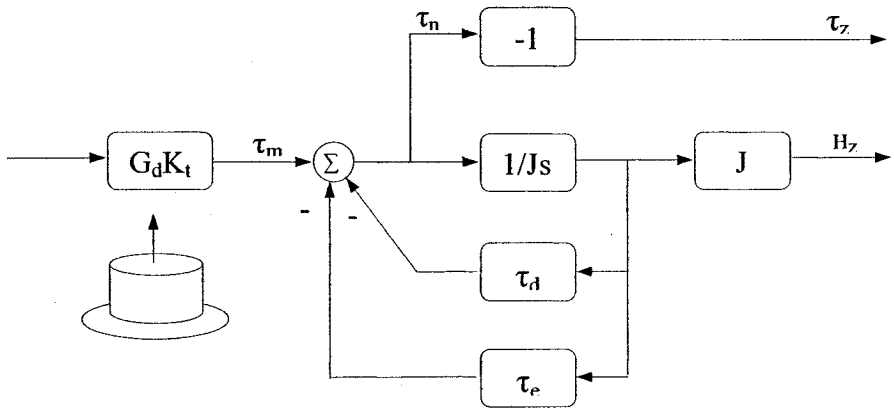

Figure 3-11: Nearly ideal reaction wheel [5]

To obtain the transfer function of the reaction wheel as illustrated in Figure 3-11, the input and output signals should be specified. Considering the output signal $y(s)$ is the generated torque which is applied to the spacecraft, and the input signal is provided by the controller, the actuator transfer function becomes:

$$\frac{y(s)}{u(s)} = -\frac{(G_d k_t J)s}{Js + (\tau_d + \tau_e)} \tag{3.30}$$

- **PID Controller**

General transfer function of a PID controller is specified by the following expression.

$$y_R(s) = K_p(1 + \frac{1}{T_I s} + T_D s) \tag{3.31}$$

where K_p indicates a proportional gain and T_I and T_D are integral and derivative coefficients, respectively.

- **Body Dynamics**

The dynamics of the rigid body of a satellite is specified by equation (3.20). By substituting equations (3.20), (3.29) and (3.30), in equation (3.27) we have:

$$F(s) = \frac{(G_d K_t J)sF_c(s)}{-I_{yy}(G_d K_t J)s^3 F_c(s) + Js + \tau_d + \tau_e} \tag{3.32}$$

As mentioned earlier, we try to approximate our system by a second order system to control it. For this purpose, the system characteristics were used to obtain a second order system.

We now apply the above controlled system to the three axes model of the spacecraft as shown in Figure 3-8, with the detailed model of the reaction wheel as depicted in Figure 3-5, and the spacecraft dynamics as modeled by equation (3.7). By using "fminsearch" function in Matlab, the optimized values for the PID controller parameters, *P*, *I* and *D* can

be obtained. The "Fminsearch" is a non-linear optimization method to find the minimum of a scalar function of several variables. This method works based on Nelder-Mead optimization simplex method [52]. In this function, one may specify the desired output behavior to the model of the system. Running the program for a specified number of times, which can be specified by '*optimset*' parameter, this function tries to find the best set of values for the parameters P, I and D to obtain the closest output to the desired output. Using this method with *optimset* parameters set to 100 for the above mentioned specifications the following optimized values for the controller parameters, P, I, and D, are obtained:

$P= -2400$, $I= -9.83$, and $D= 8666$.

To justify the good performance of the designed PID controller, three reference command signals as shown in Figure 3-12 are considered and applied to the system. Simulation results of the closed loop non-linear model of the ACS of the satellite are illustrated in Figure 3-13.

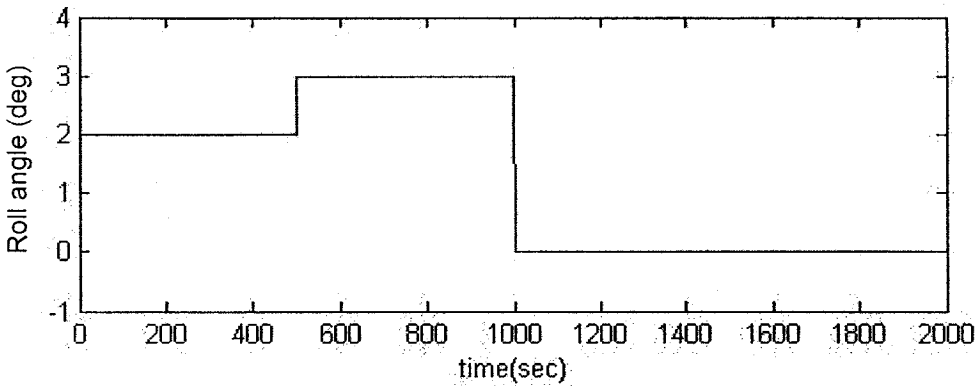

(a)

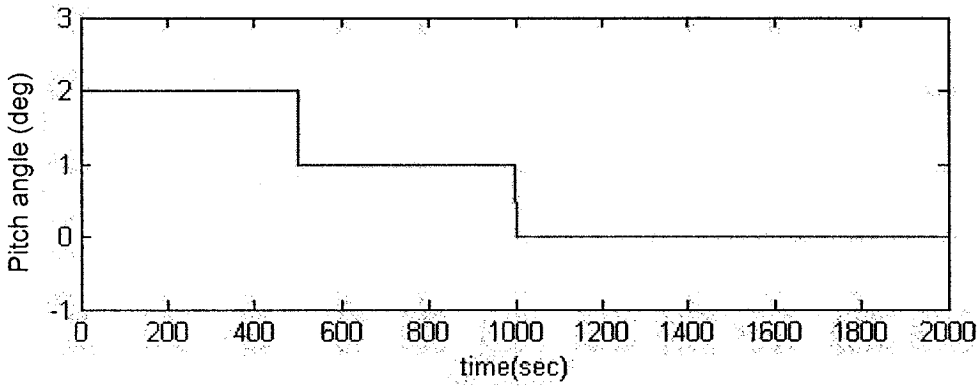

(b)

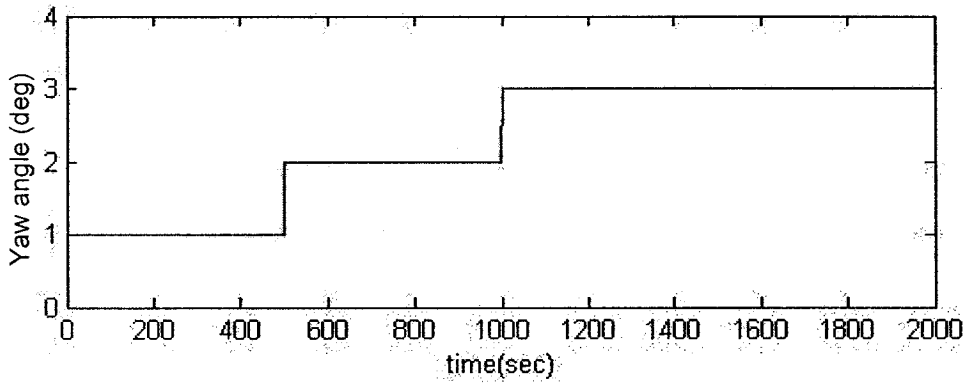

(c)

Figure 3-12: The set point reference commands for a scheduled different maneuvers for the spacecraft (a) roll axis, (b) pitch axis and (c) yaw axis

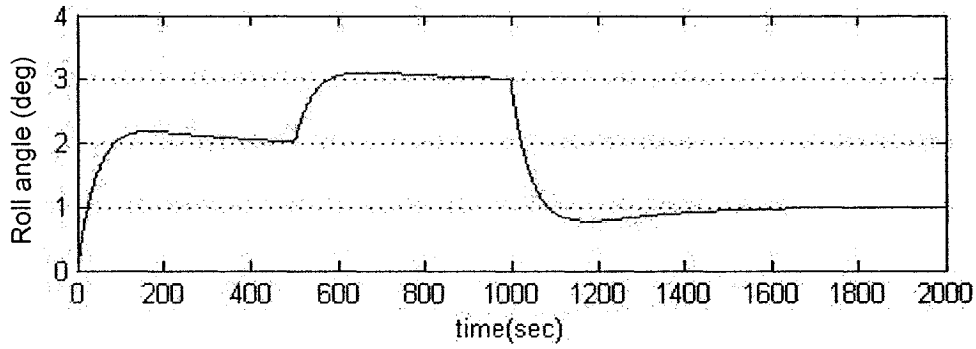

(a)

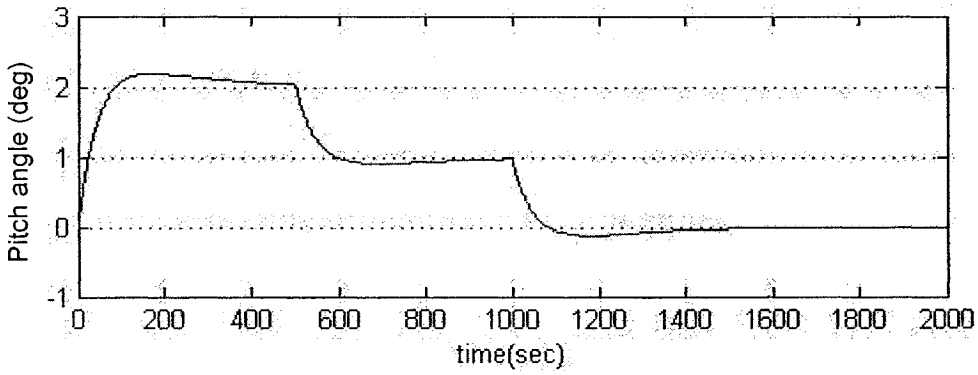

(b)

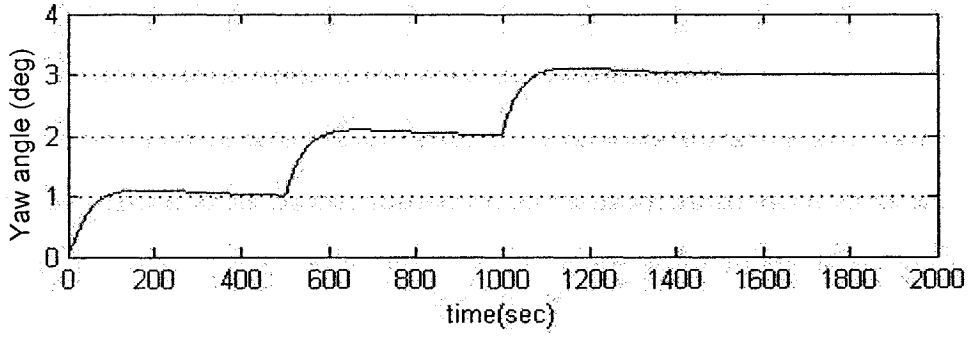

(c)

Figure 3-13: The actual outputs of the closed loop non-linear spacecraft following the desired reference commands shown in Figure 3-12 (a) roll axis, (b) pitch axis and (c) yaw axis

As shown in Figure 3-13, the satellite system outputs follow the reference command signals. Furthermore, the results satisfy the required system specifications as well. Since, under healthy condition, the structure of the attitude control system follows the reference command signal, this system is now qualified for the purpose of fault detection and diagnosis.

3.3. Conclusion

In this chapter, model based fault detection and diagnosis techniques have been introduced and discussed. Furthermore, system specifications for the considered attitude control system of the spacecraft are determined and the optimized design is presented considering these specifications. The chapter ends with simulation results to justify the developed closed loop control design. In the next chapter, this architecture is used for the purpose of fault detection and diagnosis.

Chapter 4 : Parity Space and Linear Observer-based Customized Design

In this chapter, two approaches to fault detection and diagnosis (FDD) as presented in Chapter 2, i.e. the parity space equation and the linear observer approaches are customized and developed for the attitude control dynamic model of a satellite as discussed in Chapter 3. After completing the fault detection design, safe limits or safe boundaries are determined and applied to the residuals for compensating modeling discrepancies and effects of unpredictable noise and disturbances.

4.1. Parity Space FDD Design

As discussed earlier in Chapter 2, to design a model based fault detection and diagnosis (FDD) system, one needs to know the dynamics of the system. Toward this end, we have presented in Chapter 3 the spacecraft attitude control system model and characteristics. In this section, the system dynamics obtained in Chapter 3 will be used for the purpose of design and investigation of the parity space approach to the problem of fault detection and diagnosis. To develop the parity space architecture and for sake of simplicity a single axis block diagram of Figure 3-9 is used by disregarding the coupling properties that are presented in the full 3-axis system.

In Figure 3-9 the controller block diagram is substituted by a PID controller as designed in Chapter 3. For the actuator block, the schematic of Figure 3-11 is used and the plant

block in the diagram is substituted by the spacecraft attitude dynamics by neglecting the coupling properties, as specified in equation (2.25).

By making the above substitutions, the detailed block diagram of Figure 3-9 is now illustrated as shown below:

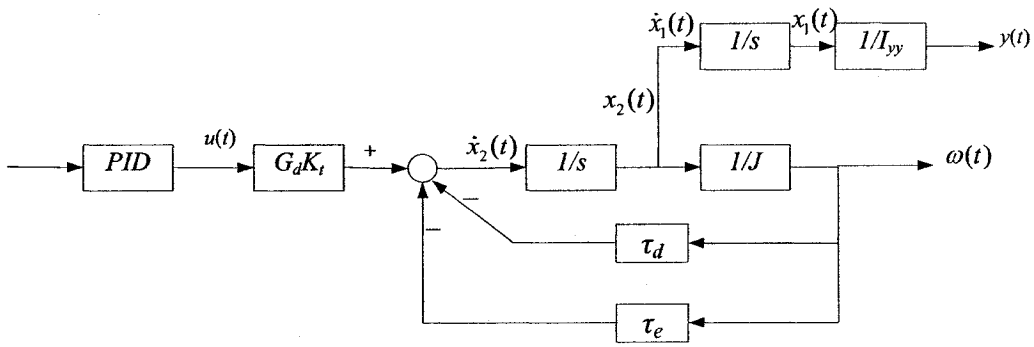

Figure 4-1: The linear block diagram of a single axis spacecraft attitude control system (pitch axis)

Using Figure 4-1, the overall state space representation of the system is obtained as follows:

$$\begin{cases} \dot{x}_1(t) = x_2(t) \\ \dot{x}_2(t) = -\left(\dfrac{\tau_d + \tau_e}{J}\right) x_2(t) + G_d K_t u(t) \\ y = -\dfrac{1}{I_{yy}} x_1(t) \end{cases} \tag{4.1}$$

where x_1 and x_2 are the system states as shown in the figure, $u(t)$ is the controlled input and $y(t)$ is the spacecraft output (spacecraft axis angle). The other parameters have already been explained in previous chapters.

In our research we first design the parity space equations for the system specified by equation (4.1). Next, we apply this design to the fully nonlinear and high fidelity model of the system as shown in Figure 3-8. Whereas, in Figure 3-8, the equation (3.7) is used to describe the dynamics of the spacecraft, the coupling effects are taken into consideration and the block diagram of Figure 3-5 substitutes the actuator block.

For the purpose of designing the parity space fault detection system, the following assumption is made:

Assumption: There is no access to the output of the reaction wheel and we have only access to the output of the satellite system (that is attitude angles).

Using the input and output measured signals, the block diagram of the fault detection system is specified as illustrated in Figure 4-2. In this figure, the FDI system is fed by system inputs and the spacecraft outputs, and the FDI system output is the residual signal. The outputs of the spacecraft are selected to be the attitude angles.

As it can be seen from equation (4.1), the system illustrated in Figure 4-1 is an LTI (Linear and Time Invariant) system. By introducing the matrix T according to equation (2.35), the Cayley-Hamilton theorem of equation (2.40) is now used to obtain the parameter $\overline{n}$, which indicates the number of derivatives that are required in matrix T for the system to be observable through spacecraft output measurements.

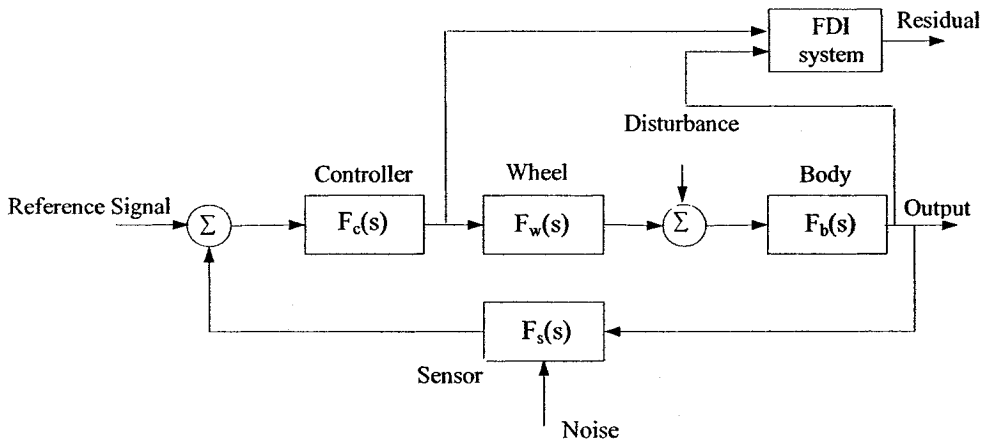

Figure 4-2: A one axis FDI system block diagram

Following equation (2.34), we have:

$$y = -\frac{1}{I_{yy}} x_1 \tag{4.2}$$

so that by differentiation in time we get:

$$\dot{y}(t) = -\frac{1}{I_{yy}} \dot{x}_1(t)$$

or equivalently

$$\dot{y}(t) = -\frac{1}{I_{yy}} x_2(t) \tag{4.3}$$

Similarly, by taking the second and third order differentiations in time we have

$$\ddot{y} = \frac{\tau_d + \tau_e}{I_{yy} J} x_2(t) - \frac{G_d K_t}{I_{yy}} u(t) \tag{4.4}$$

and

$$\ddot{y} = -\frac{1}{I_{yy}}\left(\frac{\tau_d + \tau_e}{J}\right)^2 x_2(t) + \frac{\tau_d + \tau_e}{I_{yy} J} G_d K_t u(t) - \frac{G_d K_t}{I_{yy}} \dot{u}(t) \tag{4.5}$$

Following the above procedure we may write:

$$\begin{bmatrix} y \\ \dot{y} \\ \ddot{y} \\ \dddot{y} \\ \vdots \\ y^{(n)} \end{bmatrix} = \begin{bmatrix} \frac{1}{I_{yy}} & 0 \\ 0 & -\frac{1}{I_{yy}} \\ 0 & \frac{1}{I_{yy}} \frac{\tau_d + \tau_e}{J} \\ 0 & -\frac{1}{I_{yy}} \left(\frac{\tau_d + \tau_e}{J}\right)^2 \\ \vdots & \vdots \\ 0 & \frac{(-1)^n}{I_{yy}} \left(\frac{\tau_d + \tau_e}{J}\right)^{n-1} \end{bmatrix} \begin{bmatrix} x_1 \\ x_2 \end{bmatrix} + \tag{4.6}$$

$$\begin{bmatrix} 0 & 0 & \cdots & 0 \\ 0 & 0 & \cdots & 0 \\ \frac{-G_d K_t}{I_{yy}} & 0 & \cdots & 0 \\ \frac{1}{I_{yy}} G_d K_t \frac{\tau_d + \tau_e}{J} & \frac{-G_d K_t}{I_{yy}} & \cdots & 0 \\ \vdots & \vdots & \cdots & \vdots \\ \frac{(-1)^{n-1}}{I_{yy}} G_d K_t \left(\frac{\tau_d + \tau_e}{J}\right)^{n-2} & \frac{(-1)^{n-2}}{I_{yy}} G_d K_t \left(\frac{\tau_d + \tau_e}{J}\right)^{n-3} & \cdots & \frac{-G_d K_t}{I_{yy}} \end{bmatrix} \begin{bmatrix} u \\ \dot{u} \\ \vdots \\ u^{(n-2)} \end{bmatrix}$$

Comparing the above equation with equation (2.35), it follows clearly that the matrix T is of rank 2. Now, using equation (2.40), $\bar{n}=2$; and therefore the matrix $T(\bar{n}-1)$ characterizes the part of the system state that is observable from the spacecraft output sensors.

Consequently, the first derivative of the output will be sufficient, and the equation (4.6) will reduce to:

$$\begin{bmatrix} y(t) \\ \dot{y}(t) \end{bmatrix} = \begin{bmatrix} \frac{1}{I_{yy}} & 0 \\ 0 & -\frac{1}{I_{yy}} \end{bmatrix} \begin{bmatrix} x_1(t) \\ x_2(t) \end{bmatrix} \tag{4.7}$$

Now to obtain the parity values, we introduce the nonzero vector $\Omega = [\omega_1 \quad \omega_2]$, such that:

$$[\omega_1 \quad \omega_2] \begin{bmatrix} \frac{1}{I_{yy}} & 0 \\ 0 & -\frac{1}{I_{yy}} \end{bmatrix} = 0 \tag{4.8}$$

Since the two rows of matrix T are linearly independent, the only solution for the vector Ω would be zero to satisfy equation (4.8). Consequently constructing higher order derivatives is offered. In that case, the system states are still observable and the nonzero vector Ω can be computed. Computing one more derivative, equation (4.6) becomes:

$$\begin{bmatrix} y(t) \\ \dot{y}(t) \\ \ddot{y}(t) \end{bmatrix} = \begin{bmatrix} \frac{1}{I_{yy}} & 0 \\ 0 & -\frac{1}{I_{yy}} \\ 0 & \frac{1}{I_{yy}} \frac{\tau_d + \tau_e}{J} \end{bmatrix} \begin{bmatrix} x_1(t) \\ x_2(t) \end{bmatrix} + \begin{bmatrix} 0 & 0 & 0 \\ 0 & 0 & 0 \\ \frac{G_d K_t}{I_{yy}} & 0 & 0 \end{bmatrix} \begin{bmatrix} u(t) \\ \dot{u}(t) \\ \ddot{u}(t) \end{bmatrix} \tag{4.9}$$

and equation (4.8) reduces to:

$$\begin{bmatrix} \omega_1 \\ \omega_2 \\ \omega_3 \end{bmatrix}^T \begin{bmatrix} \frac{1}{I_{yy}} & 0 \\ 0 & -\frac{1}{I_{yy}} \\ 0 & \frac{1}{I_{yy}} \frac{\tau_d + \tau_e}{J} \end{bmatrix} = 0 \tag{4.10}$$

Using equation (4.10), it can be seen that there exists only one linearly independent solution for Ω, and that is given as follows

$$\Omega = \begin{bmatrix} 0 & \frac{\tau_d + \tau_e}{J} & 1 \end{bmatrix} \tag{4.11}$$

The components of the row vector Ω are known as parity values. To obtain the parity equation, the expression (2.39) is used, namely

$$\begin{bmatrix} \omega_1 \\ \omega_2 \\ \omega_3 \end{bmatrix}^T \left[\begin{bmatrix} y(t) \\ \dot{y}(t) \\ \ddot{y}(t) \end{bmatrix} - \begin{bmatrix} 0 & 0 & 0 \\ 0 & 0 & 0 \\ \frac{G_d k_t}{I_{yy}} & 0 & 0 \end{bmatrix} \begin{bmatrix} u(t) \\ \dot{u}(t) \\ \ddot{u}(t) \end{bmatrix} \right] = r \tag{4.12}$$

which leads to the following equation for the residual error:

$$r = \ddot{y}(t) + \frac{\tau_d + \tau_e}{J} \dot{y}(t) - \frac{G_d k_t}{Iyy} u(t) \tag{4.13}$$

Equation (4.13) is considered as the parity equation for our satellite system. Applying the parity equation to the healthy system of Figure 4-1, we get:

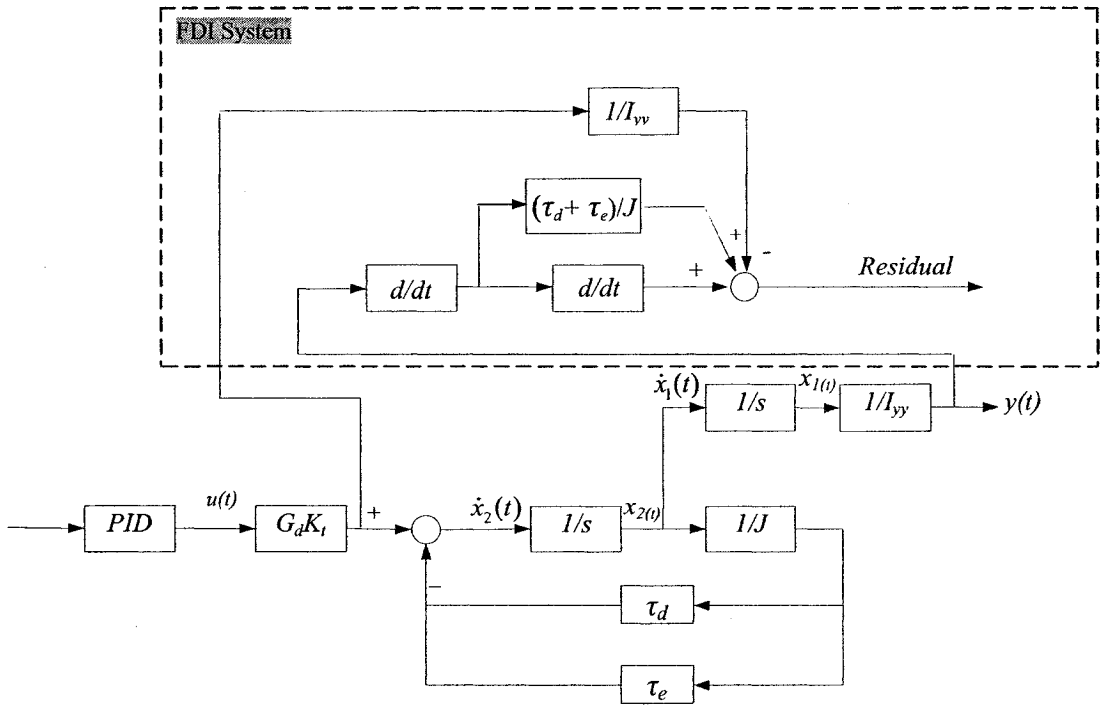

Figure 4-3: Parity equation approach to fault detection and diagnosis as applied to the linear single axis model of the spacecraft

The simulation results of Figure 4-3 are obtained under different conditions in the following section.

4.1.1. Simulation Results

To qualify the performance of the designed parity space-based method as illustrated in Figure 4-3, a number of scenarios are applied to the system to generate residual signals. These scenarios are obtained by maneuvering the spacecraft over a reference command set point and same initial conditions.

1. **Reference command signal**

   The residual is generated corresponding to various number of input signals in the range of 5 to 15 degrees. The simulated results correspond to the reference signal of 1, 7 and 15 degrees are illustrated in Figure 4-4.

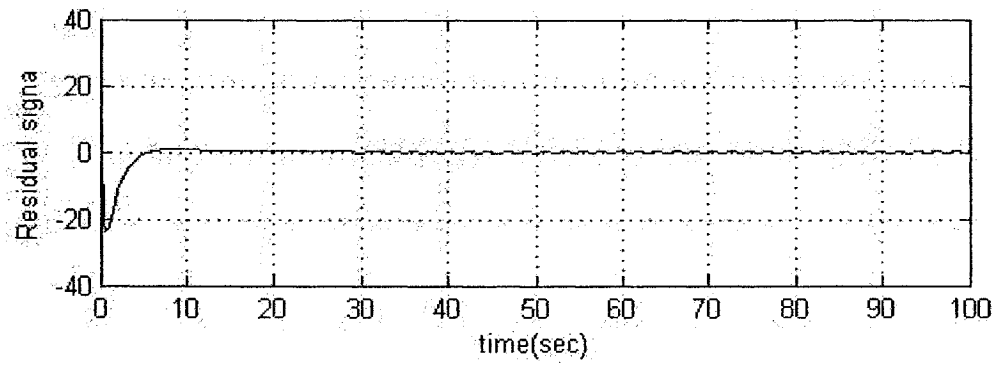

(a) Residual signal corresponding to the reference command input signal of 1°

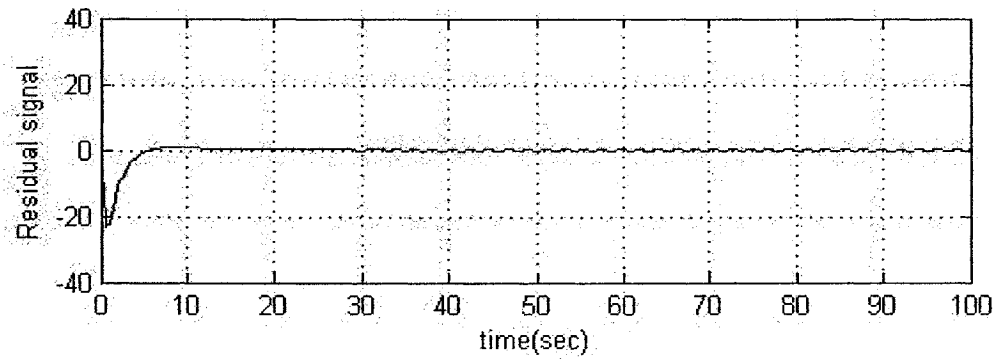

(b) Residual signal corresponding to the reference command input signal of 7°

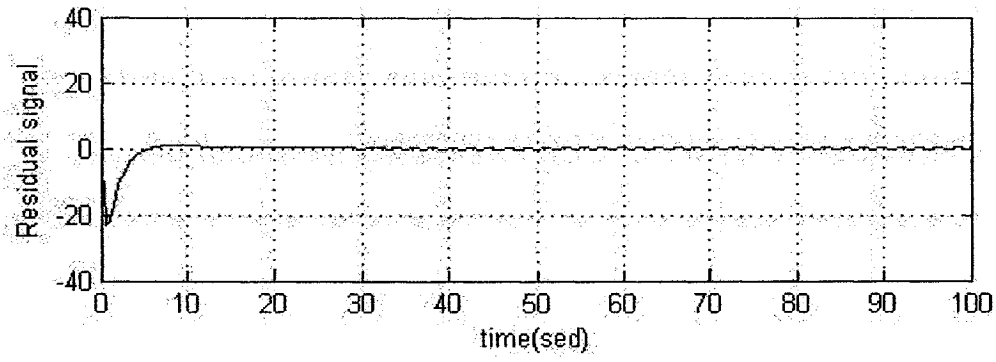

(c) Residual signal corresponding to the reference command input signal of 15°

Figure 4-4: The residual signal generated corresponding to the input signal of (a) 1°, (b) 7°, and (c) 15°

2. Initial conditions

To verify the influence of the initial conditions on the pattern of the residual signal, input signals with different pattern are applied to the system. The input signal pattern together with the residual generated correspond to that is shown in Figure 4-5.

As it can be seen from Figures 4-4 and 4-5, the residual errors will converge to zero, which is the ideal residual signature for a healthy system. Furthermore, the transient response time interval is less than 10 sec. These properties of residual signals provide them with sufficient qualifications to be used as signals for detecting and isolating faults.

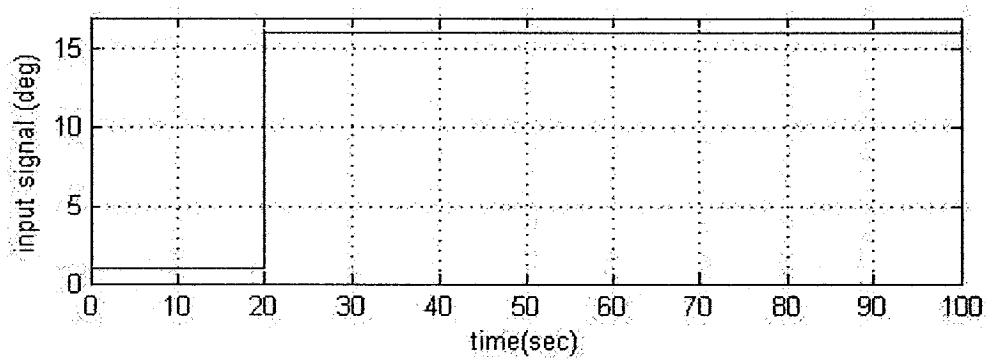

(i) Input signal

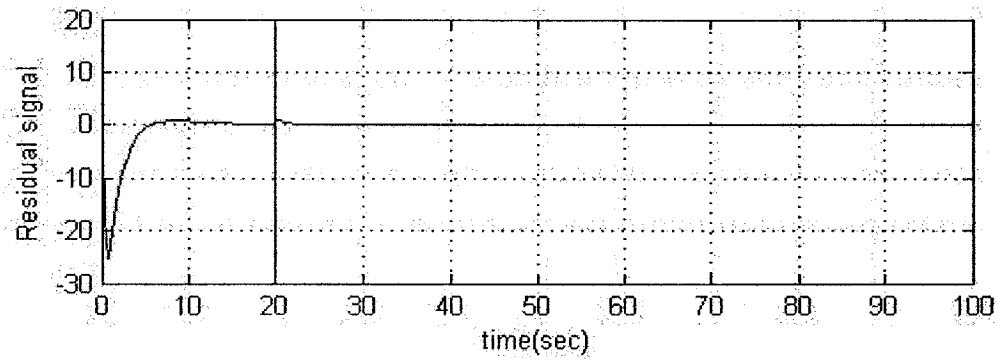

(ii) Residual signal

(a) The residual signal of figure (ii) is generated due to the input signal of plot (i)

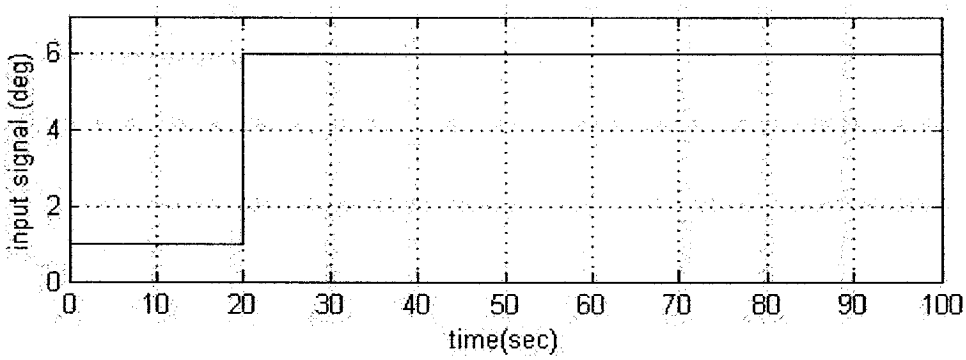

(i) Input signal

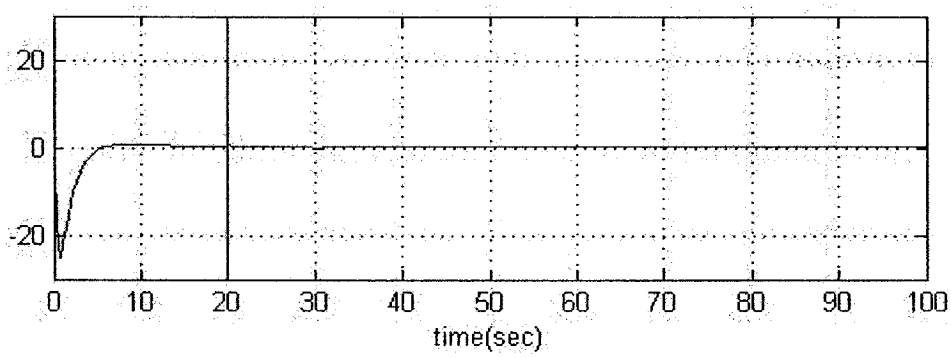

(ii) Residual signal

(b) The residual signal of figure (ii) is generated due to the input signal of plot (i)

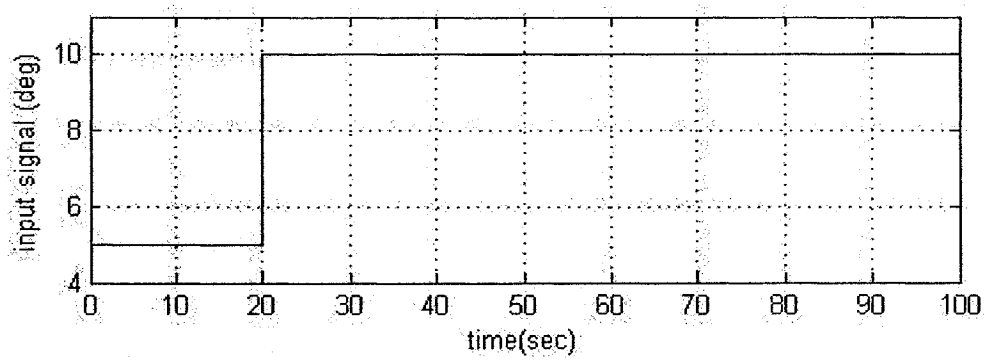

(i) Input signal

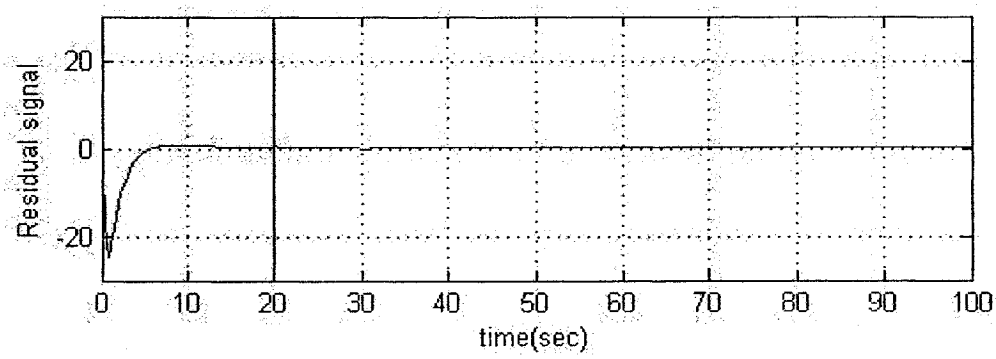

(ii) Residual signal

(c) The residual signal of figure (ii) is generated due to the input signal of plot (i)

Figure 4-5: Residual generated corresponding to different initial conditions applied through different input signals of (a), (b) and (c).

4.2. Linear Observer FDI Design (State Estimation Approach)

To get a better appreciation of the functionality and advantages of the parity space approach, our results for this method are compared to those of a linear observer approach to fault detection and diagnosis. A linear observer can be designed according to the descriptions given in Chapter 2. To design a linear observer the model of the system as illustrated in Figure 4-1 is used. The designed FDI scheme is then applied to a system that has the detailed representation of the reaction wheel and by considering the coupling effects of the spacecraft attitude dynamics.

As described earlier in Chapter 2, the estimator dynamic representation can be given by:

$$\dot{\hat{x}}(t) = A\hat{x}(t) + Bu(t) + Ge(t).$$

The state space representation of the whole system is expressed by equation (4.1). Using equation (4.1), the matrices A, B and C, introduced in Chapter 2 are specified as follows:

$$\begin{cases} A = \begin{bmatrix} 0 & 1 \\ 0 & -\dfrac{\tau_e + \tau_d}{J} \end{bmatrix} \\ B = \begin{bmatrix} 0 \\ G_d K_t \end{bmatrix} \\ C = \begin{bmatrix} -\dfrac{1}{I_{yy}} & 0 \end{bmatrix} \end{cases}$$

To obtain the observer gain, G, the transient response of the residual should be taken into consideration. The performance of the system during the steady state phase is of interest

also. Consequently, obtaining the gain, G, such that the residual transient response lasts less than the system transient response (t_s), is achievable. Using this condition, the gain matrix G is obtained as follows:

$$G=\begin{bmatrix} g1 \\ g2 \end{bmatrix}=\begin{bmatrix} -1000 \\ -20 \end{bmatrix}$$

using the following parameters $\tau_e=0.029$ V/rad/sec, $\tau_d=0$, $J=0.0077$ N-m-s^2, $K_t=0.029$ N-m/A, $G_d=0.19$ A/V and $I_{yy}=5$ N-m-s^2.

The observer method uses both input and output of the system to estimate the states of the system. According to the assumption we made earlier, the output of the actuator is not measurable, and we only have access to the output of the spacecraft. Therefore, as illustrated in Figure 4-2, the input of the actuator and output of the spacecraft are used as reference signals for the estimator block to obtain the estimate of the system states.

4.2.1. Simulation Results

For the purpose pf comparison, the same conditions that were studied in Section 4.2.1 have been applied to the linear observer-based approach and the residuals are obtained and are shown in Figure 4-7:

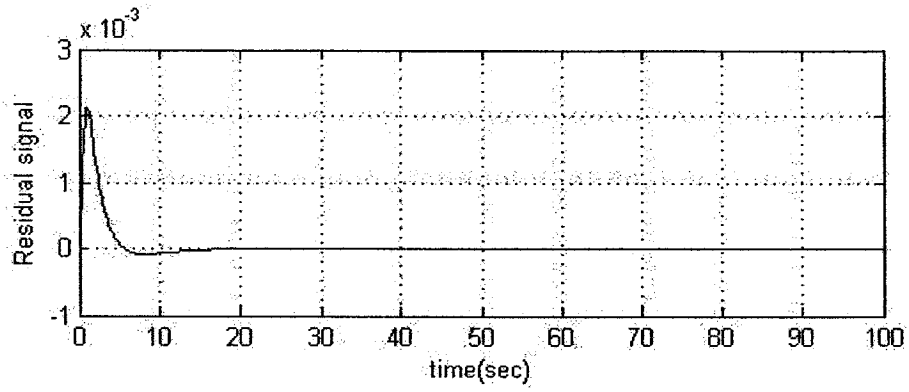

(a)

Residual signal corresponding to the reference command input signal of 1°

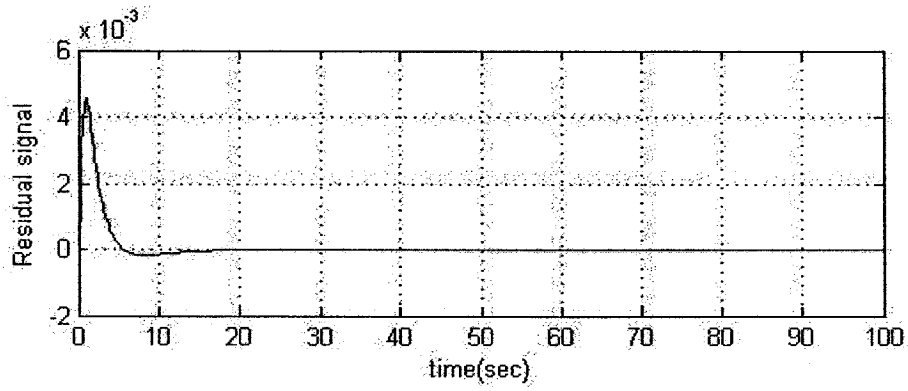

(b)

Residual signal corresponding to the reference command input signal of 7°

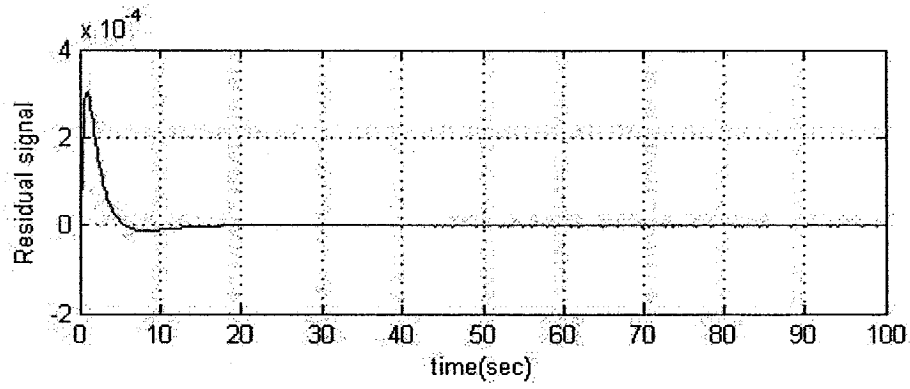

(c)

Residual signal corresponding to the reference command input signal of 15°

Figure 4-6: The residual signal generated corresponding to the input signal of (a) 1°,(b) 7°, and (c) 15°

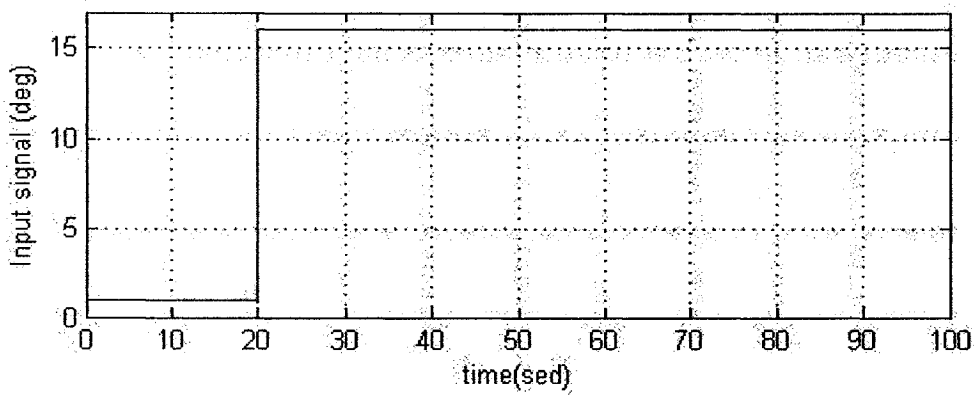

(i) Input signal

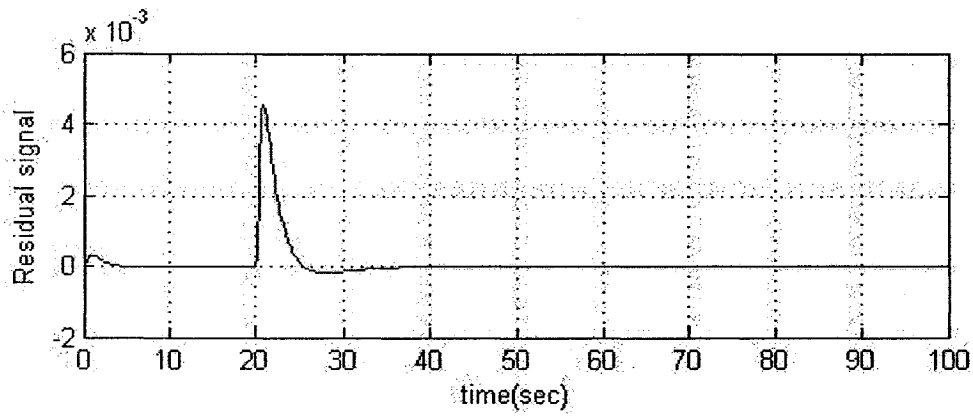

(ii) Residual signal

(a) The residual signal in figure (ii) is generated due to the input signal of figure (i)

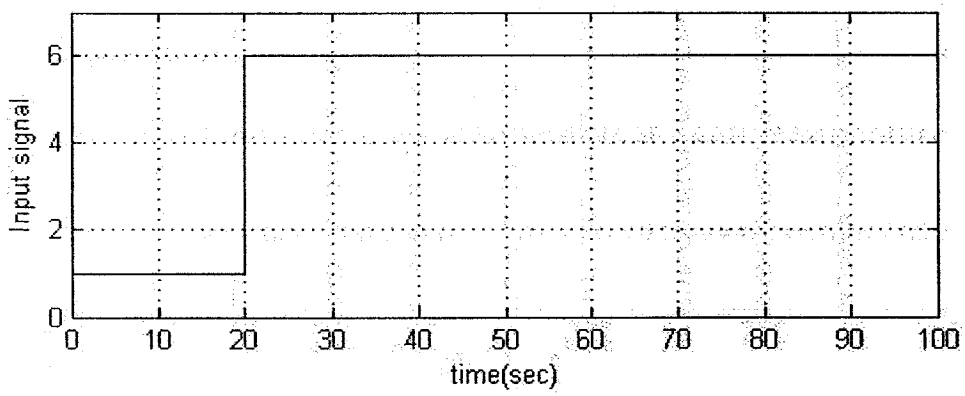

(i) Input signal

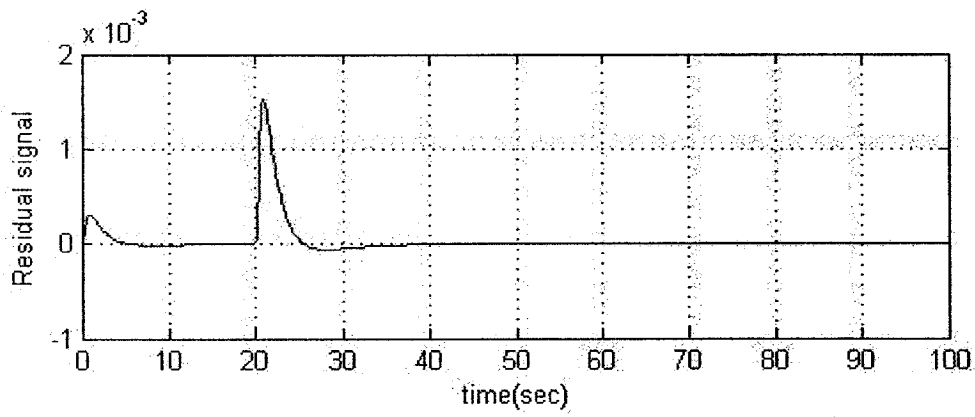

(ii) Residual signal

(b) The residual signal in figure (ii) is generated due to the input signal of figure (i)

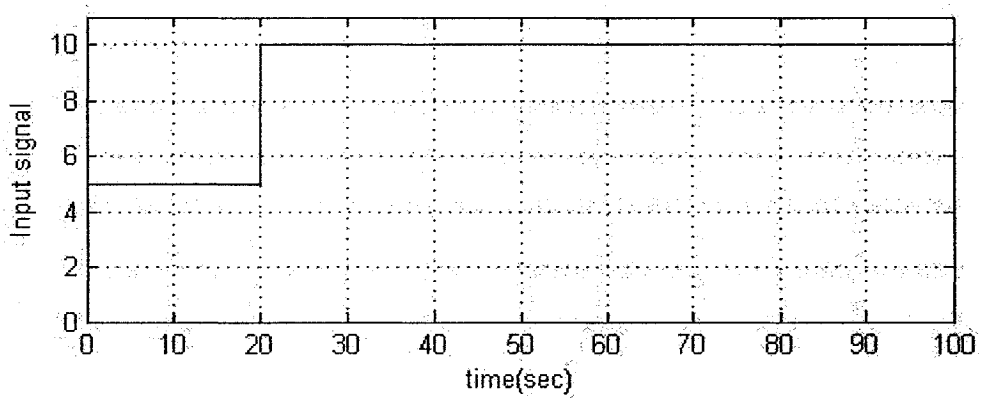

(i) Input signal

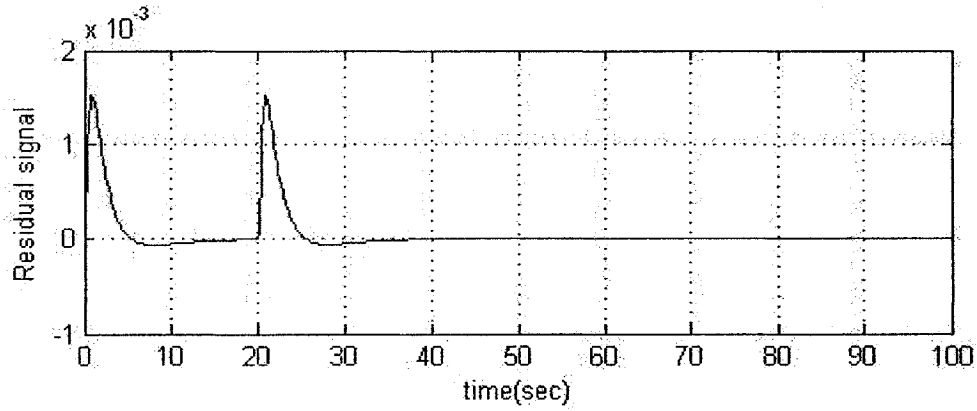

(ii) Residual signal

(c) The residual signal in figure (ii) is generated due to the input signal of figure (i)

Figure 4-7: Residual generated corresponding to different initial conditions applied for different input signals (a), (b) and (c).

Figure 4-7 shows the residual signal. As shown, the transient response for the residual converges to zero is less than 10 seconds, which satisfies our requirements for the settling time of the residual.

4.3. Safe Limits

Both parity space and observer methods developed in earlier subsections are required to be evaluated by applying them to a detailed block diagram of the attitude control dynamics of the spacecraft. The application of the above designed FDI systems to the spacecraft of Figure 3-8 will result in certain problems due to presence of disturbances and noise, system modeling discrepancies and the coupling effects of the spacecraft attitude dynamics. Safe limits should be specified such that the generated residual does not exceed them in presence of nominal noise and disturbance conditions. However, residuals should distinguishably cross over the threshold boundaries in presence of faults. Robustness of the system has a direct relation with selecting proper safe limits. As mentioned earlier, safe limits can be either fixed or variable. In this thesis, variable safe limits or safe boundaries are obtained corresponding to extensive set of simulations conducted under different conditions for each axis. These conditions may be specified as different inputs and diverse range of initial conditions together with random signals representing noise and disturbances. Furthermore, it should be noted that by running a large number of simulations the idea of variable threshold limits was derived, since the residual signal's band is seen to be related to the system input.

4.3.1.1. Selection of the Safe Limit

To obtain safe limits corresponding to residual generated through parity space-based and linear observer-based approaches to fault detection and diagnosis, extensive set of simulations are conducted. The standard deviation approach for this purpose did not work as the deviation of residual signals from the mean value is linearly independent from the input signal. Consequently, the limits are determined experimentally, and a set of relations between the reference signal and the mean value of the residual are obtained for each spacecraft attitude axis. The resulting safe limits are implemented for a set of reference command input signals of 1° to 15°, and work properly in this interval.

These limits are applied to the residual signals and the results are shown in Figures 4-7, 4-8 and 4-9 for the parity space approach and Figures 4-10, 4-11 and 4-12, for the linear observer approach corresponding to the input set point command of 5°. Since the residual signal is to be utilized in the steady state response, the safe limits are also designed to compensate the influence of the disturbances and noise and the system modeling mismatches in the steady state responses. Considering the fact that noise is a Gaussian random signal with zero mean and standard deviation of 0.06 deg, the simulated results depict the selected safe limits from the reference time index of t=500 sec which corresponds to the settling time of the response of the closed loop attitude system.

The limits could be applied to the system using the following set of expressions for both the parity space and linear observer approaches:

- Parity space-based approach

- Safe limits for the roll axis of the spacecraft:

$$Roll\ Axis\ Residual\ Mean \pm 0.00018\ (Spacecraft\ roll\ axis\ angle)^{0.8794}$$

- Safe limits for the pitch axis of the spacecraft:

$$Pitch\ Axis\ Residual\ Mean \pm 0.00021\ (Spacecraft\ pitch\ axis\ angle)^{0.366}$$

- Safe limits for the yaw axis of the spacecraft:

$$Yaw\ Axis\ Residual\ Mean \pm 0.00018\ (Spacecraft\ yaw\ axis\ angle)^{0.9173}$$

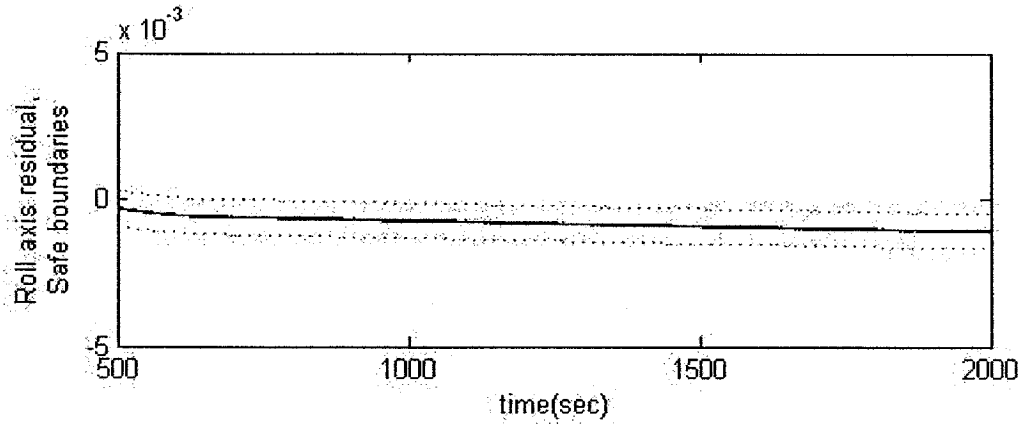

Figure 4-8: Safe limits derived and applied to the roll axis residual (parity space)

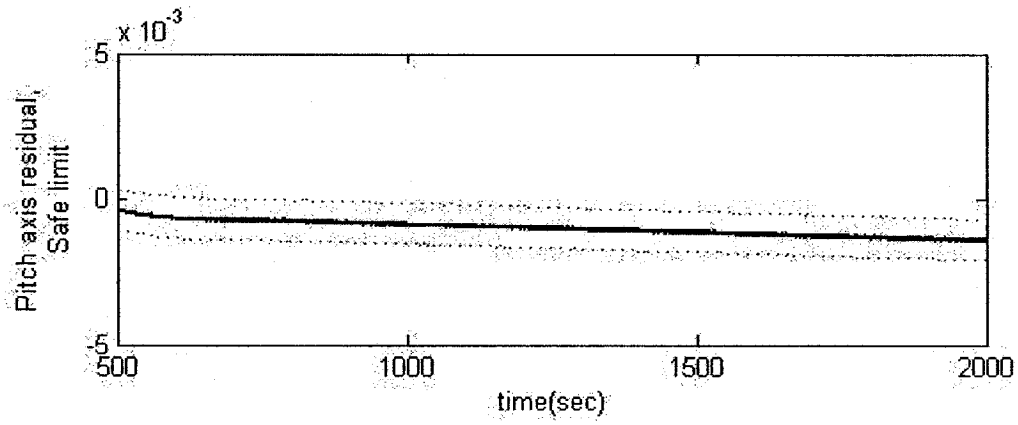

Figure 4-9: Safe limits derived and applied to the pitch axis residual (parity space)

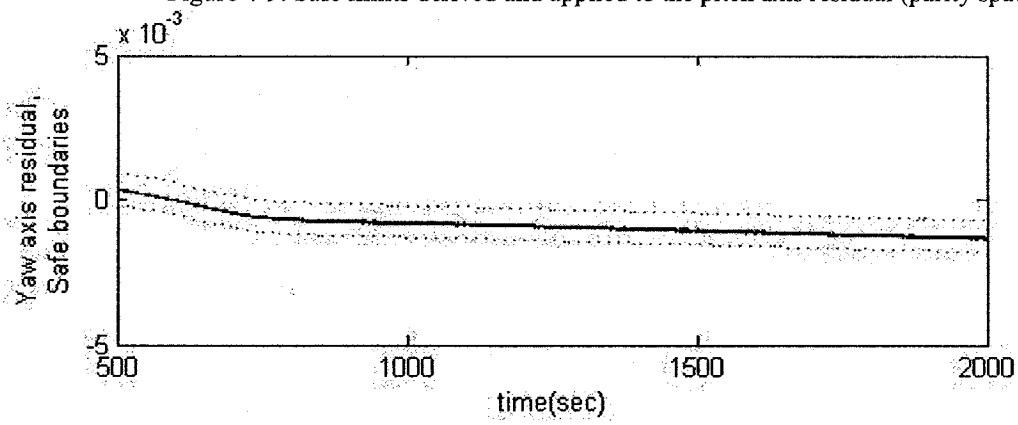

Figure 4-10: Safe limits derived and applied to the yaw axis residual (parity space)

- Linear observer-based approach

- Safe limits for the roll axis of the spacecraft

Roll Axis Residual Mean ± $(1.36\times10^{-5}$ *(Spacecraft roll axis angle)+* $2.27\times10^{-5})$

- Safe limits for the pitch axis of the spacecraft

Pitch Axis Residual Mean ± $(5.4\times10^{-4}$ *(Spacecraft pitch axis angle)–*$4.4\times10^{-4})$

- Safe limits for the yaw axis of the spacecraft

Roll Axis Residual Mean ± $(1.36\times10^{-5}$ *(Spacecraft yaw axis angle)+* $2.27\times10^{-5})$

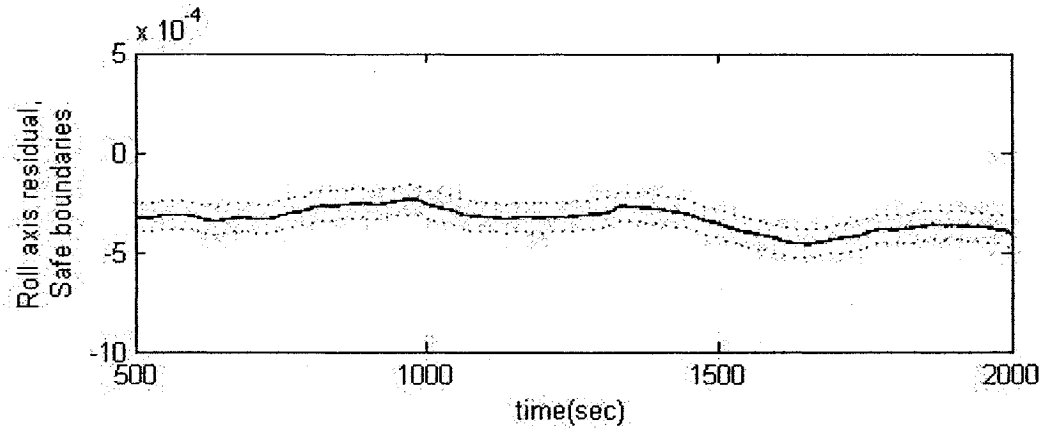

Figure 4-11 : Safe limits derived and applied to the roll axis residual (linear observer)

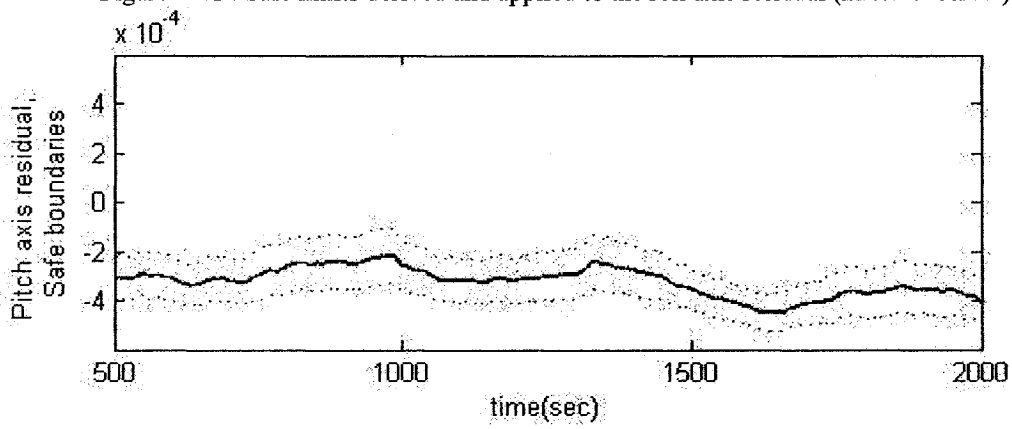

Figure 4-12: Safe limits derived and applied to the pitch axis residual (linear observer)

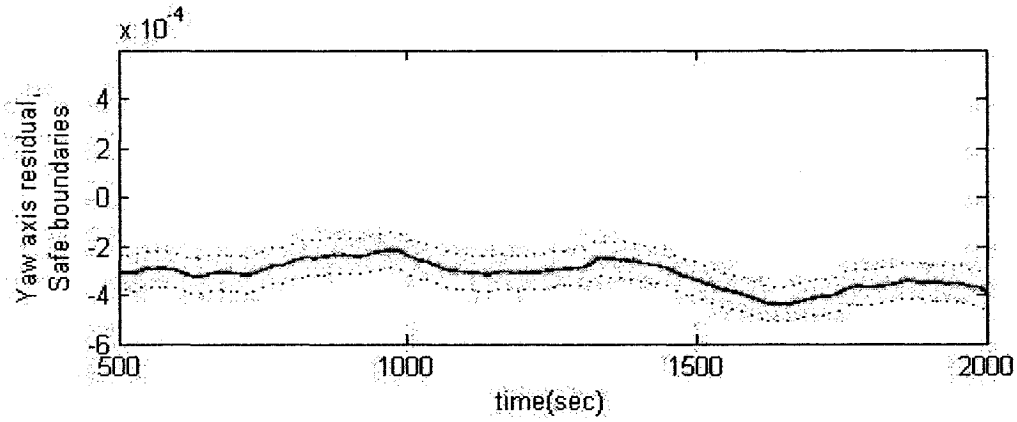

Figure 4-13: Safe limits derived and applied to the yaw axis residual (linear observer)

As shown from the above equations, the safe limits are dependent on the satellite output, therefore are functions of input signals.

4.4. Conclusion

In this chapter, a parity space approach and a linear observer approach to FDI are presented and specific algorithms for the satellite's ACS system are designed. The design was augmented by applying proper safe limits to the resulting generated residuals. In the next chapter, these FDI systems are applied to a faulty model of the spacecraft ACS system, and their performances under different types of faults in the V_{BUS} and K_t of the reaction wheel are investigated.

Chapter 5 : Comparative Analysis and Simulation Results

As mentioned in Chapter 1, in this thesis the occurrence of two types of faults, namely in K_t and V_{BUS} of a reaction wheel in the attitude control system of a spacecraft is considered. In this chapter, various scenarios for the occurrence of faults in the above mentioned components are considered. Both linear observer-based and parity space-based approaches are designed and implemented in Chapter 4 for the purpose of fault detection and diagnosis in the attitude control system of the spacecraft. In this chapter our objective is to compare the relative advantages and disadvantages of these two schemes.

5.1. Fault in K_t

In this section, first the sensitivity of both observer-based and parity space-based approaches to faults are evaluated and determined. Next, different types of faults (that is permanent and intermittent) are applied to the reaction wheel of the satellite system. Furthermore, the cross coupling characteristics of the satellite dynamics on the performance of the FDI schemes are investigated.

5.1.1. Sensitivity

Sensitivity is a function of a fault detection system that is determined by the minimum amount of fault which is detectable by the utilized fault detection system. Various simulations have shown that the sensitivity of both linear observer-based and parity space-based approaches to fault detection strongly depend on input signals that are

applied to the system. Due to this fact, the sensitivity of the two considered approaches is investigated under two different reference trajectory signals.

The sensitivity of the parity space-based and the linear observer-based schemes for the roll axis are shown in Figure 5-1 corresponding to the reference input signal of *1* degree and Figure 5-2 corresponding to the reference input signal of *5* degrees. In both these figures the fault has occurred at $t=700$ sec.

As mentioned earlier, fault or failure can be specified as any change in the parameters of the system such that it leads to an unacceptable result. Using this specification, to implement the fault in the parameter K_t in the reaction wheel of the spacecraft ACS, the parameter K_t is manipulated according to the following equation:

$$\begin{cases} K_t & t < 700 \\ K_t + AK_t & t \geq 700 \end{cases} \tag{5.1}$$

where the coefficient A is specified such that the residual crosses over the safe limits, which specify the threshold boundaries of the sensitivity of the FDI system.

As can be seen from Figure 5-1, the value of the coefficient A for the linear observer-based scheme is equal to *0.09*, while this value for the parity space-based approach to fault detection is equal to *0.05*. This shows clearly that in the roll axis of the spacecraft, the parity space scheme is capable of detecting smaller magnitude of faults as compared to the observer-based scheme for this specified reference set point.

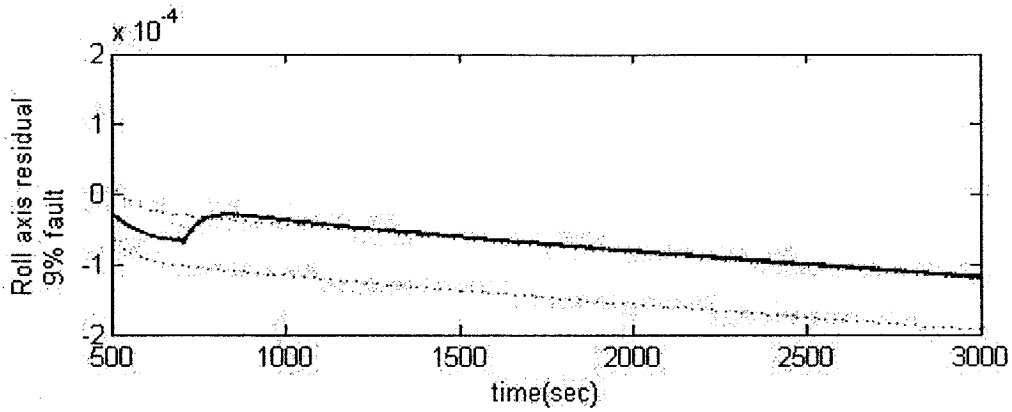

(a) Linear observer fault detection for 9% fault

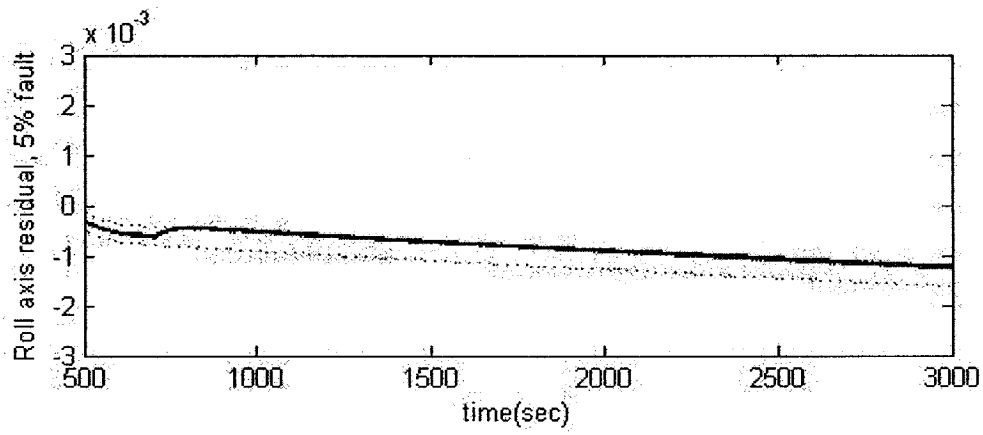

(b) Parity space fault detection for 5% fault

Figure 5-1: The minimum amount of fault in the roll axis that is detected by (a) linear observer-based and (b) Parity space-based schemes for a reference set point angle of 1°

According to the earlier results stated in this section, the sensitivity of the fault detection system is dependent on the system input as well. To investigate the influence of the system input on the residual signal, the results presented above are now obtained for a different reference command signal. These results are illustrated in Figure 5-2:

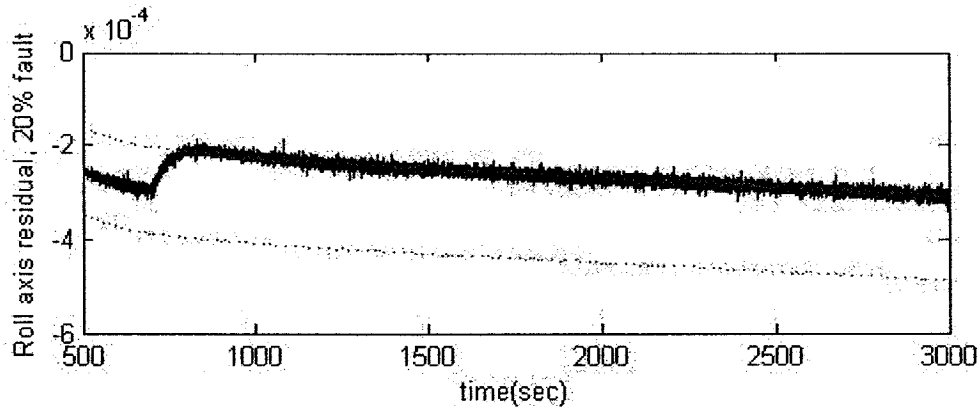

(a) Linear observer fault detection for 20% fault

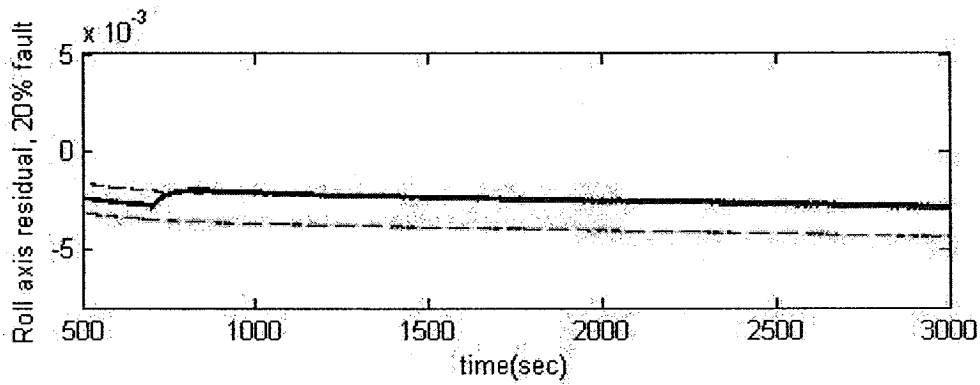

(b) Parity space fault detection for 20% fault

Figure 5-2: The minimum amount of fault in the roll axis that is detected by (a) linear observer-based and (b) parity space-based scheme for a reference set point angle of 5°

As can be seen from the above figure, the value of the coefficient A in equation (5.1), is equal to *0.20* for both fault detection approaches. It is obvious that the larger the reference command signal is, the less sensitive the fault detection system becomes to occurrence of fault. This is more dominant in the parity space-based scheme for the roll axis than a linear observer-based scheme. For the other two spacecraft axes, the results are now summarized in Table 5-1.

Input signal set point		*Linear observer approach to FD*	*Parity space approach to FD*
	Applied axis	Min detected amount, (Coefficient *A*)	Min detected amount, (Coefficient *A*)
1 (deg)	Roll axis	0.09	0.05
	Pitch axis	0.25	0.05
	Yaw axis	0.10	0.09
5 (deg)	Roll axis	0.20	0.20
	Pitch axis	6	0.10
	Yaw axis	0.30	0.20

Table 5-1: Sensitivity of the two fault detection (FD) approaches to occurrence of faults in the component K_t

As can be seen from Table 5-1, in general the sensitivity of the parity space-based approach to fault in K_t is higher than that of the linear observer approach. The most significant difference appears in the pitch axis for the input set point signal of *5* degrees, for which the coefficient *A* for the linear observer-based approach is *60* times bigger than the coefficient *A* for the parity space-based approach. This large difference arises due to the fact that the noise and disturbances applied to the system influence the residual generated by the linear observer-based approach a lot more than the residual obtained by the parity space-based approach, specially in the pitch axis. To compensate for the influences of these disturbances and noises, the safe limits with larger variance and wider threshold bands should be applied to the system. This will reduce the sensitivity of the fault detection system to the fault as well. To substantiate this fact, the following set of figures show simulation results for the pitch axis.

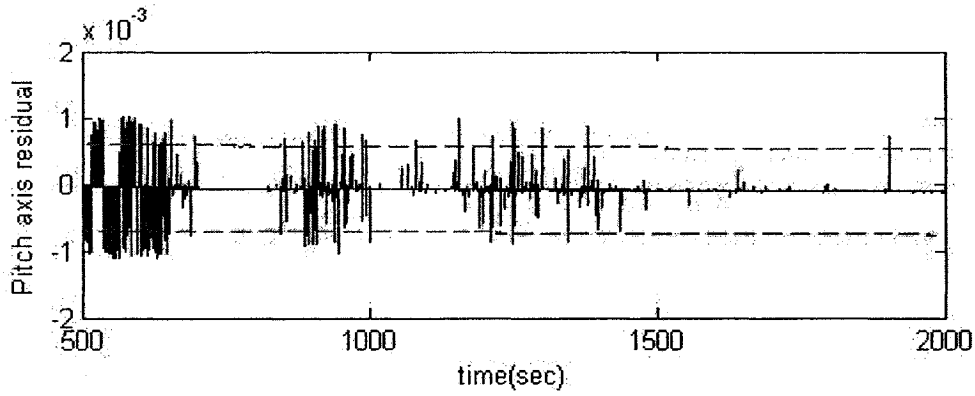

(a) The pitch axis residual when a fault with a loss of effectiveness of 80% of K_t is occurred in the roll axis of the spacecraft

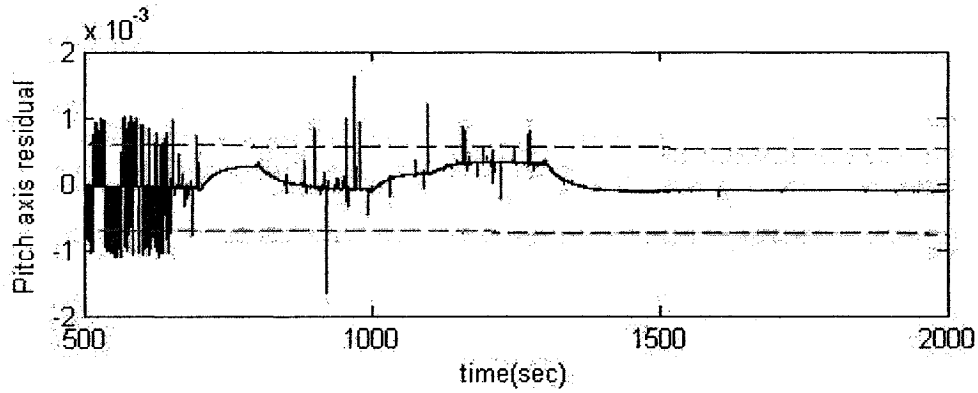

(b) The pitch axis residual when a fault with a loss of effectiveness of 70% of K_t is occurred in the pitch axis of the spacecraft

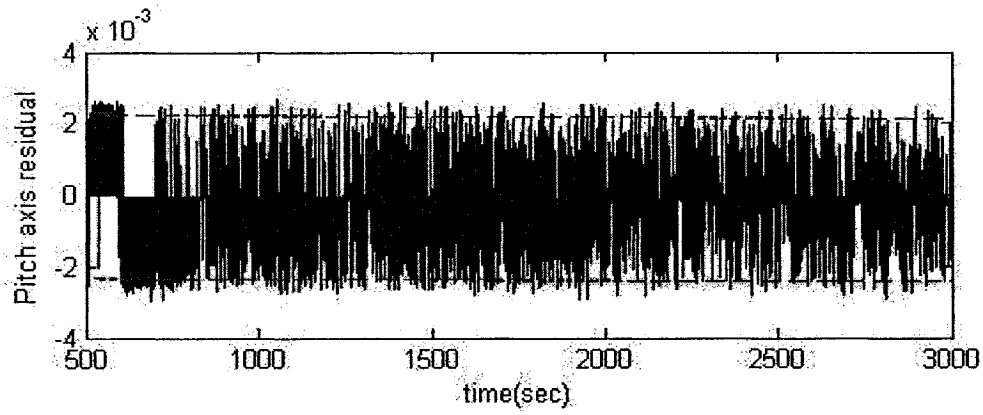

(c) The pitch axis residual when a fault with a loss of effectiveness of 80% of K_t is occurred in the yaw axis of the spacecraft

Figure 5-3: The effects of noise and disturbances on the residual generated by the pitch axis of a spacecraft when (a) faults occur in the roll axis, (b) faults occur in the pitch axis, and (c) faults occur in the yaw axis of the spacecraft

The results shown in Figure 5-3 restrict the designer to apply wider threshold band limits for residuals generated by the pitch axis.

5.1.2. Permanent Faults

A permanent fault is characterized as a fault that occurs at a given point in time and continues affecting the system thereafter. Now that the sensitivity of the fault detection systems is verified, a comparative analysis on the fault detection times corresponding to these methods are of special interest to be investigated. For this purpose, permanent faults which are sufficiently large in magnitude to be detected by both approaches are considered.

The permanent fault is set to be applied to the reaction wheel of the satellite system at the time instant t=700 sec, under the following conditions:

$$\begin{cases} reference\ command\ signal\ (system\ input\ signal) = 2(\text{deg}) \\ f = AK_t \qquad\qquad for \quad A = 0.7 \end{cases}$$

The simulation results implementing the above specified fault in the reaction wheel of the roll axis are illustrated in Figure 5-4.

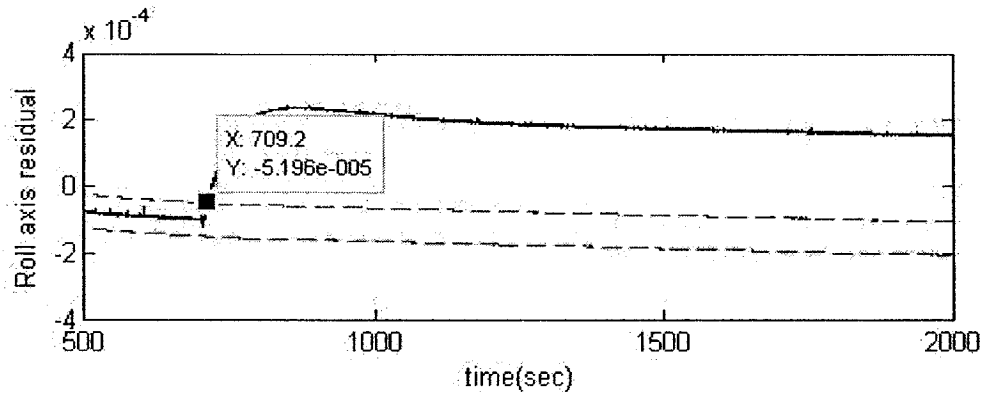

(a) Linear observer fault detection

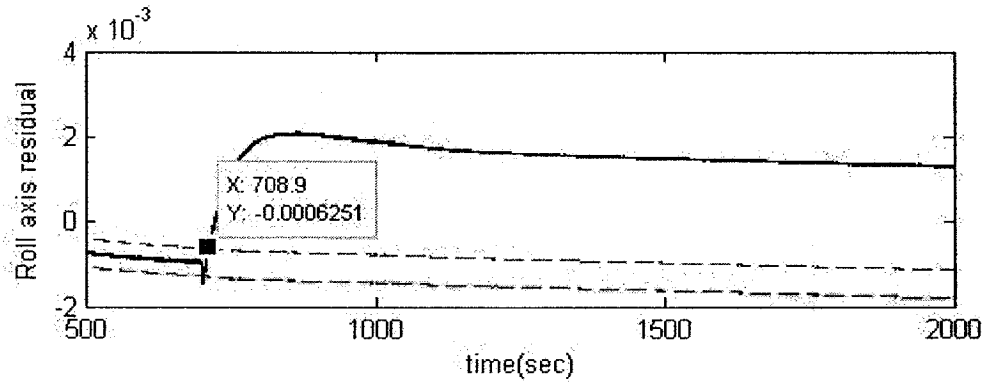

(b) Parity space fault detection

Figure 5-4: The delay in detecting of a fault in the roll axis by using (a) linear observer and (b) parity space approaches

Figure 5-4 (a) depicts the results by using a linear observer-based and Figure 5-4 (b) depicts the results by using the parity space-based approach. Various simulations show that the residual signal caused due to only noise, remains or ripples out of the safe limits after a short period of time in the order of 1 to 3 seconds. As a result, the fault detection time is set to be 3 seconds after the residual crosses over the safe limits. If during these 3 seconds the residual remains outside of the threshold band then one would consider that a fault is detected.

In the above figure, X specifies the time of detecting a fault while Y specifies the magnitude of the residual at that time. The results for the other two axes are summarized in Table 5-2.

Input signal set point		*Linear observer approach to FD*	*Parity space approach to FD*
	Applied axis	Detection time (sec)	Detection time (sec)
2 (deg)	Roll axis	709.2	708.9
	Pitch axis	Not detected	708.0
	Yaw axis	711.9	708.1

Table 5-2: Detection times for the linear observer-based and parity space-based approaches to fault detection

It can be seen from the above table that the delay in the detection time in parity space-based approach is smaller than the delay in the detection time of the linear observer-based approach. Having a small delay in the detection time, as mentioned earlier in Chapter 2, is one of the requisites for a fault detection system. As in the previous case, it is shown here that having wide safe thresholds in the pitch axis has caused a problem in detecting the fault using a linear observer approach. The residual did not cross over the safe thresholds in the linear observer-based approach, while the same fault is detected by the parity space-based approach, *8* seconds after it has occurred. The results for the pitch axis are shown in Figure 5-5. Figure 5-5 (a) shows the safe limits when applied to the residual generated by the linear observer-based approach. Due to its variance, the residual does not cross over the safe limits threshold and therefore the fault is not detected. In this figure the effects of noise on the residual has led one in selecting a wide band for safe limit thresholds as seen during the time interval before the 700 seconds. However, Figure 5-5(b) shows the residual signal as a result of implementation of the parity space-based

fault detection scheme which crosses over the safe limits thresholds. As a result, the fault can be detected by the parity space-based method.

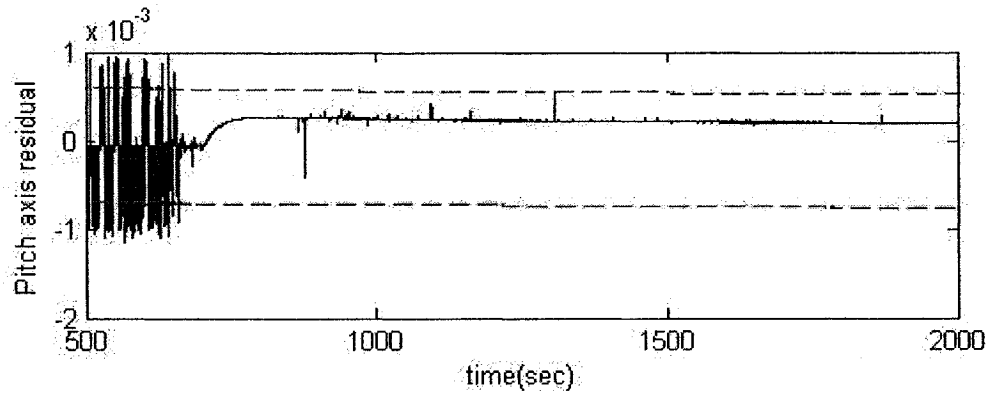

(a) Linear observer fault detection

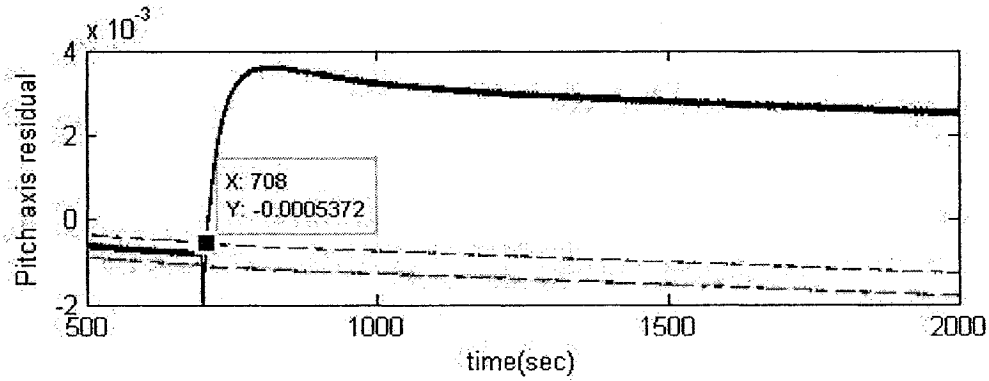

(b) Parity space fault detection

Figure 5-5: The delay in detecting of a fault in the pitch axis by using (a) linear observer-based and (b) parity space-based approaches

5.1.3. Intermittent Faults

An intermittent fault, as illustrated in Figure 5-6, is specified so that it affects the system during only a limited period of time. In this section intermittent faults are injected to the component K_t of the reaction wheel in the attitude control system of the spacecraft. The component K_t is infected such that:

$$\begin{cases} K_t & t < 700 \text{ sec} \\ K_t - A_1 K_t & 700 \le t < 800 \text{ sec} \\ K_t & 800 \le t < 1000 \text{ sec} \\ K_t - A_2 K_t & 1000 \le t < 1100 \text{ sec} \\ K_t - A_3 K_t & 1100 \le t < 1300 \text{ sec} \\ K_t & t \ge 1300 \text{ sec} \end{cases}$$

where the coefficients A_1, A_2 and A_3 are set to be *1*, *0.9*, and *1.5*, respectively. The main goal for the present test case is to verify that when a fault vanishes, the residual will also get back within the safe limits thresholds.

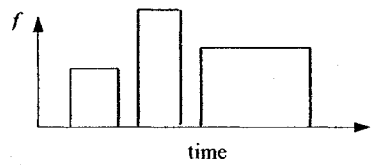

Figure 5-6: Intermittent fault

The fault considered is now to be detected by utilizing both linear observer-based and parity space-based approaches. The simulation results for the roll axis are shown in Figure 5-7. The results for both detection approaches are compared with one another in terms of detection capability and delay in the time of detection. The results are summarized in Table 5-3. In Table 5-3, it was shown that the K_t fault that occurred at time *700* sec in the roll axis of the spacecraft is detected at the time *715.8* sec by the linear observer and the time *712.2* sec by the parity space fault detection systems. This fault disappears at the time *800* sec, however, the fault removal is detected at *916.1* sec by the linear observer and *899.3* sec by the parity space fault detection systems. Consequently, the intermittent fault is easily detected by both FD approaches although with some delay in time. The behavior of the residual signal in the case of occurrence of intermittent fault in the roll axis is illustrated in Figure 5-7. This figure shows that the

residual signal follows the fault pattern, and when a fault disappears the residual returns back within its safe limits thresholds. The differences between the two approaches in detecting the above specified intermittent faults as illustrated in Table 5-3, are in (a) detection time, and (b) the detectibility of the fault that is applied to the pitch axis.

Time	Detection time in the roll axis		Detection time in the pitch axis		Detection time in the yaw axis	
	Linear observer	Parity space	Linear observer	Parity space	Linear observer	Parity space
700 (sec)	715.8	712.2	Not detected	708.2	712.4	712
800 (sec)	916.1	899.3	Not detected	903.2	950.8	923
1000 (sec)	1020	1020	Not detected	1014	1014	1014
1100 (sec)	1106	1104	Not detected	1104	1106	1103
1300 (sec)	1382	1307	Not detected	1378	1420	1400

Table 5-3: Detection time for the linear observer-based and parity space-based schemes to intermittent faults

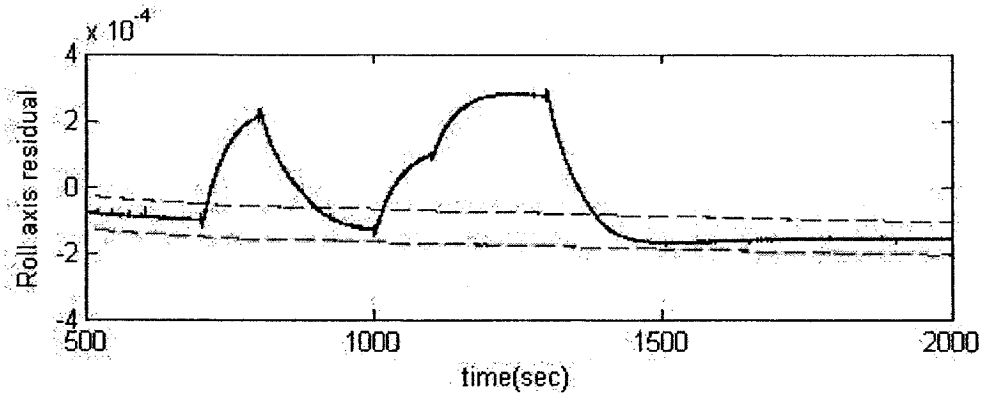

(a) Linear observer fault detection

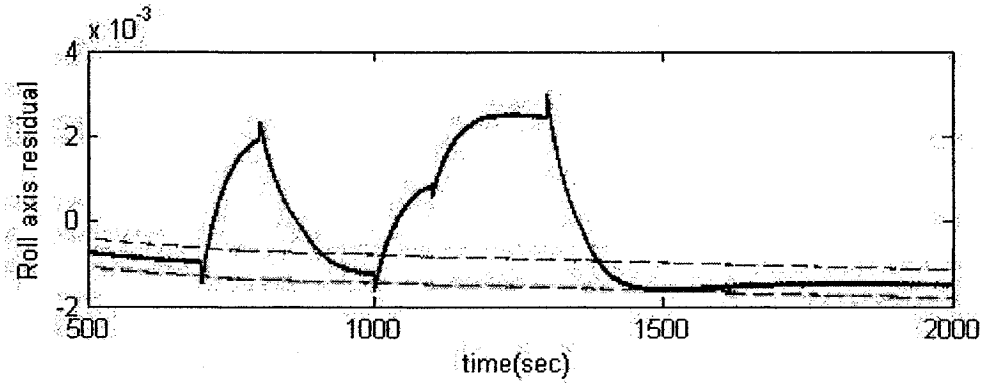

(b) Parity space fault detection

Figure 5-7: Intermittent fault detection in the roll axis for the (a) linear observer-based and (b) parity space-based approaches

5.2. Fault in the V_{BUS}

In this section the performance of linear observer-based and parity space-based methods to fault detection and diagnosis is verified subject to occurrence of faults in the V_{BUS} variable of the reaction wheel in the attitude control system of the spacecraft. A comparison of the performance of the above two methods to this type of fault is investigated. The results obtained will provide one with information on the performance of each method under different types of faults occurred in this component.

5.2.1. Sensitivity

As mentioned earlier an important requirement for a fault detection system is its sensitivity to different types of faults. In this section we investigate this issue for the two designed fault detection systems corresponding to the occurrence of faults in the V_{BUS} component of the reaction wheel of the ACS. The simulated results for the roll axis are illustrated in Figure 5-8.

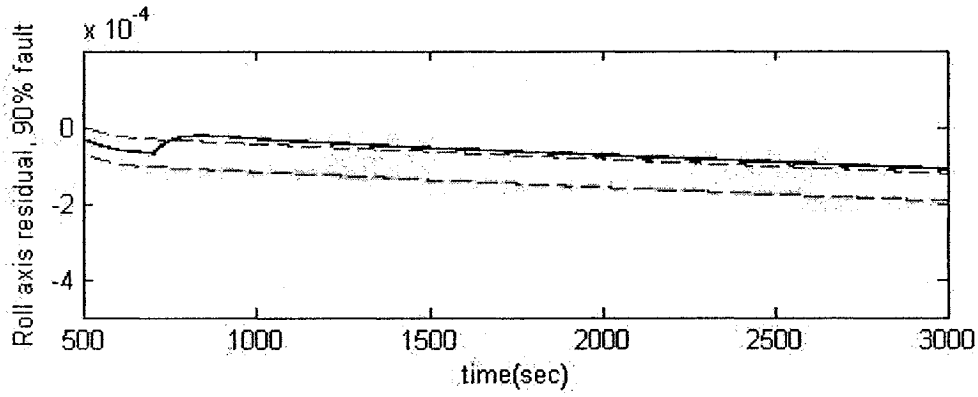

(a) Linear observer fault detection

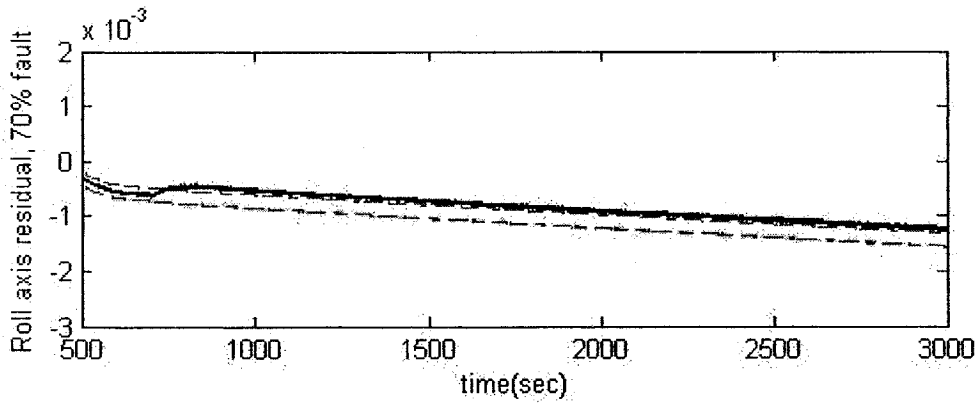

(b) Parity space fault detection

Figure 5-8: Minimum V_{BUS} fault in the roll axis detected by (a) linear observer-based and (b) parity space-based approaches

To obtain the previous result, the reference set point command signal applied to the satellite system is set to 1 degree, and the fault occurs at the time instant 700 seconds

characteristics. The fault that is injected to the reaction wheel of the satellite system has the following characteristics:

$$\begin{cases} V_{BUS} & t < 700 \\ V_{BUS} + AV_{BUS} & t \geq 700 \end{cases};$$

According to the simulation results shown in Figure 5-8, the coefficient A in the above equation is equal to 0.9 for the linear observer-based approach and 0.7 for the parity space-based approach. This shows that the sensitivity of the parity space approach to this type of fault is higher when compared with the sensitivity of the linear observer-based approach. The results obtained for the other two axes as well as a different reference set point command signal of the spacecraft are summarized and compared relatively in Table 5-4.

Input signal set point command		***Linear observer approach to FD***	***Parity space approach to FD***
	Applied axis	Min detected value, (Coefficient A)	Min detected value, (Coefficient A)
1 (deg)	Roll axis	0.90	0.70
	Pitch axis	2.00	0.70
	Yaw axis	0.90	0.70
5 (deg)	Roll axis	1.80	0.90
	Pitch axis	30.00	0.80
	Yaw axis	1.80	0.90

Table 5-4: Sensitivity of the linear observer-based and parity space-based approaches to fault detection to the occurrence of faults in the V_{BUS} component

5.2.2. Permanent and Intermittent Faults

To complete verification of the performance of the designed fault detection methods under the assumption of occurrence of faults in the bus voltage of the reaction wheel, permanent and intermittent faults that are detectable by both methods are applied to the

reaction wheel of the ACS system. The characteristics of the permanent faults as well as intermittent faults that are applied to the V_{BUS} component are given below:

- Permanent faults:

$$\begin{cases} V_{BUS} & t < 700 \\ V_{BUS} + AV_{BUS} & t \geq 700 \end{cases}$$

where A is equal to 2, and

- Intermittent faults:

$$\begin{cases} V_{BUS} & t < 700 \text{ sec} \\ V_{BUS} - A_1 V_{BUS} & 700 \leq t < 800 \text{ sec} \\ V_{BUS} & 800 \leq t < 1000 \text{ sec} \\ V_{BUS} - A_2 V_{BUS} & 1000 \leq t < 1100 \text{ sec} \\ V_{BUS} - A_3 V_{BUS} & 1100 \leq t < 1300 \text{ sec} \\ V_{BUS} & t \geq 1300 \text{ sec} \end{cases}$$

where A_1, A_2, and A_3 are equal to 1.2, 1.1 and 1.7, respectively. The simulated results are obtained to evaluate the performance requirements of both methods as discussed in Chapter 2, including the delay in the detection time and the rate of the correct detection. These attributes are verified under a reference set point command signal that is equal to 2 degrees. These results are summarized in Table 5-5 and Table 5-6.

As shown in Table 5-5, the delay in the detection time is smaller in the parity space-based approach when compared to the linear observer-based approach. Clearly, the main difference is in detecting a fault in the pitch axis. The V_{BUS} fault applied to the pitch axis

can not be detected by the linear observer-based approach since the safe limits thresholds can not be determined successfully for this axis. The simulated results for the pitch axis are illustrated in Figure 5-9, which shows the threshold ranges of the safe limits corresponding to both approaches.

Input signal set point command		*Linear observer-based approach to FD*	*Parity space-based approach to FD*
2 (deg)	Applied axis	Detection time (sec)	Detection time (sec)
	Roll axis	727.8	714.4
	Pitch axis	Not detected	708.0
	Yaw axis	742.6	718.9

Table 5-5: Detection time of the linear observer-based and parity space-based approaches to a permanent fault

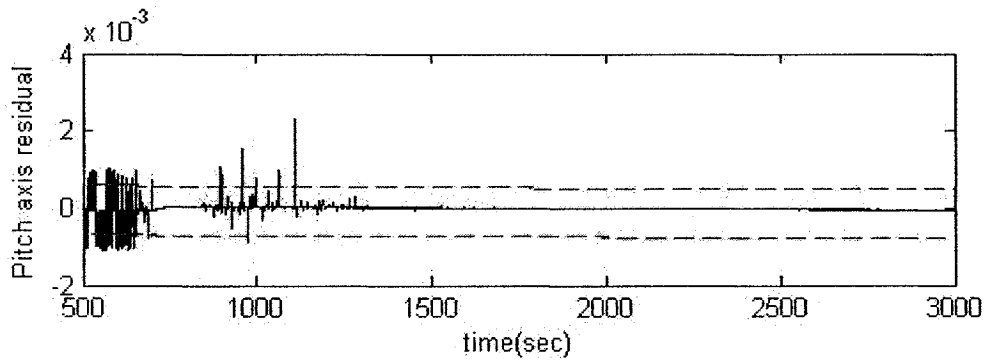

(a)Linear observer fault detection

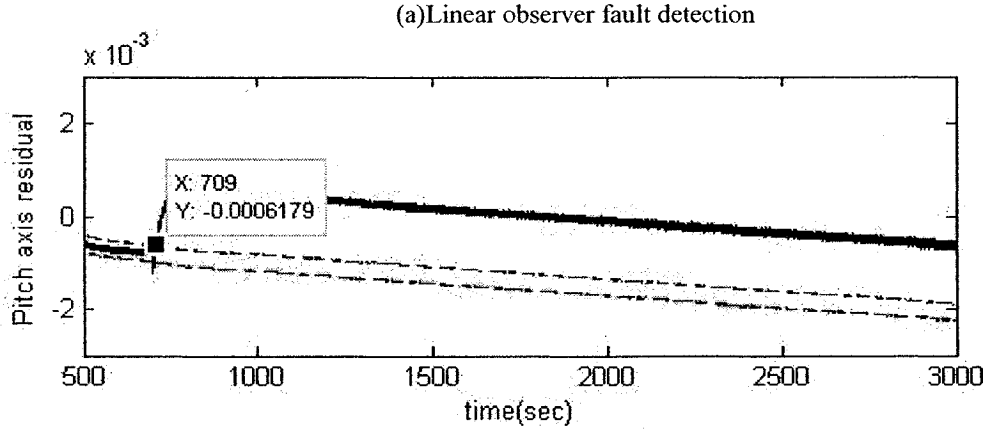

(b) Parity space fault detection

Figure 5-9: Permanent fault detection in the pitch axis for (a) linear observer-based and (b) parity space-based approaches

The simulation results for the occurrence of intermittent faults in the roll axis are provided in Figure 5-10. The comparison between linear observer-based and parity space-based approaches is shown in Table 5-6.

Fault Injection Time Instant	Detection time in the roll axis		Detection time in the pitch axis		Detection time in the yaw axis	
	Linear observer	Parity space	Linear observer	Parity space	Linear observer	Parity space
700 (sec)	Not detected	736.2	Not detected	715	Not detected	759
800 (sec)	Not detected	837.7	Not detected	831.3	Not detected	892
1000 (sec)	Not detected	1020	Not detected	1020	Not detected	1037
1100 (sec)	1120	1104	Not detected	1104	1118	1103
1300 (sec)	1348	1335	Not detected	1355	1411	1350

Table 5-6: Detection time of the linear observer and parity space approaches to intermittent faults

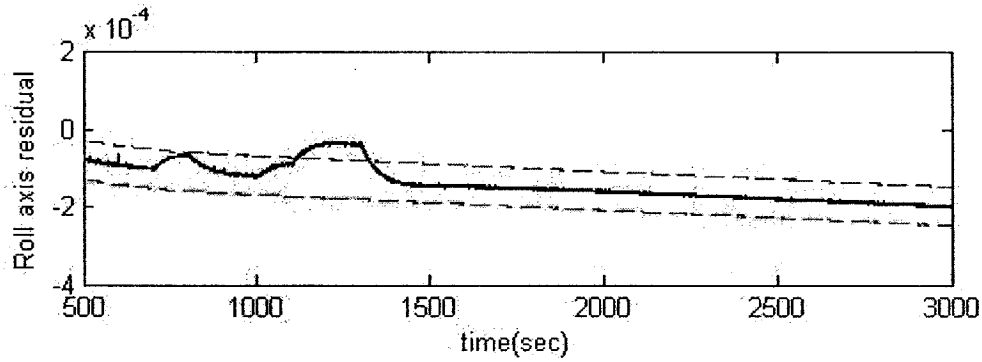

(a)Linear observer fault detection

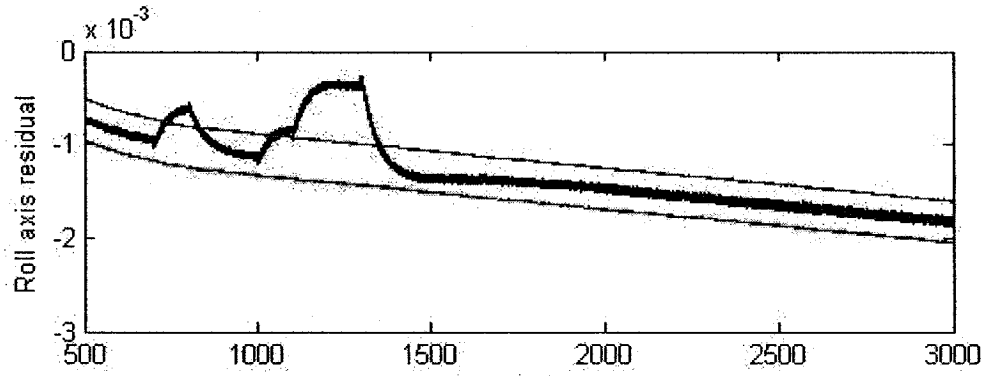

(b) Parity space fault detection

Figure 5-10: Detection of the intermittent fault in the V_{BUS} in the roll axis for the (a) linear observer-based and (b) parity space-based approaches

5.3. Multiple Faults in K_t and V_{BUS}

One of the most important requirements for the fault detection and diagnosis system is the capability of being able to detect multiple faults. This means that from the generated residual signal, the system is required to detect if multiple faults have occurred and if so to be able to isolate them. To verify this property for our proposed parity space fault detection system, different scenarios are considered and implemented in this section. It was shown earlier in simulated results of Figures 5-1, 5-2 and 5-7 that the changes in the residual signals for the faults in K_t have the same behaviors, as that of the residuals generated due to the occurrence of faults in V_{BUS}. Due to this fact, multiple faults in one

axis can not be detected and isolated simultaneously. Consequently, we have restricted our verification investigations to multiple faults in different axes. The scenarios and case studies that we have pursued are specified in Table 5-7:

Scenario/Case Study	Roll Axis	Pitch Axis	Yaw Axis
1	V_{BUS}	K_t	No fault
2	V_{BUS}	No fault	K_t
3	K_t	K_t	No fault
4	K_t	No fault	K_t
5	V_{BUS}	V_{BUS}	No fault
6	V_{BUS}	No fault	V_{BUS}

Table 5-7: Multiple fault scenarios and case studies

In the above table the applied faults in K_t and V_{BUS} follow the specifications and characteristics as follows:

$$\begin{cases} K_t & t < 700 \\ K_t + AK_t & t \geq 700 \end{cases}; \text{ where } A=0.7$$

$$\begin{cases} V_{BUS} & t < 700 \\ V_{BUS} + AV_{BUS} & t \geq 700 \end{cases}; \text{ where } A=2$$

Different simulations have indeed shown that occurrence of faults in different axes of the spacecraft corresponding to K_t and V_{BUS} components are independent of each other. On the other hand, any fault in one of these components does not affect the residual generated in the other two axes. To support this fact, the residuals generated from the linear observer and parity space designed approaches for these scenarios and case studies

are shown in Figures 5-11, 5-12, 5-13, 5-14, 5-15 and 5-16 for all the roll, pitch and yaw axes.

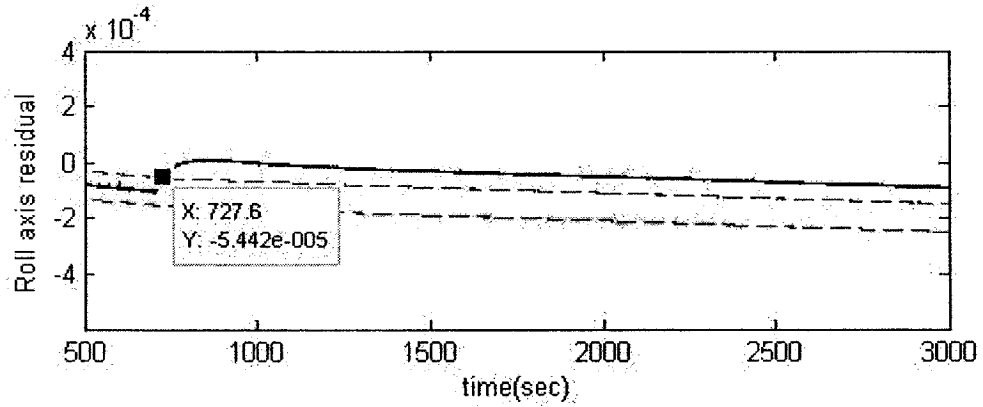

(i)

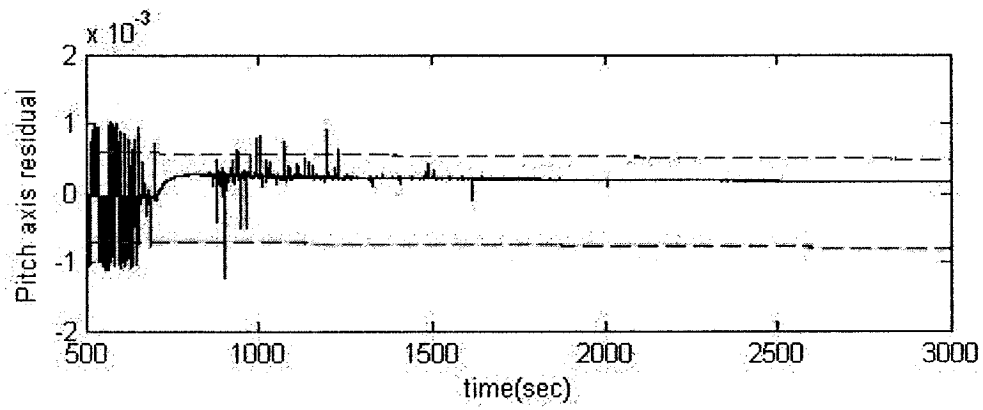

(ii)

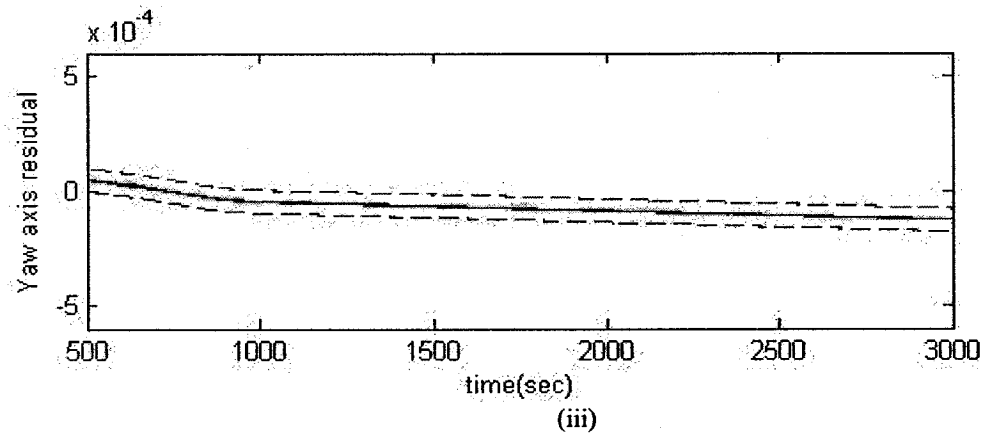

(iii)

(a) Linear observer fault detection

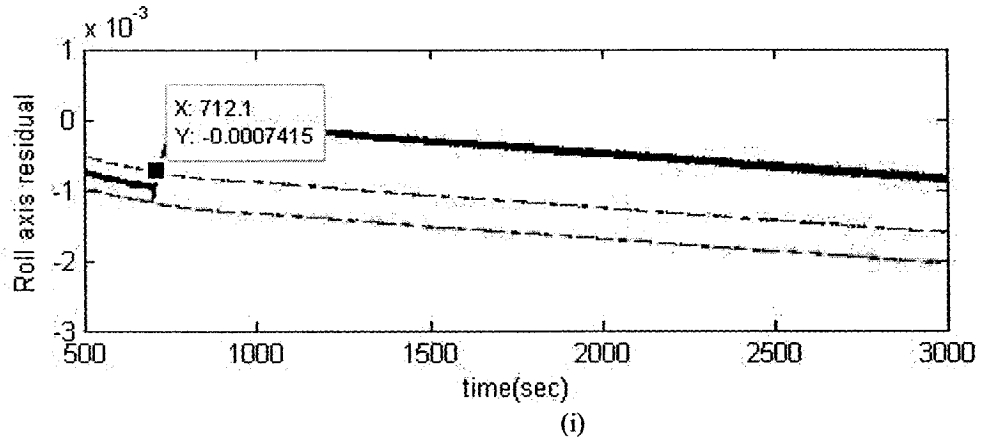

(i)

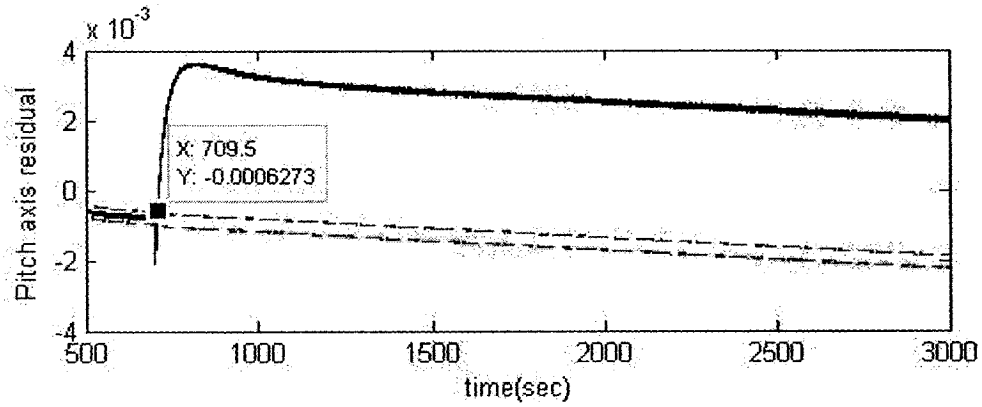

(ii)

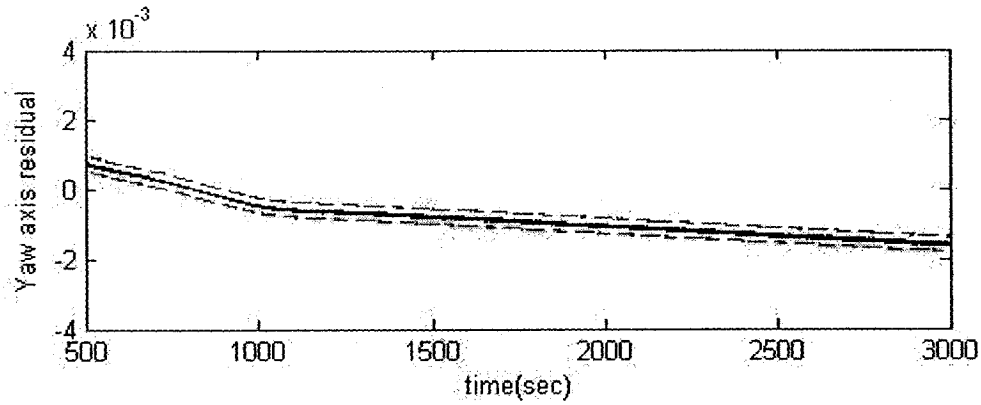

(iii)

(b) Parity space fault detection

Figure 5-11: Multiple faults in V_{BUS} in the roll axis and K_t in the pitch axis that are detected by (a) linear observer-based, and (b) parity space-based approaches

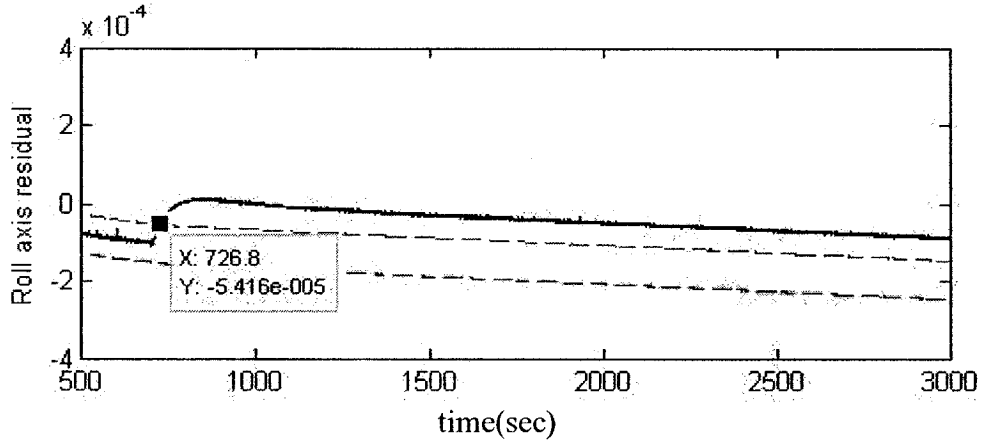

(i)

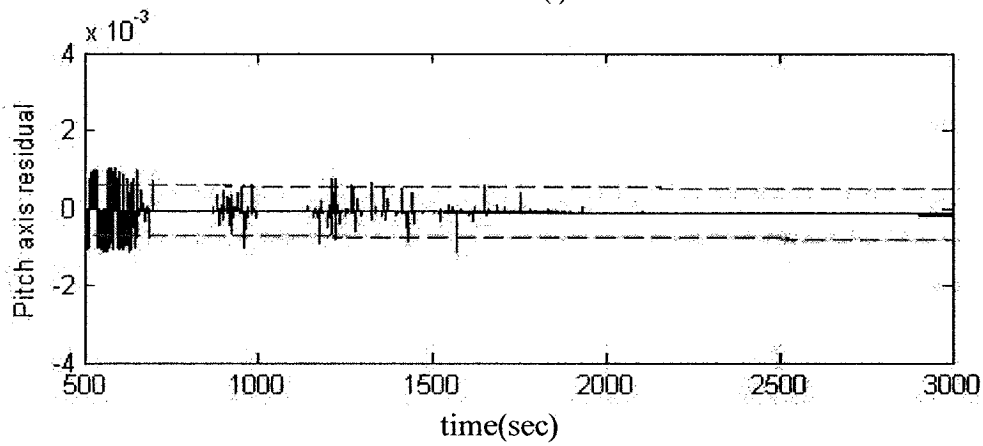

(ii)

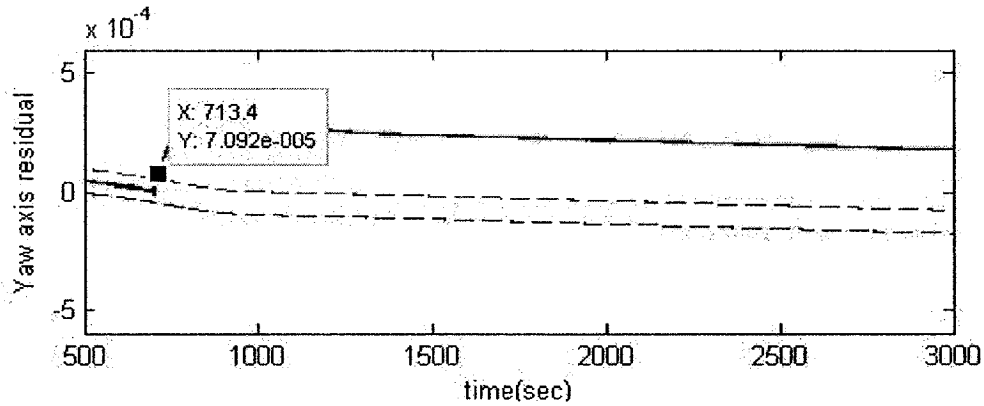

(iii)

(a) Linear observer fault detection

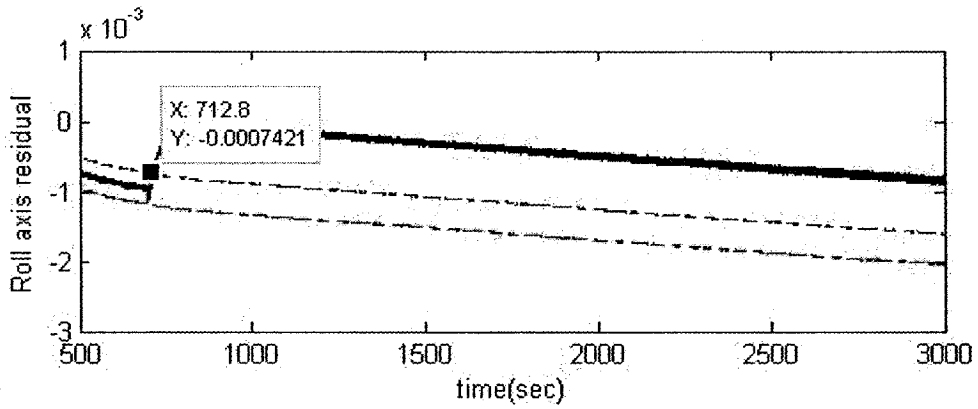

(i)

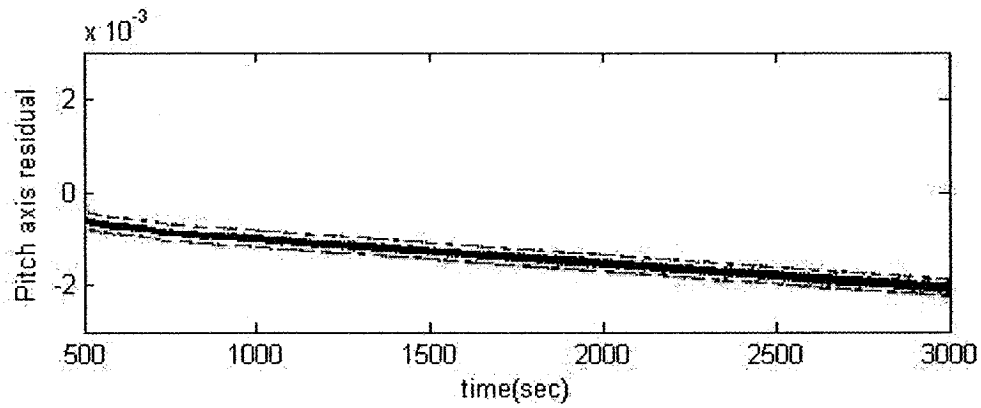

(ii)

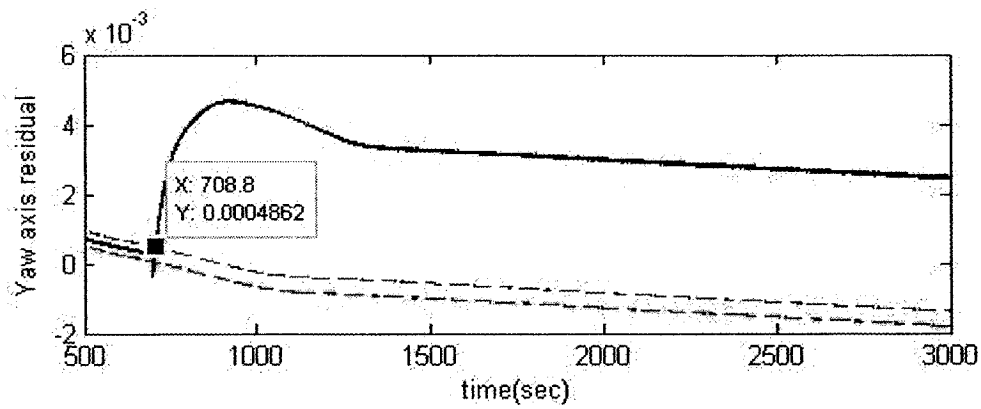

(iii)

(b) Parity space fault detection

Figure 5-12: Multiple faults in V_{BUS} in the roll axis and K_t in the yaw axis that are detected by (a) linear observer-based, and (b) parity space-based approaches

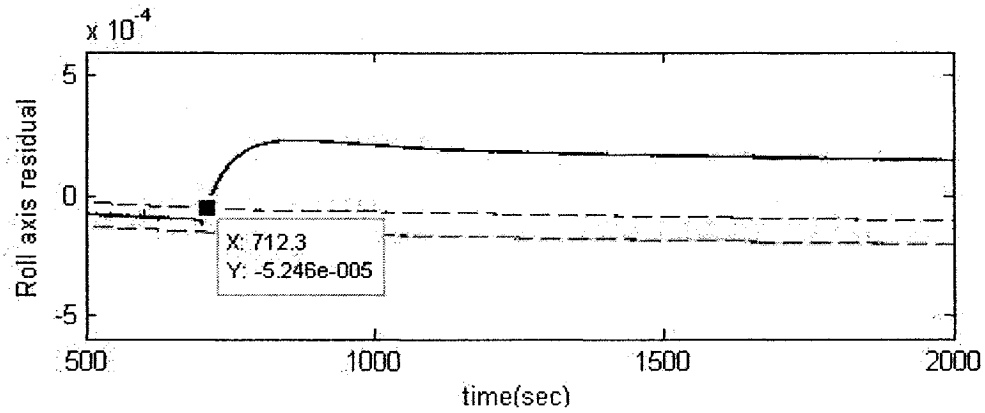

(i)

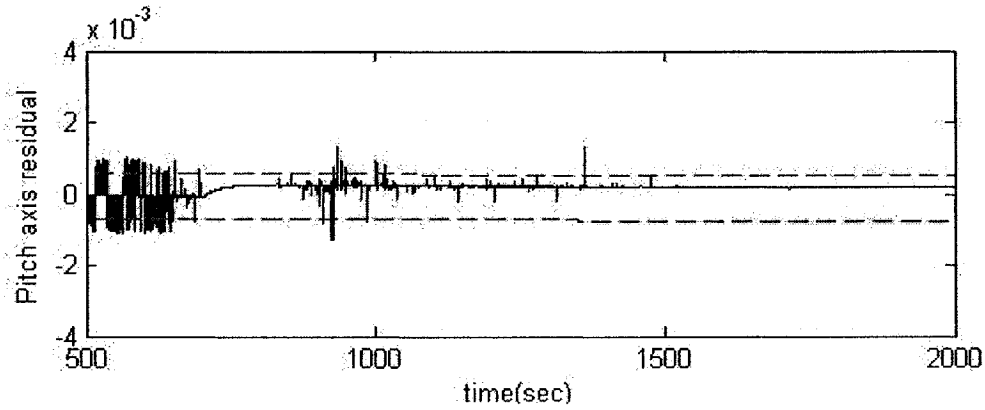

(ii)

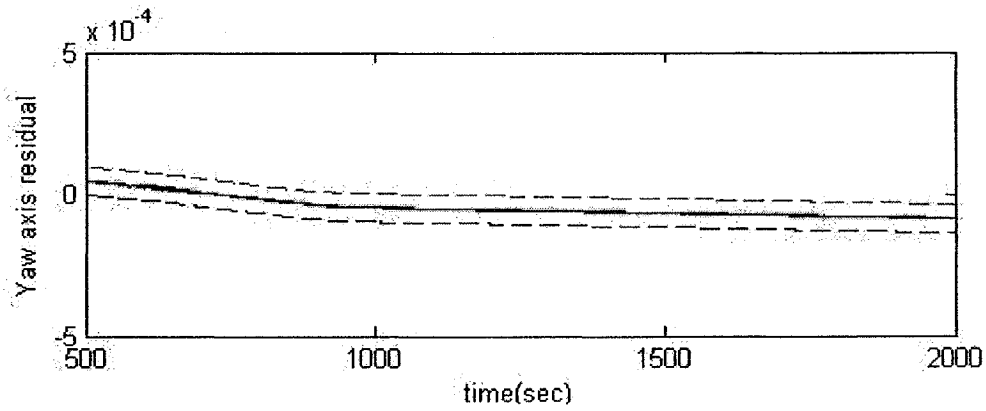

(iii)

(a) Linear observer fault detection

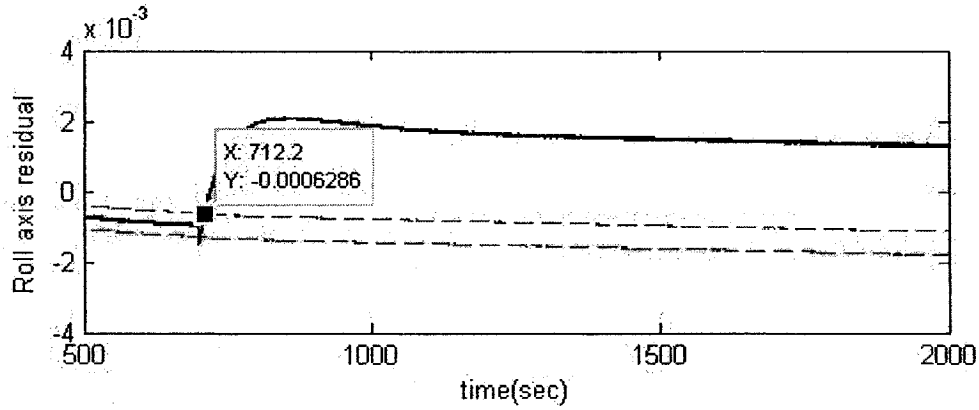

(i)

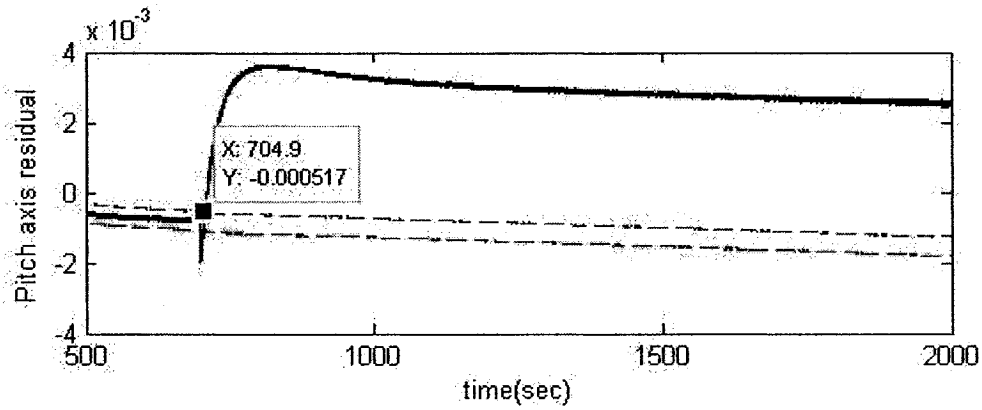

(ii)

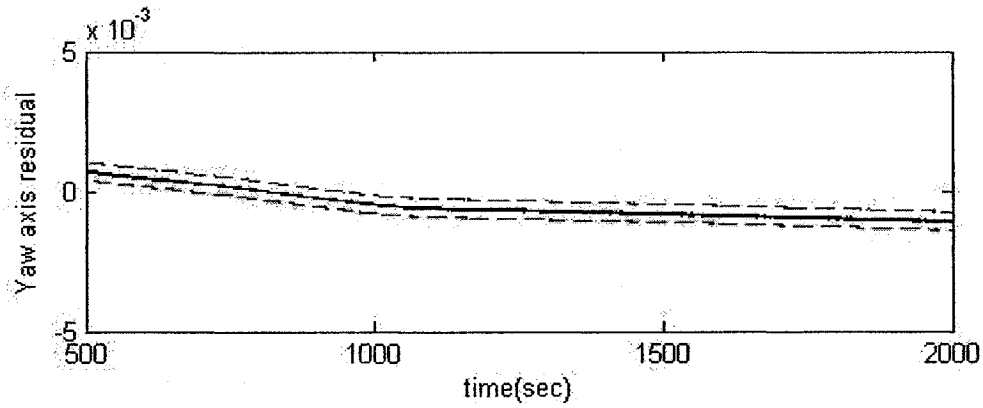

(iii)

(b) Parity space fault detection

Figure 5-13: Multiple faults in K_i in the roll and pitch axes that are detected by (a) linear observer-based, and (b) parity space-based approaches

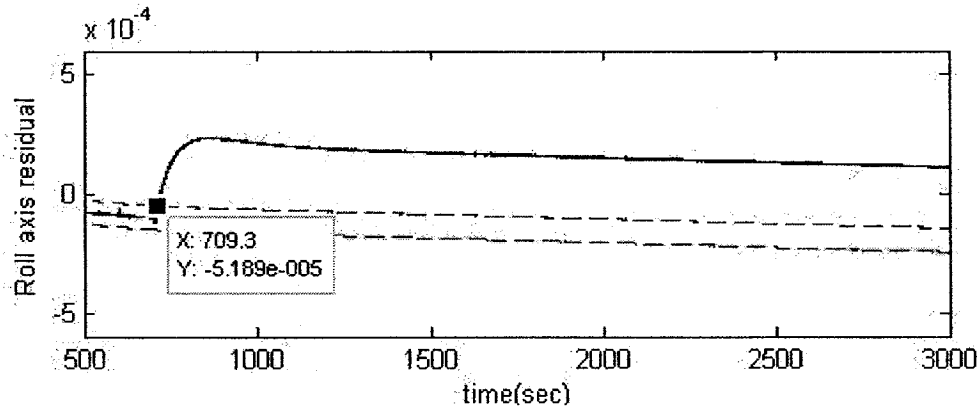

(i)

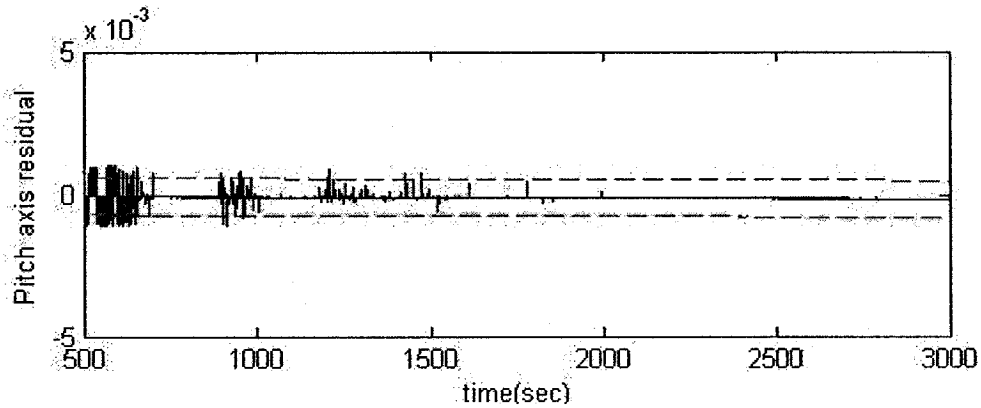

(ii)

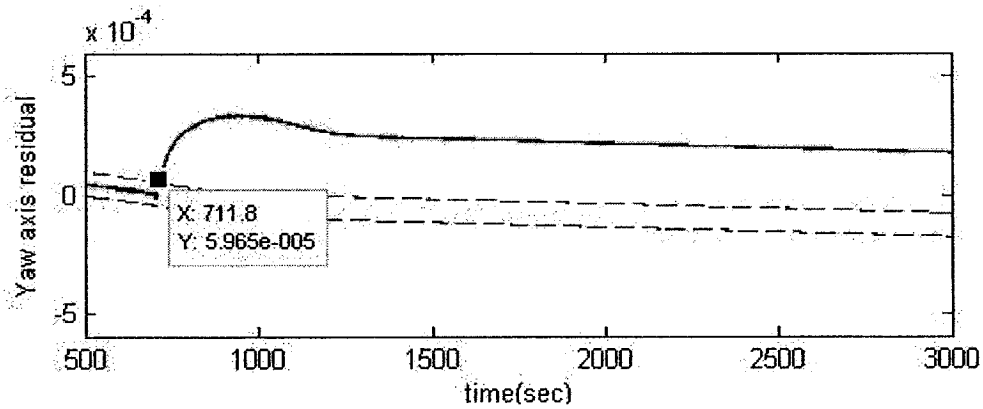

(iii)

(a) Linear observer fault detection

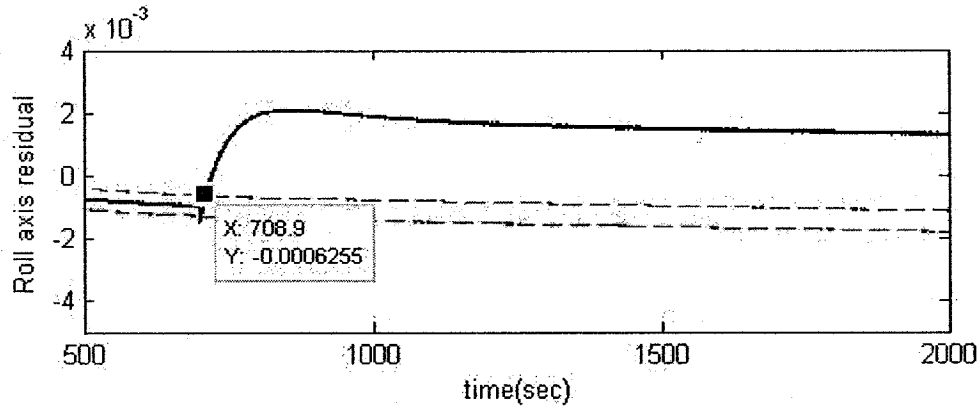

(i)

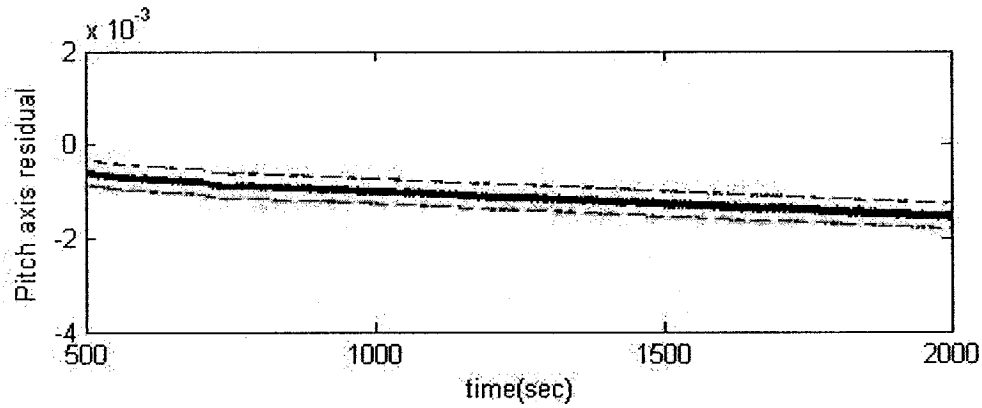

(ii)

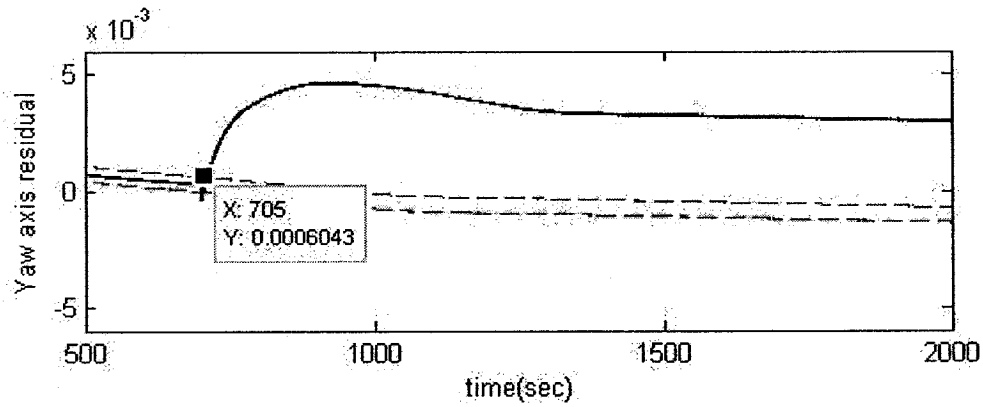

(iii)

(b) parity space fault detection

Figure 5-14: Multiple faults in K_t in the roll and yaw axes that are detected by (a) linear observer-based, and (b) parity space-based approaches

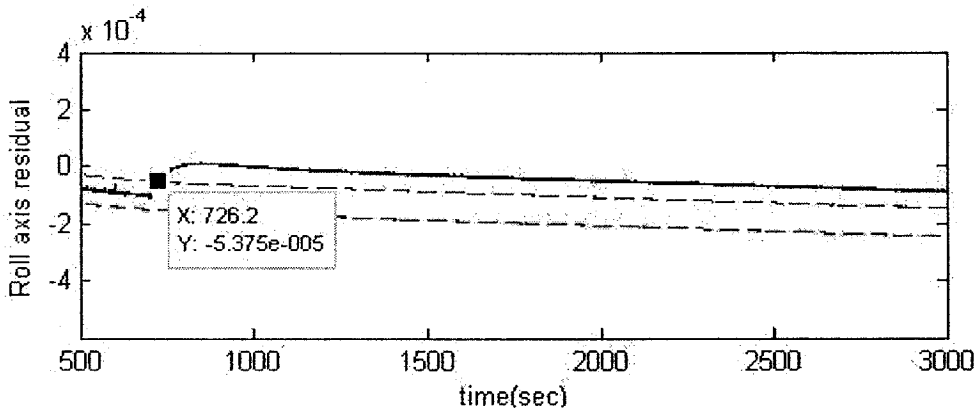

(i)

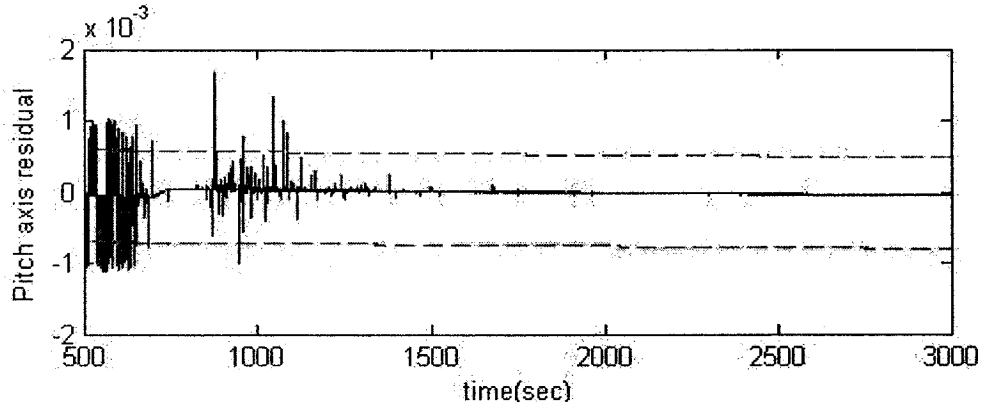

(ii)

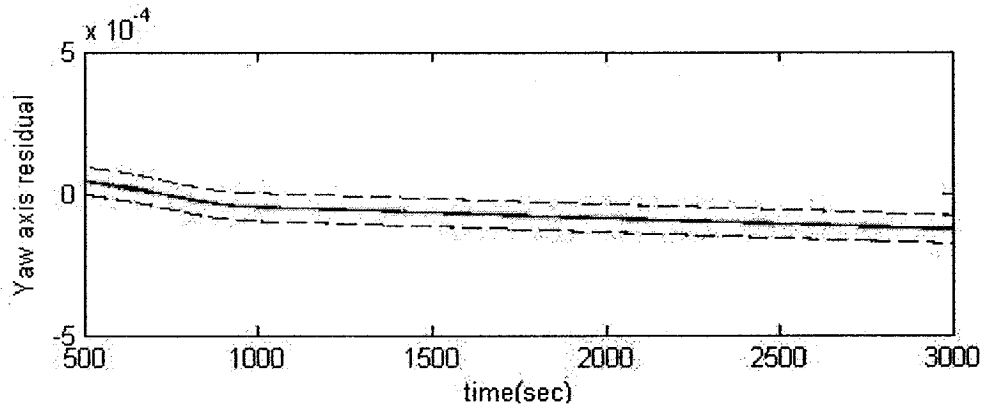

(iii)

(a) Linear observer fault detection

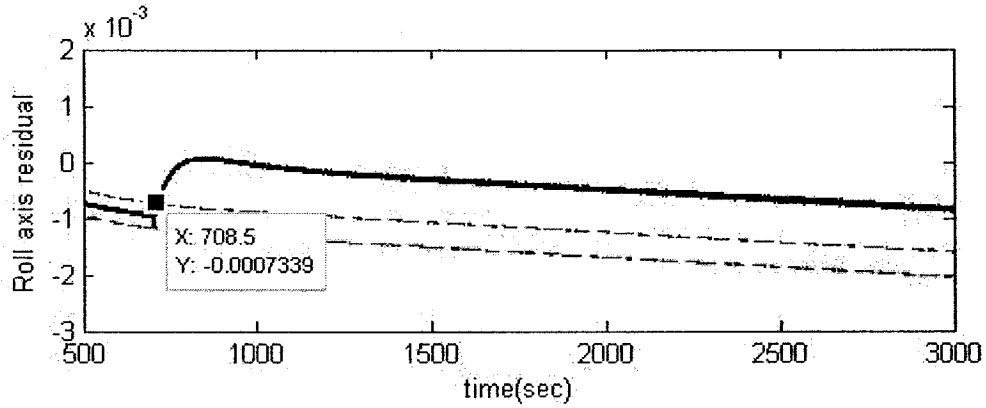

(i)

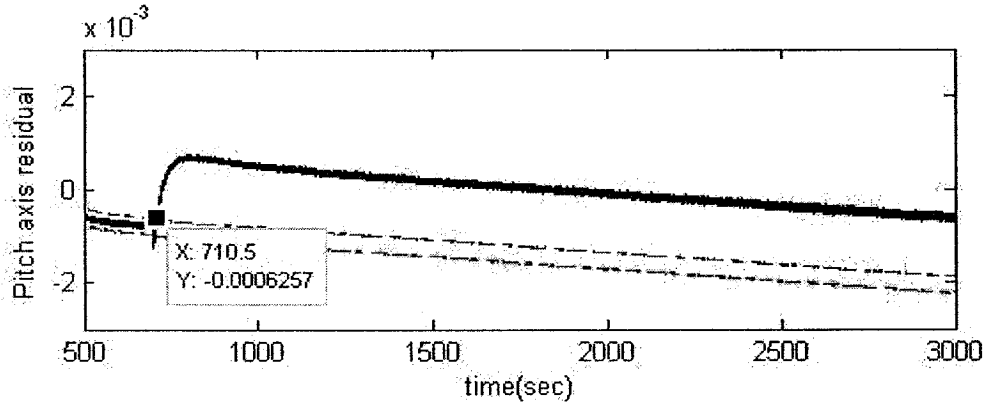

(ii)

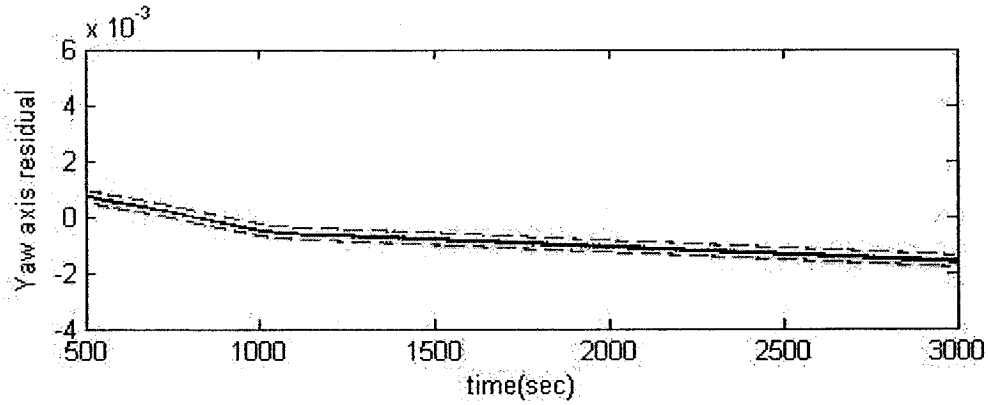

(iii)

(b) Parity space fault detection

Figure 5-15: Multiple faults in V_{BUS} in the roll and pitch axes that are detected by (a) linear observer-based, and (b) parity space-based approaches

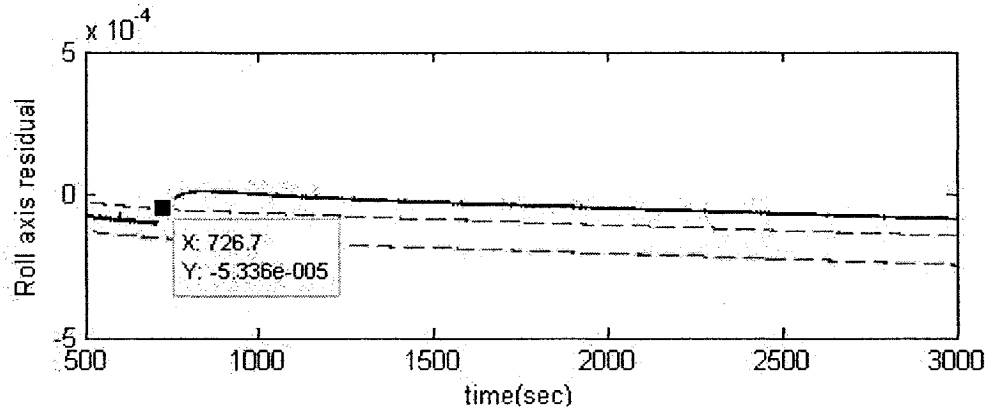

(i)

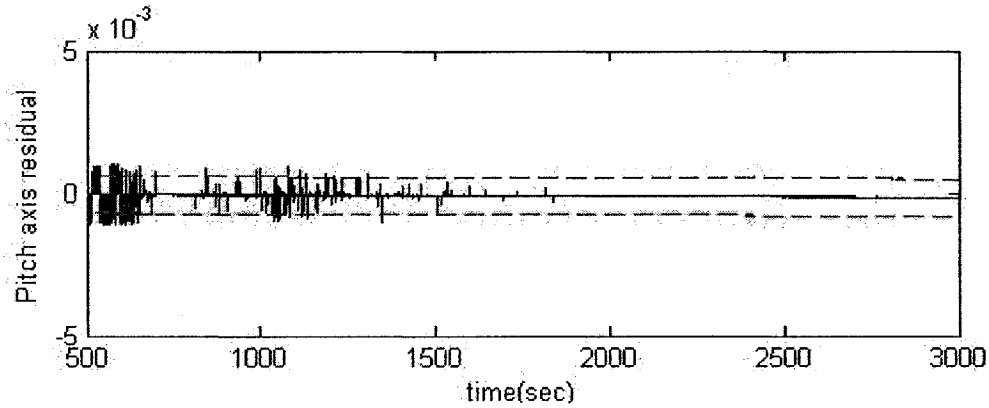

(ii)

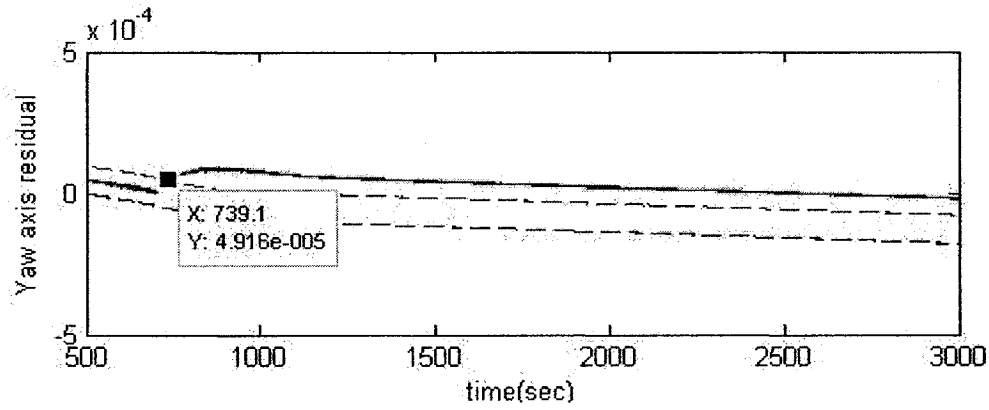

(iii)

(a) Linear observer fault detection

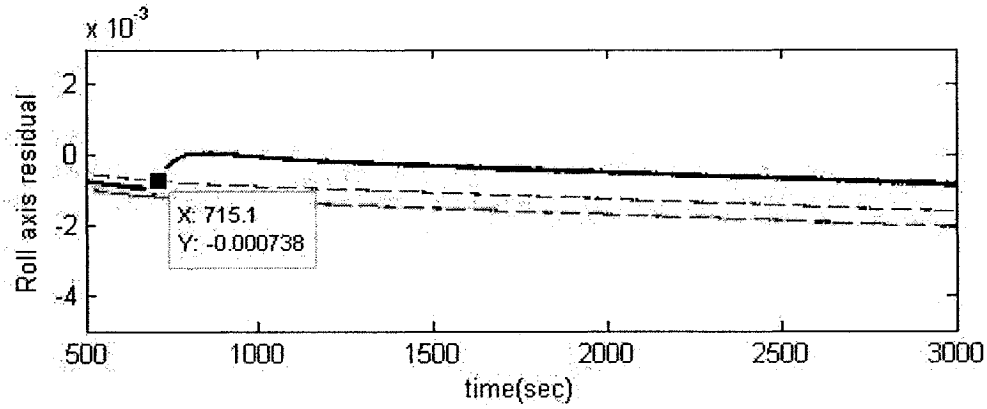

(i)

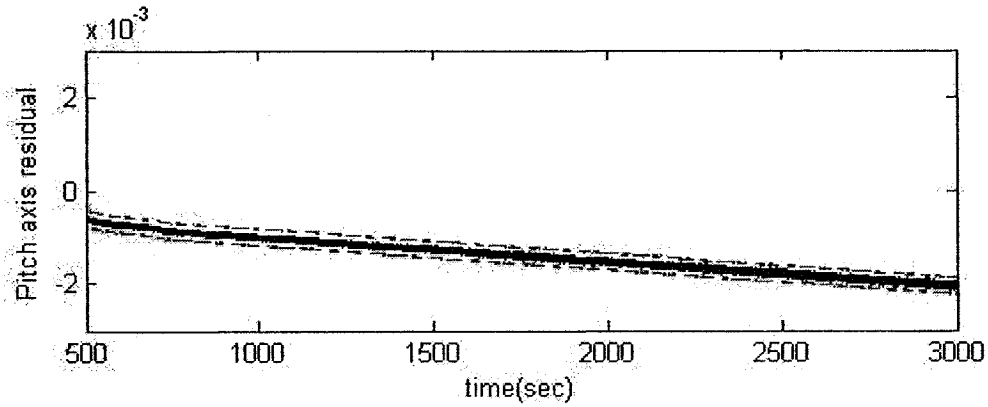

(ii)

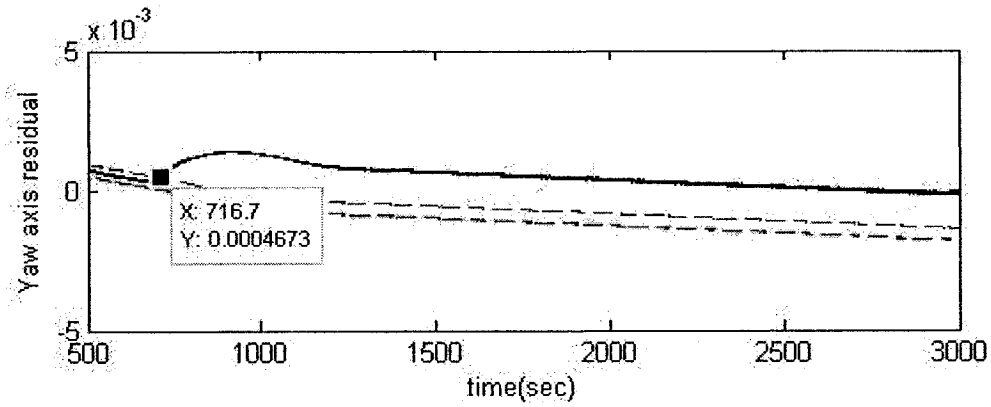

(iii)

(b) Parity space fault detection

Figure 5-16: Multiple faults in V_{BUS} in the roll and yaw axes that are detected by (a) linear observer-based, and (b) parity space-based approaches

The results obtained from these figures are summarized in Table 5-8 for the linear observer-based approach, and Table 5-9 for the parity space-based approach.

Case study	Linear observer-based FD method					
	Roll Axis		Pitch Axis		Yaw Axis	
	Detected	Detection time(sec)	Detected	Detection time(sec)	Detected	Detection time(sec)
1	✓	727.6	×	–		
2	✓	726.8			✓	713.4
3	✓	712.3	×	–		
4	✓	709.3			✓	711.8
5	✓	726.2	×	–		
6	✓	726.7			✓	739.1

Table 5-8: Detectability and the detection time for the linear observer scheme to multiple faults in the roll, pitch and the yaw axes according to Table 5-7

Case study	Parity space-based FD approach					
	Roll Axis		Pitch Axis		Yaw Axis	
	Detected	Detection time	Detected	Detection time	Detected	Detection time
1	✓	712.1	✓	709.5		
2	✓	712.8			✓	708.8
3	✓	712.2	✓	704.9		
4	✓	708.9			✓	705
5	✓	708.5	✓	710.5		
6	✓	715.1			✓	716.17

Table 5-9: Detectability and the detection time for the parity space scheme to multiple faults in the roll, pitch and the yaw axes according to Table 5-7.

According to the above figures, clearly the applied fault to the pitch axis cannot be detected by the linear observer approach. Furthermore, it is shown that occurrence of fault in the V_{BUS} component of the reaction wheel in the pitch axis and the yaw axis, reduces the delay time for the detection of fault in V_{BUS} component in the roll axis (case studies 5 and 6).

It is not yet possible to isolate the faulty component or components in the related faulty axis of the spacecraft. This is because of the fact that the residual pattern is the same for the occurrence of fault in the two studied components in this thesis.

5.4. Conclusion

In this chapter, the main advantages of the parity space approach over the linear observer approach are investigated and demonstrated through extensive simulation results. In addition to the improved sensitivity of the parity space approach one should also note its capability in detection of faults in the pitch axis. As shown through simulated results, the residuals generated by the linear observer approach are seriously influenced by noise, so that one needs to set the safe limits thresholds having a wider band to prevent detecting noise as faults. This has decreased the sensitivity of the linear observer approach mainly in the pitch axis. Furthermore, due to the similarity of the generated residual signals correspond to both K_t and V_{BUS} faults, the detection systems don't have the ability to isolate these different faults.

A number of scenarios and case studies have also been investigated to demonstrate the simultaneous detection and isolation capabilities of the parity space approach when compared to the linear observer approach.

Chapter 6 : Conclusions and Future Work

In this thesis, a parity space approach was developed, implemented and evaluated for fault detection and diagnosis of a reaction wheel in the spacecraft attitude control system (ACS). Since, an ACS is a complex system composed of different components, the process of fault detection and diagnosis is restricted to two components in the ACS reaction wheel. The model considered for the ACS reaction wheel is a high fidelity representation. The dynamics of the reaction wheel and the corresponding nonlinear attitude control system is covered in details. The components considered for fault injection are the current constant, K_t, which is a constant that converts the current input to a torque corresponding to that current, and the bus voltage, V_{BUS} of the reaction wheel.

To obtain a better validation of the performance capabilities of our proposed parity space-based fault detection and isolation technique, the results are compared to those of the linear observer-based method. The results obtained could be summarized as follows:

1. Development and implementation of the parity space approach to the ACS of a satellite for the first time in the literature.
2. The parity space approach is shown to be more sensitive to occurrence of faults. The fault ranges that can be detected by this method in the roll and the yaw axes are about two times smaller than the fault ranges that a linear observer-based method is sensitive to. However, the main advantage of the parity space-based method over the linear observer approach to fault detection appears in detecting

faults in the *pitch* axis. As illustrated in Chapter 5, noise and disturbances influence the pitch axis residual signal for the linear observer which makes the design of sensitive safe limits impossible, whereas these effects for the parity space approach are not present.

3. As far as detection capabilities are concerned both approaches are able to detect faults in both K_t and V_{BUS} components. The main difference between the methods as mentioned before, is in the amount and severity of faults that they can detect.
4. Observer-based approach requires a more time consuming design process. (e.g. in terms of the detection of the observer gains through a trial and error process), whereas the design procedure for the parity space approach is quite straight forward and does not require any tuning parameters and trial and error process.
5. Due to the differences in the architecture of observer-based and parity space approaches, namely in terms of the corresponding filter structures different sensitivities to noise and disturbance may be obtained.

Future Work

The future work that we can envisage for research beyond the developed work in this thesis can be summarized as follows:

1- **Fault diagnosis-** The residuals that are generated by the parity space approach do not provide sufficient information for fault diagnosis. Generally, for the purpose of fault diagnosis, different residuals should be generated, each residual sensitive to one type of fault. Improving the proposed system for the goal of fault diagnosis can be considered as a research area for future work.

2- **Fault detection in other reaction wheel components-** Fault detection in all of the components of the reaction wheel could not be covered in this thesis. The verification of influences of faults in other components by utilizing our proposed parity space method will result in better evaluation of this technique and is therefore of great interest to be investigated in future.

3- **Increasing sensitivity of the fault detection system-** The sensitivity of a fault detection method depends on initial conditions. As illustrated in Chapter 5, the sensitivity of our proposed method, specially in case of fault detection in the bus voltage is not quite satisfactory. Improvement in this area should be considered in future work.

4- **Verification over other ACS signals-** This work is based on the assumption that not all signals in the attitude control system of the spacecraft is measured. As an extension to this work, instead of signals obtained from the spacecraft, one can consider other outputs in the attitude control system and use them in the fault detection system as additional information for improving our proposed scheme.

5- **Improvement in detection delay time-** Having a real time fault detection system is one of the main goals in this area. Another promising future work could be improving and minimizing the detection delay time.

7 References

[1] M. C. Weisskope, B. Brinkman, C. Canizares, G. Garmire S. Murray and L. P. V. Speybroeck, "An Overview of the Performance and Scientific Results from the Chandra x-ray Observer", Astronomical Society of the Pacific, vol. 114, pp.1–24, 2002.

[2] F. Bauer, J. Bristow, D. Folta , K Hartman, and David Quinn, "Satellite Formation Flying Using An Innovative Autonomous Control System (AUTOCON) Environment", American Institute of Aeronautics and Astronautics, Inc. pp. 1-10, 1997.

[3] P. W. Fortescue, G. Swinerd, K.W. Angel, and J. P. W. Stark, "Spacecraft Systems Engineering", 3rd Edition, Published by John Wiley and Sons, 2003.

[4] J. R. Wertz, "Spacecraft Attitude Determination and Control", Published by Springer, 1978.

[5] B. Bialke, "High Fidelity Mathematical Modeling of Reaction Wheel Performance", in 21st Annual American Astronautical Society Guidance and Control Conference, AAS, Paper 98-063, 1998.

[6] D. J. Sahnow, H. W. Moos, T. B. Ake, J. Andersen, B. G. Andersson, M. Andre, D. Artis, A. F. Berman, W. P. Blair, K. R. Brownsberger, H. M. Calvani, P. Chayer, S. J. Conard, P. D. Feldman, S. D. Friedman, A. W. Fullerton, G. A. Gaines, W. C. Gawne, J. C. Green, M. A. Gummin, T. B. Jennings, J. B. Joyce, M. E. Kaiser, J. W. Kruk, D. J. Lindler, D. Massa, E. M. Murphy, W. R. Oegerle, R. G. Ohl, B. A. Roberts, M. L. Romelfanger, K. C. Roth, R. Sankrit, K. R. Sembach, R. L. Shelton, O. H. W. Siegmund, C. J. Silva, G. Sonneborn, S. R. Vaclavik, H. A. Weaver, and E. Wilkinson, "On-Orbit

Performance of the *Far Ultraviolet Spectroscopic Explorer* Satellite", The American Astronomical Society, vol. 538, pp. L7-L11, 2000.

[7] E. Asphaug, "Adventures in Near-Earth Object Exploration", Science vol. 312, no. 5778, pp. 1328 – 1329, 2006.

[8] H. E. Rauch, "intelligent fault diagnosis and control reconfiguration", IEEE control system vol. 14, no. 3, pp. 6-12, 1994.

[9] Y.Zhang. X.R. Li, "Detection and diagnosis of sensor and actuator failures using IMMestimator", IEEE transaction, vol. 34, no. 4, pp. 1293-1313, 1998.

[10] J. J. Gertler, "Survey of model-based failure detection and isolation in complexplants", IEEE Control System Magazine, vol. 8, no. 6, pp. 3-11, 1998.

[11] E. Jackson, "Real-time model-based fault detection and diagnosis for automated systems", Dynamic Modeling Control Applications for Industry Workshop, IEEE Industry Applications Society, pp. 26-28, 1997.

[12] R. Mehra, C. Rago, S. Seereeram, "Autonomous failure detection, identification and fault-tolerantestimation with aerospace applications", IEEE Aerospace Conference Proceedings, vol. 2, pp. 133-138, 1998.

[13] R. J. Patton, J. Chen, "Review of parity space approaches to fault diagnosis for aerospace systems", Journal of Guidance, Control & Dynamics, vol. 17, no. 2, pp. 278-285, 1994.

[14] R. Dearden, T. Willeke, F. Hutter, R. Simmons, V. Verma, "Real-time Fault Detection and Situational Awareness for Rovers: Report on the Mars Technology Program Task", Proceeding of IEEE conference, 2004

[15] E. M. Atkins, R. H. Miller, T. Van Pelt, K. D. Shaw, W. B. Ribbens, P. D. Washabaugh, D. S. Bernstein, "An Autonomous Aircraft for Flight Control and Trajectory Planning Research", Proceeding of American Control Conference, vol.2, pp. 689-693, 1998.

[16] H. E. Rauch, "Autonomous control reconfiguration", IEEE Control System Magazine, vol. 15, no. 6, pp. 37-48, 1995.

[17] P. J. Adamovits, B. Pagurek, "Simulation (model) based fault detection and diagnosis of aspacecraft electrical power system", IEEE Ninth conference on Artificial Intelligence for Applications, pp. 422-428, 1993.

[18] D. A. Rennels, "Architectures for fault-tolerant spacecraft computers", Proceeding of the IEEE, vol. 66, no. 10, pp. 1255-1268, 1978.

[19] P. Smith, "Hidden Markov models and neural networks for fault detection indynamic systems", Neural Networks for Signal Processing III. Proceedings of IEEE-SP Workshop, pp. 582-592, 1993.

[20] A. J. Gonzalez, R. A. Morris, F. D. Mckenzie, D. J. Carreira, B. K. Gann, "Model-based, real-time control of electrical power systems", IEEE Transactions on Systems, Man and Cybernetics, Part A, vol. 26, no. 4, pp. 470-482, 1996.

[21] M. Hecht, H. Hecht, E. Shokri, "Adaptive Fault Tolerance for Spacecraft", IEEE Proceeding on Aerospace Conference Proceedings, vol. 5, pp. 521-533, 2000.

[22] F. Hutter, R. Deareden, "Efficient On-line Fault Diagnosis for Non-Linear Systems", Proceeding of the 7th International Symposium on Artificial Intelligence and symbolic Computation, 2003.

[23] I Naoki, O, Shiro, Y, Takehisa, "Spacecraft fault diagnosis using a data mining", Proceedings of the twenty-third international symposium on space technology and science (Selected papers), vol. 2 , pp. 1431-1436, 2002.

[24] S. Simani, C. Fantuzzi and R. J. Patton, "Model-Based Fault Diagnosis in Dynamic Systems Using Identification Techniques", Published by Springer, 2002.

[25] P. M. Frank, "Fault Diagnosis in Dynamic Systems Using Analytical and Knowledge-based Redundancy- A Survey and Some New Results", Automatica, vol. 26, no. 3, pp. 459-474, 1990.

[26] R. Isermann, "Process fault detection based on modeling and estimation methods. A survey", Automatica. vol. 20, no. 4, pp. 387-404. 1984.

[27] M. Yoshimura, P. M. Frank, X. Ding, "Survey of robust residual generation and evaluation methods in observer-based fault detection systems", Journal of Process Control, vol. 7, no. 6, pp. 403-424, 1997.

[28] P. P. Harihara, K. Kyusung, A. G. Parlos, "Signal-based versus model-based fault diagnosis-a trade-off in complexity and performance", 4th IEEE International Symposium on Diagnostics for Electric Machines, Power Electronics and Drives, pp. 277-282, 2003.

[29] E. Y. Chow, A. S. Willsky, "Analytical Redundancy and the Design of Robust Failure Detection Systems", IEEE Transactions on Automatic Control, vol. AC-29, no. 7, 1984.

[30] R. J. Patton, "Fault Detection and Diagnosis in Aerospace Systems Using Analytical Redundancy", Computing and Control Engineering Journal, pp.127-136, 1991.

[31] S. I. Mofizul, T. Wu, G. Ledwich, "A novel fuzzy logic approach to transformer fault diagnosis", IEEE Transactions on Dielectrics and Electrical Insulation. vol. 7, no. 2, pp. 177-186, 2000.

[32] Y. Maki, K. A. Loparo, "A neural-network approach to fault detection and diagnosis inindustrial processes", IEEE transaction on Control Systems Technology, vol. 5, no. 6, pp. 529-541, 1997.

[33] A. Wolfram, D. Fussel, T. Brune, R. Isermann, "Component-based multi-model approach for fault detection anddiagnosis of a centrifugal pump", American Control Conference, vol. 6, pp. 4443-4448, 2001.

[34] R. Isermann, "Model-based Fault Detection and Diagnosis-Status and Applications", Annual Review in Control, vol. 29, pp. 71-85, 2005.

[35] V. Venkatasubramanian, R. Rengaswamy, K. Yin, S. N. Kavuri, "A Review of Process Fault Detection and Diagnosis Part I: Quantitative Model-based Methods", Computers and Chemical Engineering, vol. 27, pp. 293-311, 2003.

[36] R. Isermann. "Supervision, Fault Detection and Fault Diagnosis Methods: an Introduction", Control Engineering Practice, vol. 5, no. 5, pp. 639-652, 1997.

[37] R. J. Patton, P. M. Frank and R. N. Clark, "Issues of Fault Diagnosis for Dynamic systems", Published by Springer, 2000.

[38] M. Mesbahi and F. Y. Hadaegh, "Formation Flying Control of Multiple Spacecraft via Graphs, Matrix Inequalities, and Switching", Journal of Guidance, Control and Dynamics, vol. 24, no. 2, pp. 369-377, 2001.

[39] B. Wie, "Space Vehicle Dynamics and Control", Published by AIAA, 1998.

[40] M. Haji. H.A. Toliyat, "Pattern Recognition-a Technique for Induction Machines Rotor fault Detection", IEEE transaction, vol. 16, no. 4, pp. 312-317, 2001.

[41] K. Ogata, "Modern Control Engineering", third Edition, 1997.

[42] Z. Bubnicki, "Modern Control Theory", Springer, 2005.

[43] J. Gertler, "Generating directional residuals with dynamic parity equations", Proc. IFAC/IMACS Symp. SAFEPROCESS'91. Baden Baden (G), 1991.

[44] J.A.Geymayr, N. F. Ebecken, "Fault-Tree Analysis: a Knowledge-Engineering Approach", IEEE Transactions, vol. 44, no. 1, pp. 37-45, 1995.

[45] R. W. Brockett, Finite Dimentional Linear Systems, Wiley, New York, 1970.

[46] E. Y. Chow, A. S. Willsky, "Issue in the development of a general algorithm for reliable failure detection", In Proc. of the 19th Conf. on Decision & Control, Albuquerque, NM, 1980.

[47] J. Chen, R. J. Patton, "Robust Model-Based Fault Diagnosis for Dynamic Systems", Kluwer Academic, 1999.

[48] P. M. Frank, "Enhancement of robustness on observer-based fault detection", International Journal of Control, vol. 59, no. 4, pp. 995-983, 1994.

[49] P. M. Frank, X, Ding, "Survey of robust residual generation and evaluation methods in observer-based fault detection system", Journal of Process Control, vol. 7, no. 6, pp. 403-424, 1997.

[50] I. E. Potter, M. C. Suman, "Thresholdless redundancy management with array of skewed instruments", Technical Report AGARDOGRAPH-224, AGARD, Integrity in Electronic Flight Control Systems, 1977.

[51] K. C. Daly, E. Gai, J. V. Harrison, "Generalized likelihood test for FDI in redundancy sensor configurations", Journal of Guidance, Control & Dynamics, vol. 2, no. 1, pp. 9-17, 1979.

[52] R. R. Barton, J. S. Ivey, "Nelder-Mead Simplex Modifications for Simulation Optimization", Management Science, vol. 42, no. 7, pp. 954-973, 1996.

[53] W. B. Chubb, S. M. Seltzer, "Skylab Attitude and pointing control System", George C. Marsball Space Flight Center, Ala 35812. National Aeronautic & Space Administration, Washington D.C., 1971.

[54] S. M. El-shal, and A. S. Morris, "A Fuzzy Expert System for Fault Detection in Statistical Process Control of Industrial Process", IEEE Transaction, vol. 30, no. 2, pp. 281-289, 2000.

[55] H. Azarnoush, "Fault Diagnosis in Spacecraft Attitude Control System", Master's thesis, Concordia University, 2005.